ELEMENT-FREE GALERKIN METHOD FOR PLANE STRESS PROBLEMS

A THESIS SUBMITTED TO
THE GRADUATE SCHOOL OF NATURAL AND APPLIED SCIENCES
OF
MIDDLE EAST TECHNICAL UNIVERSITY

BY

FATMA DİLAY AKYAZI

IN PARTIAL FULFILLMENT OF THE REQUIREMENTS
FOR
THE DEGREE OF MASTER OF SCIENCE
IN
MECHANICAL ENGINEERING

FEBRUARY 2010

Approval of the thesis:

ELEMENT-FREE GALERKIN METHOD FOR PLANE STRESS PROBLEMS

submitted by **FATMA DİLAY AKYAZI** in partial fulfillment of the requirements for the degree of **Master of Science in Mechanical Engineering Department, Middle East Technical University** by,

Prof. Dr. Canan Özgen
Dean, Graduate School of **Natural and Applied Sciences** _____

Prof. Dr. Suha Oral
Head of Department, **Mechanical Engineering** _____

Prof. Dr. Suha Oral
Supervisor, **Mechanical Engineering Dept.**, **METU** _____

Examining Committee Members:

Prof. Dr. Ahmet Bülent Doyum
Mechanical Engineering Dept., METU _____

Prof. Dr. Suha Oral
Mechanical Engineering Dept., METU _____

Prof. Dr. Haluk Darendeliler
Mechanical Engineering Dept., METU _____

Prof. Dr. Suat Kadıoğlu
Mechanical Engineering Dept., METU _____

Assoc. Dr. Mustafa Uğur Polat
Civil Engineering Dept., METU _____

Date: _____

I hereby declare that all information in this document has been obtained and presented in accordance with academic rules and ethical conduct. I also declare that, as required by these rules and conduct, I have fully cited and referenced all material and results that are not original to this work.

Name, Last Name :

Signature :

ABSTRACT

ELEMENT-FREE GALERKIN METHOD FOR PLANE STRESS PROBLEMS

Akyazı, Fatma Dilay
M.Sc., Department of Mechanical Engineering
Supervisor: Prof. Dr. Suha Oral

February 2010, 129 pages

In this study, the Element-Free Galerkin (EFG) method has been used for the analysis of plane stress problems. A computer program has been developed by using FORTRAN language. The moving least squares (MLS) approximation has been used in generating shape functions. The results obtained by the EFG method have been compared with analytical solution and the numerical results obtained by MSC. Patran/Nastran. The comparisons show that the mesh free method gives more accurate results than the finite element approximation with less computational effort.

Keywords: Mesh Free Methods, Element-Free Galerkin Method, Plane Stress

ÖZ

DÜZLEMSEL GERİLME PROBLEMLERİ İÇİN ELEMAN BAĞIMSIZ GALERKİN YÖNTEMİ

Akyazı, Fatma Dilay

Yüksek Lisans, Makina Mühendisliği Bölümü

Tez Yöneticisi: Prof. Dr. Suha Oral

Şubat 2010, 129 sayfa

Bu çalışmada, Eleman Bağımsız Galerkin (EBG) yöntemi düzlemsel gerilme problemlerinin analizinde kullanılmıştır. FORTRAN dilinde bir bilgisayar programı geliştirilmiştir. Hareketli en küçük kareler (HEK) yaklaşımı ise biçim fonksiyonlarını oluşturmak için kullanılmıştır. EBG yöntemiyle elde edilen sonuçlar, analitik yöntemle ve MSC. Patran/Nastran ile elde edilen sayısal sonuçlarla karşılaştırılmıştır. Karşılaştırmalar göstermiştir ki, ağsız yöntem daha az hesaplama çabasıyla sonlu elemanlar yaklaşımından daha iyi sonuç vermektedir.

Anahtar Kelimeler: Ağsız Yöntemler, Eleman Bağımsız Galerkin Yöntemi, Düzlemsel Gerilme

To my dear friend Efruz and my dearest Erdem

ACKNOWLEDGEMENTS

I express sincere appreciation to my supervisor Prof. Dr. Suha Oral for his great guidance, advice, criticism, systematic supervision, and insight throughout the study.

My dear friend Mehmet Efruz Yalçın is gratefully acknowledged for his self denying support, encouragement and faith in me.

I want to thank my beloved friend Erdem Aksoy for his support, patience and inspiration. I would not have handled my busy scheduled term without his vitalizing presence.

I also want to thank my family, my mother Nergiz Akyazı, my father Ali Turan Akyazı, my sisters Yeliz Oymak and Yelda Akyazı and my brother Kubilay Cenk Oymak for their encouragement and generosity.

The cooperation and support of my friends, especially Yasemin Olcay deserves to be acknowledged for her interesting discussions and support during my thesis study.

Finally, I am thankful to my company TAI-TUSAŞ Inc. for letting of my thesis.

TABLE OF CONTENTS

ABSTRACT iv
ÖZ v
ACKNOWLEDGEMENTS vii
TABLE OF CONTENTS viii
LIST OF TABLES x
LIST OF FIGURES xii
LIST OF SYMBOLS xvi
CHAPTER
1. INTRODUCTION 1
1.1. Mesh Free Methods 1
1.2. The Advantages of the Mesh Free Methods 2
1.3. Scope of the Study 3
2. REVIEW OF LITERATURE 4
3. THE ELEMENT-FREE GALERKIN METHOD 10
3.1. Node Generation 12
3.2. Shape Functions 15
3.3. Formulation 18
4. NUMERICAL EXAMPLES 25
4.1. Cantilever Beam under Parabolic End Load 26
4.2. Cantilever Beam under Uniform Transverse Load 55
4.3. A Square Plate with Hole under Uniform Distributed Load at both sides 77
5. CONCLUSION 112
REFERENCES 114

APPENDICES

A. GAUSSIAN QUADRATURE 118
B. VISUALIZATION 121
B.1 Creating Elements from an External File 121
B.2 Data Preparation Procedure for CATIA 126
C. CODE ALGORITHM 129

LIST OF TABLES

TABLES

Table 4.1.1 Comparison of the displacements in x direction 29
Table 4.1.2 Comparison of the displacements in y direction 30
Table 4.1.3 Comparison of the σ_x results 32
Table 4.1.4 Comparison of the σ_{xy} results 34
Table 4.1.5 Comparison of the displacements in x direction 37
Table 4.1.6 Comparison of the displacements in y direction 38
Table 4.1.7 Comparison of the σ_x results 40
Table 4.1.8 Comparison of the σ_{xy} results 42
Table 4.1.9 Comparison of the displacements in x direction 44
Table 4.1.10 Comparison of the displacements in y direction 46
Table 4.1.11 Comparison of the σ_x results 47
Table 4.1.12 Comparison of the σ_{xy} results 49
Table 4.1.13 Comparison of the displacements in x direction 51
Table 4.1.14 Comparison of the displacements in y direction 52
Table 4.1.15 Comparison of the σ_x results 53
Table 4.1.16 Comparison of the σ_{xy} results 54
Table 4.2.1 Comparison of the displacements in y direction 56
Table 4.2.2 Comparison of the σ_x results 58
Table 4.2.3 Comparison of the σ_{xy} results 60
Table 4.2.4 Comparison of the displacements in y direction 62
Table 4.2.5 Comparison of the σ_x results 64
Table 4.2.6 Comparison of the σ_{xy} results 66
Table 4.2.7 Comparison of the displacements in y direction 68
Table 4.2.8 Comparison the σ_x results 70
Table 4.2.9 Comparison of the σ_{xy} results 72

Table 4.2.10 Comparison of the displacements in y direction 74
Table 4.2.11 Comparison of the σ_x results 75
Table 4.2.12 Comparison of the σ_{xy} results 76
Table 4.3.1 Comparison of the displacements in x direction 78
Table 4.3.2 Comparison of the displacements in y direction 80
Table 4.3.3 Comparison of the σ_x results 81
Table 4.3.4 Comparison of the σ_y results 83
Table 4.3.5 Comparison of the σ_{xy} results 85
Table 4.3.6 Comparison of the displacements in x direction 91
Table 4.3.7 Comparison of the displacements in y direction 92
Table 4.3.8 Comparison of the σ_x results 94
Table 4.3.9 Comparison of the σ_y results 96
Table 4.3.10 Comparison of the σ_{xy} results 98
Table 4.3.11 Comparison of the displacements in x direction 100
Table 4.3.12 Comparison of the displacements in y direction 102
Table 4.3.13 Comparison of the σ_x results 103
Table 4.3.14 Comparison of the σ_y results 105
Table 4.3.15 Comparison of the σ_{xy} results 107
Table 4.3.16 Comparison of the displacements in x direction 109
Table 4.3.17 Comparison of the displacements in y direction 110
Table 4.3.18 Comparison of the σ_x results 111
Table A.1 Abscissae and Weight Coefficients of the Gaussian Quadrature Formula 119
Table A.2 Abscissae and Weight Coefficients of the Gaussian Quadrature Formula used for Boundary Integration Points [28] 120

LIST OF FIGURES

FIGURES

Figure 3.1 The background mesh of a problem domain 11
Figure 3.1.1 Nodes in a problem domain 12
Figure 3.1.2 Delaunay triangulation 13
Figure 3.1.3 Node distribution on a background mesh 14
Figure 3.1.4 Node and integration point distribution on a background mesh 15
Figure 3.3.1 Representation of an Influence Domain (ID) 18
Figure 4.1.1 A cantilever beam subjected to parabolic end loading 26
Figure 4.1.2 The background mesh 28
Figure 4.1.3 Node distribution on the background mesh 28
Figure 4.1.4 Node and integration point distribution on the background mesh 28
Figure 4.1.5 Graphical comparison of displacements in x direction 29
Figure 4.1.6 Graphical comparison of displacements in y direction 31
Figure 4.1.7 σ_x distribution obtained by Patran/Nastran 33
Figure 4.1.8 Graphical comparison of σ_x results 33
Figure 4.1.9 σ_{xy} distribution obtained by Patran/Nastran 35
Figure 4.1.10 Graphical comparison of σ_{xy} results 35
Figure 4.1.11 The background mesh 36
Figure 4.1.12 Node distribution on the background mesh 36
Figure 4.1.13 Node and integration point distribution on the background mesh 36
Figure 4.1.14 Graphical comparison of displacements in x direction 37
Figure 4.1.15 Graphical comparison of displacements in y direction 39
Figure 4.1.16 σ_x distribution obtained by Patran/Nastran 41
Figure 4.1.17 Graphical comparison of σ_x results 41
Figure 4.1.18 σ_{xy} distribution obtained by Patran/Nastran 43
Figure 4.1.19 Graphical comparison of σ_{xy} results 43

Figure 4.1.20 Graphical comparison of displacements in x direction..... 45
Figure 4.1.21 Graphical comparison of displacements in y direction..... 46
Figure 4.1.22 σ_x distribution obtained by Patran/Nastran 48
Figure 4.1.23 Graphical comparison of σ_x results 48
Figure 4.1.24 σ_{xy} distribution obtained by Patran/Nastran 50
Figure 4.1.25 Graphical comparison of σ_{xy} results 50
Figure 4.1.26 Graphical comparison of displacements in x direction..... 51
Figure 4.1.27 Graphical comparison of displacements in y direction..... 52
Figure 4.1.28 Graphical comparison of σ_x results 53
Figure 4.1.29 Graphical comparison of σ_{xy} results 54
Figure 4.2.1 A cantilever beam subjected to uniform transverse loading..... 55
Figure 4.2.2 Graphical comparison of displacements in y direction..... 57
Figure 4.2.3 σ_x distribution obtained by Patran/Nastran 59
Figure 4.2.4 Graphical comparison of σ_x results 59
Figure 4.2.5 σ_{xy} distribution obtained by Patran/Nastran 61
Figure 4.2.6 Graphical comparison of σ_{xy} results 61
Figure 4.2.7 Graphical comparison of displacements in y direction..... 63
Figure 4.2.8 σ_x distribution obtained by Patran/Nastran 65
Figure 4.2.9 Graphical comparison of σ_x results 65
Figure 4.2.10 σ_{xy} distribution obtained by Patran/Nastran 67
Figure 4.2.11 Graphical comparison of σ_{xy} results 67
Figure 4.2.12 Graphical comparison of displacements in y direction..... 69
Figure 4.2.13 σ_x distribution obtained by Patran/Nastran 71
Figure 4.2.14 Graphical comparison of σ_x results 71
Figure 4.2.15 σ_{xy} distribution obtained by Patran/Nastran 73
Figure 4.2.16 Graphical comparison of σ_{xy} results 73
Figure 4.2.17 Graphical comparison of displacements in y direction..... 74
Figure 4.2.18 Graphical comparison of σ_x results 75
Figure 4.2.19 Graphical comparison of σ_{xy} results 76
Figure 4.3.1 A square plate with hole subjected to uniform distributed side loading 77
Figure 4.3.2 Geometry reduction and boundary condition application 77
Figure 4.3.3 Graphical comparison of displacements in x direction..... 79

Figure 4.3.4 Graphical comparison of displacements in y direction..... 80
Figure 4.3.5 σ_x distribution obtained by Patran/Nastran 82
Figure 4.3.6 Graphical comparison of the σ_x results 82
Figure 4.3.7 σ_y distribution obtained by Patran/Nastran 84
Figure 4.3.8 Graphical comparison of σ_y results 84
Figure 4.3.9 σ_{xy} distribution obtained by Patran/Nastran 86
Figure 4.3.10 Graphical comparison of the σ_{xy} results 86
Figure 4.3.11 The background mesh distribution 87
Figure 4.3.12 Node distribution in the problem domain 88
Figure 4.3.13 Node distribution on the background mesh 89
Figure 4.3.14 Node and integration point distribution on the background mesh..... 90
Figure 4.3.15 Graphical comparison of displacements in x direction..... 91
Figure 4.3.16 Graphical comparison of displacements in y direction..... 93
Figure 4.3.17 σx distribution obtained by Patran/Nastran..... 95
Figure 4.3.18 Graphical comparison of σ_x results 95
Figure 4.3.19 σ_y distribution obtained by Patran/Nastran 97
Figure 4.3.20 Graphical comparison of σ_y results 97
Figure 4.3.21 σ_{xy} distribution obtained by Patran/Nastran 99
Figure 4.3.22 Graphical comparison of σ_{xy} results 99
Figure 4.3.23 Graphical comparison of displacements in x direction..... 101
Figure 4.3.24 Graphical comparison of displacements in y direction..... 102
Figure 4.3.25 σ_x distribution obtained by Patran/Nastran 104
Figure 4.3.26 Graphical comparison of σ_x results 104
Figure 4.3.27 σ_y distribution obtained by Patran/Nastran 106
Figure 4.3.28 Graphical comparison of σ_y results 106
Figure 4.3.29 σ_{xy} distribution obtained by Patran/Nastran 108
Figure 4.3.30 Graphical comparison of σ_{xy} results 108
Figure 4.3.31 Graphical comparison of displacements in x direction..... 109
Figure 4.3.32 Graphical comparison of displacements in y direction..... 110
Figure 4.3.33 Graphical comparison of σ_x results 111
Figure A.1 Boundary line between two nodes 119

Figure B.1.1 Sample Input Excel Sheet for the Macro [32] 123
Figure B.1.2 Macro type list view 124
Figure B.1.3 Entity type selection view 124
Figure B.1.4 A multi-sections surface created by extracting the points from an excel sheet [32] 125
Figure B.2.1 Integration Points view in a CATPart 127
Figure B.2.2 Connected Lines (background meshes) view in a CATPart 127
Figure B.2.3 Connected Lines and Integration Points together view in a CATPart 128
Figure B.2.4 Surface created by the connected lines view in a CATPart 128

LIST OF SYMBOLS

σ	Normal stress
τ_{xy}	Shear stress
D	Material property matrix
ν	Poisson's ratio
ε	Normal strain
γ_{xy}	Shear strain
d_i	Distance of the i^{th} node from its integration point
x_i, y_i	Coordinate of i^{th} node
ρ_{IP}	Radius of an influence domain
w_i	Nodal weight for i^{th} node
u, v	Nodal displacement parameters in x and y directions
J_u	Error function for u
U, V	Displacements in x and y directions
Φ	Shape function matrix
B_i	Strain matrix for i^{th} node
π	Strain energy
K_{ij}	Nodal stiffness matrix
K	Total stiffness matrix
f_i	Nodal force vector for i^{th} node
F	Total force vector
Δ	Displacement matrix

CHAPTER 1

INTRODUCTION

1.1. Mesh Free Methods

Computer-aided design (CAD) tools are necessary in modeling and investigation of physical phenomena in complex engineering systems. Designing such systems necessitates either solving complex partial differential equations or discretizing the domain and using approximate methods.

The most well-known approximation methods are the finite element method (FEM) and the finite difference method (FDM). FEM requires the discretization of the domain by a finite mesh. After meshing the problem domain in a decisive manner and using the proper principle, complex partial differential equations are estimated by a set of algebraic equations. Then, by assembling the element equations, the system of algebraic equations for the problem domain can be obtained.

Meanwhile, the mesh free method (or meshless method), forms a system of algebraic equations for the problem domain without requiring a predefined mesh. Instead, mesh free methods represent the problem domain and the boundaries with sets of scattered nodes in the domain and on the boundaries. These sets of scattered nodes do not form meshes unlike the other numerical methods. That removes the obligation of having a relationship between the nodes, at least for field variable interpolation. Mesh free method is a new numerical analysis method. It has excellent accuracy and rapid convergence [1].

1.2. The Advantages of the Mesh Free Methods

The finite element method is widely used in many fields of science to perform linear or nonlinear, static or dynamic stress analysis for solids, structures or fluid flows. In a structural simulation, the FEM enables to visualize stiffness and strength of the structure parts. Although, currently, several modern and commercial FEM packages allow detailed visualization of where structures bend or twist, and indicate the distribution of stresses and displacements, the following limitations of FEM appear to be obvious [2].

The very beginning step in FEM packages is to mesh the problem domain. This process is very expensive since the analyst spends most of his/her time with the generation of the mesh and that gives it the major share within the cost of a simulation project. In order to decrease the cost, the aim should be to use more computer power than the manpower, but this is not the way in FEM packages. Thus, ideally the computer would accomplish the meshing without a man contribution.

The FEM packages produce discontinuous and less accurate stress values. In the problems having large deformations, the results are less accurate due to element distortions. Another disadvantage of FEM packages is the dependence on continuum mechanics. That is, the elements formed cannot be split or broken which disables the simulation of the fracture of material into a number of pieces. Therefore, the elements should be in one piece or totally extinguished. Otherwise, it can cause significant errors since the problem is essentially nonlinear and consequently the results are path dependent.

To avoid errors from that type of problems, instead of splitting the elements, re-meshing of the problem domain is introduced. In re-meshing, the problem domain is re-meshed to prevent the distortion of the elements and make the nodal lines coincident. Thus, the meshes would be fine and smooth. Re-mesh can be performed by manpower or a mesh generation processor can be used. However, both solutions

have considerable handicaps. Manpower is expensive and less accurate; meanwhile, the mesh generation processors should be powerful, advanced and adaptive. Furthermore, the cost of re-meshing is very high for large 3D problems.

1.3. Scope of the Study

The main objective of this study is to implement a mesh free method, which is called Element-Free Galerkin method, makes approximation based on nodes, not elements. In each plane stress problem solved, the capability and accuracy of the method is compared with analytical and FEM results. For this purpose, the parameters of the EFG are changed and the optimal parameters for the method are determined for each problem type.

The thesis covers the following chapters and their ingredients:

Chapter 2 presents the work done on the topic of the thesis. In chapter 3, the construction of the EFG mesh free program and its steps are explained. In chapter 4, the methodology of the mesh free program is given and several problems are studied. Moreover, the comparisons of different solution techniques are performed. Finally, in chapter 5, conclusion and discussion of the work done are presented.

CHAPTER 2

REVIEW OF LITERATURE

Mesh free methods emerged about thirty years ago. Its emergence can be traced back to the work by Lucy in 1977 on “Smoothed Particle Hydrodynamics (SPH) Method” [3]. Originally, SPH Method is a computational method used for the simulation of fluid flows. After, it has been used in several fields, including astrophysics, ballistics, volcanology and oceanology. SPH method is a mesh free Lagrangian method where the coordinates move with fluid. In the smoothed-particle hydrodynamics (SPH) method, fluid is divided into a number of separate elements called as particles and the distance between them known as “smoothing length”. The kernel function “smoothed” the particles over the distance which means the summation of the related properties of all the particles in the kernel range gives the physical quantity of each particle.

Lucy used mesh free method for modeling astrophysical phenomena without boundaries such as exploding stars and dust clouds. After Lucy’s work, in 1982, Monaghan introduced the “Kernel Estimate” method to carry SPH method to more rational basis [4]. However, Kernel estimation method suffers from less accuracy and the method needs to be improved by further research. Nowadays, it can be said, these methods have improved significantly.

SPH method displays tensile instability. This tension instability is solved by Reproducing Kernel Particle Method (RKPM) under the scope of Lagrangian Kernel.

In 1995 Swengle, Hicks and Attaway and in 1994 Dyka have had substantial contribution in the study of SPH method instabilities [5-6].

In 1995, Liu, Jun and Zhang have presented a correction function for Kernels while in 1996 Johnson and Biessel have presented a method to upgrade strain calculations [7-8]. Other notable modifications or corrections of the SPH method include the correction by Belytschko et al. in 1996 [9] and the integration Kernel correction by Bonet and Kulasegaram in 2000 [10].

In 1992, Moving Least Square approximation is used in a mesh free method (Galerkin Method) which is pioneered by B. Nayroles, G. Touzot and P. Villon for solving partial differential equations [11]. And they named that method as the Diffuse Element Method (DEM). DEM is advantageous over finite element methods in respect of not relying on a grid and being more precise in the calculation of the derivations of the reconstructed functions.

After them, in 1994, the method has been modified and refined by T. Belytschko, Y. Y. Lu and L. Gu and called as Element Free Galerkin (EFG) method [12]. In this method, they used the moving least-squares interpolants to construct the trial and test functions for the variational principle (weak form) and weight functions. In contradistinction to DEM, they introduced certain key differences in the implementation to improve the accuracy. Also in their paper, they illustrated these modifications with the examples where no volumetric locking occurs and the rate of convergence highly exceeded that of finite elements.

It is evident that this type of methods has considerable advantages such as consistency and stability, yet SPH method is still cheaper. Moreover, these methods have improvements toward the moving least squares and partition of unity. Since the standard, SPH method has a problem of getting accurate interpolation for the particles scattered arbitrarily, many developments were made to improve the completeness of the SPH method. One of the most important ones is the normalization approximation introduced by Johnson and Beissel in 1996 [8], the

other is the moving least squares (MLS) approximation first implicitly used by Nayroles [11] and then classified by Belytschko et al. Two approaches have been proposed to construct EFG shape functions; one is the moving least squares approximation and the other is partition of unity approximation.

MLS is a method of reconstructing continuous functions from a set of scattered nodes. The reconstructed value is calculated for a node around which a region is defined. A weighted least squares measure tended to that region. Although MLS approximation has pioneered to the development of many mesh free methods, the shape functions generated by this method do not have the Kronecker delta function property.

Instead, in 1999, a new method called the point interpolation method (PIM) was developed by G. R. Liu and Gu to construct shape functions [13]. In contrast to MLS method, this new method contains shape function which possesses Kronecker delta property.

As mentioned before, there is another method for the construction of shape functions; the partition of unity method. The generalized finite element method (GFEM) was introduced separately by Babuska et al. and by Duarte and Oden [14]. They called the method with different names; Babuska et al. called it as finite element partition of unity method and they published several articles while Duarte and Oden used the names of hp clouds or cloud-based hp finite element method [15]. The main common characteristic of these methods is the usage of a partition of unity. They described PoU as a set of functions values of which sum to the unity at each node in a domain. Using partition of unity in the construction of the shape functions prevent from numerical integration problems related to the usage of moving least squares. Furthermore, it is claimed that the use of a finite element partition of unity helps to implement the essential boundary conditions. However, presently, the moving least squares (MLS) approximation is the most popular method for generating the mesh free shape functions since it is much cheaper than the partition of unity method in integration of the stiffness matrix.

In 1999, another mesh free method has been introduced to this area, called the Renormalized Meshless Derivative (RMD) by Vila [16]. It is aimed to obtain accurate approximation of derivatives under the scope of collocation approaches via this new mesh free method.

Another success is achieved in 1998 by Bouillard and Suleau. They have succeeded in introducing a mesh free formulation to acoustic problems [17].

Meanwhile in 1999, J. Bonet and S. L. Lok published a paper which presented a new variational framework for various existing Smooth Particle Hydrodynamic (SPH) techniques and a new corrected SPH formulation [18]. They claim that to preserve angular momentum, the gradient of a linear velocity field must be calculated correctly with the SPH equations. They presented a corrected algorithm which is a combination of Kernel correction and gradient correction and they illustrated the theory with several examples related to fluid dynamics.

In 2000, J. Bonet has published another paper with S. Kulasegaram this time about 'Correction and stabilization of smooth particle hydrodynamics with application in metal forming' [10]. In the paper the SPH with the corrected kernel is referred to as corrected smooth particle hydrodynamics (CSPH). They claimed that the instability of the SPH method is based on under integration of the weak form, and they got the stability by a least-squares stabilization procedure. Further, they illustrated the improvement in SPH method in stability and accuracy aspects. They also used CSPH method to metal forming simulations and they proved the effectiveness of the method by numerical examples.

In 2001, E. O~nate, C. Sacco, and S. Idelsohn introduced a stabilized Finite Point Method (FPM), where the stabilization is based in Finite Calculus (FIC), for the mesh free analysis of incompressible fluid flow problems [19]. In the paper, it is proved to have semi-implicit numerical solution for incompressible fluids using this method with several examples.

In contrast to SPH or some element-free methods, the Meshless Local Petrov-Galerkin (MLPG) method is truly meshless method. This approach developed by Atluri and his colleagues in 1998 [20], is based on writing the local weak form of partial differential equations over overlapping local sub-domains and within these local sub-domains the integration of the weak form is also performed. This makes the method independent from any need of any kind of meshes or background cells. The MLPG method has been used in several problems in different areas such as, fracture mechanics by Atluri, Kim and Cho in 1999 [21-22] and fluid mechanics by Lin and Atluri in 2001 [23] etc.

One of the latest improvements in mesh free methods is the Space-time Meshless Collocation Method (STMCM) which is introduced by Hennadiy Netuzhylov and Andreas Zilian in 2009 [24]. The STMCM is developed with the help of Interpolating Moving Least Squares technique. Thus, it is possible to have simplified implementation of boundary conditions because the kernel function enables the fulfillment of the Kronecker delta property. In their paper, Netuzhylov and Zilian have solved numerous examples to verify this method in different problems such as interpolation problems or PDEs.

In 2008, Wenjing Zhang, Maohui Xia and Lechun Liu have published an article about a new mesh free method which is the point interpolation method based on radial basis function or RPIM [1]. They asserted that this method has not only all the advantages of mesh free methods but also the Kronecker delta function property. The main difference of this new method is to have shape function constructed by the combination of both radial and polynomial basis functions and this makes the implementation of the boundary conditions functional as the traditional finite element methods. The article also has solution for a two-dimensional static elastic problem with success.

Moreover, recently several authors have proposed to use mixed interpolations which is a combination of finite elements and mesh free methods, in order to gain the advantages of both methods.

CHAPTER 3

THE ELEMENT-FREE GALERKIN METHOD

The Element-free Galerkin (EFG) method is one of the mesh free methods which has been developed by Belytschko et al. [12]. In EFG, the moving least squares (MLS) approximation is used for construction of the shape functions and the Galerkin weak form is used to develop the discretized system equations. A background mesh is required. EFG is confirming since MLS shape functions are consistent and compatible and the constrained Galerkin approach is used to impose the essential boundary conditions.

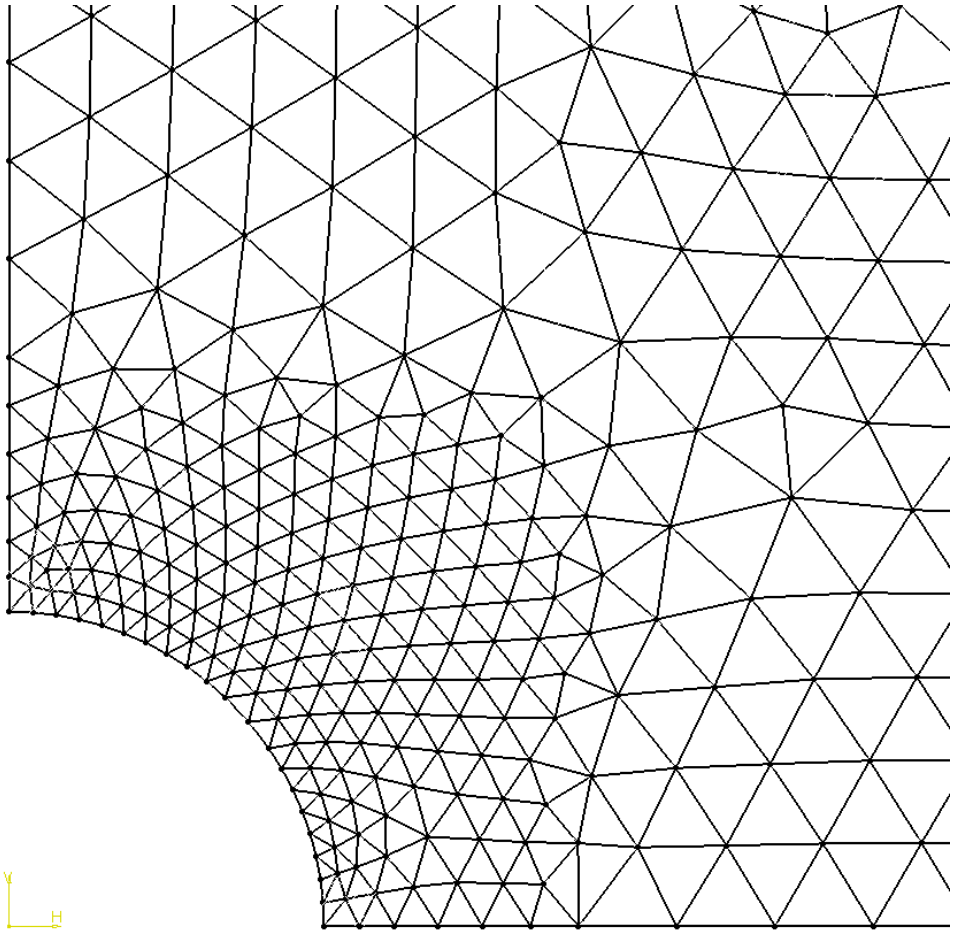

Figure 3.1 The background mesh of a problem domain

In EFG method, it is common to use high order polynomials for shape functions but even linear polynomial based functions give quite accurate results for the curved boundaries which are represented by nodes. EFG shape functions can interpolate the two nodes at any location on the boundary since the shape functions are formed by nodes in a moving local domain. Actually, there are numerous ways to perform geometric interpolation to simplify the geometry by varied software in the computer. Moreover, it is very essential to simplify the model mathematically.

3.1. Node Generation

The problem domain is represented by a set of scattered nodes, as schematically illustrated in Figure 3.1.1.

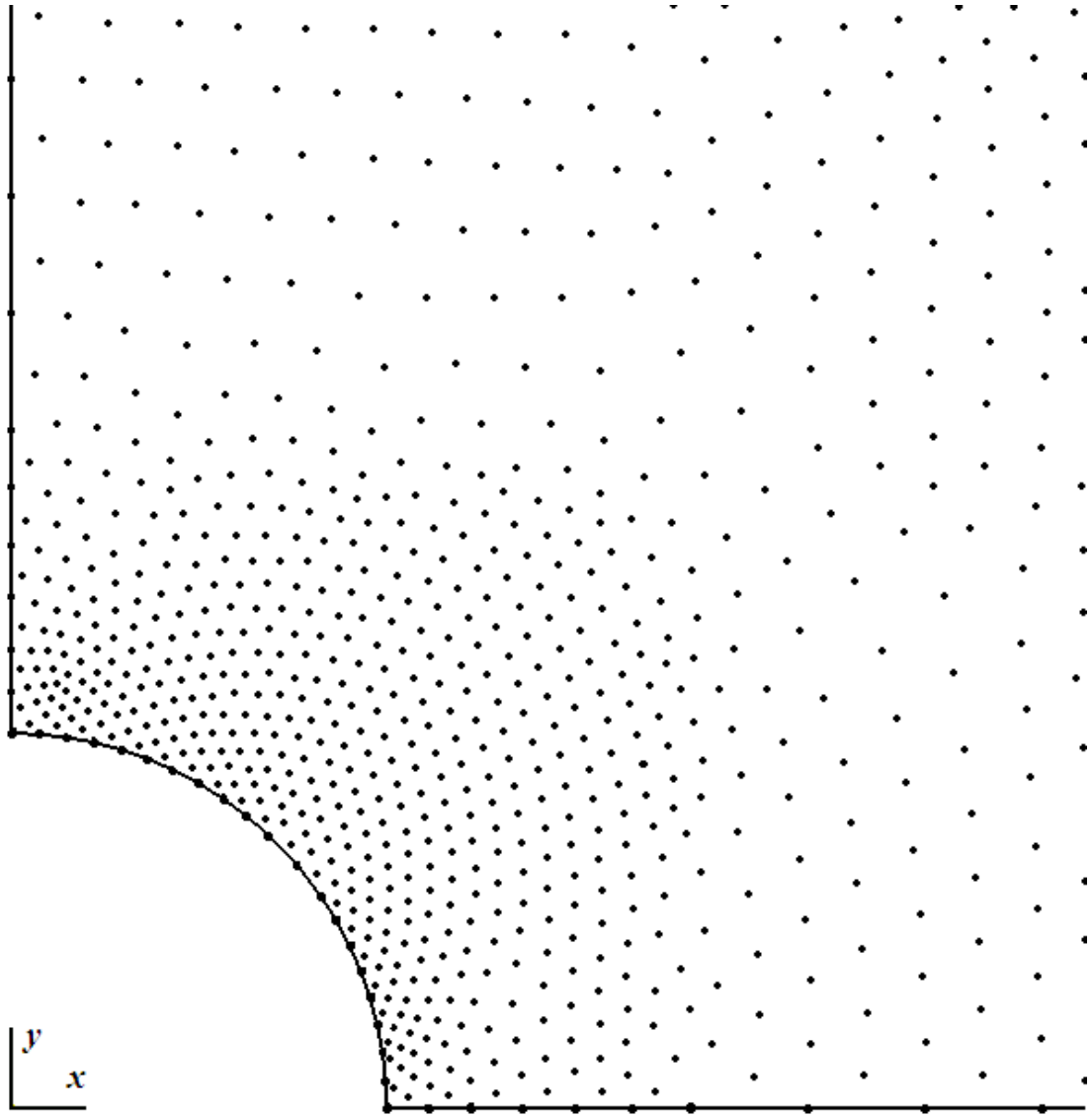

Figure 3.1.1 Nodes in a problem domain

One of the advantages of using a mesh free method is that it does not require meshes or elements. There is no need to use meshes or elements for field variable interpolation. Instead, the nodes are scattered in the problem domain. Moreover, the node generation can be fully automated without any human intervention. This

automated programs based on triangulation (since the most convenient mesh to use is a mesh of triangular cells) algorithm (e.g. Delaunay triangulation [25]) are very simple, easy to find and available for both 2D and 3D domains. For an analyst, using such algorithms really reduces the time of an analysis process.

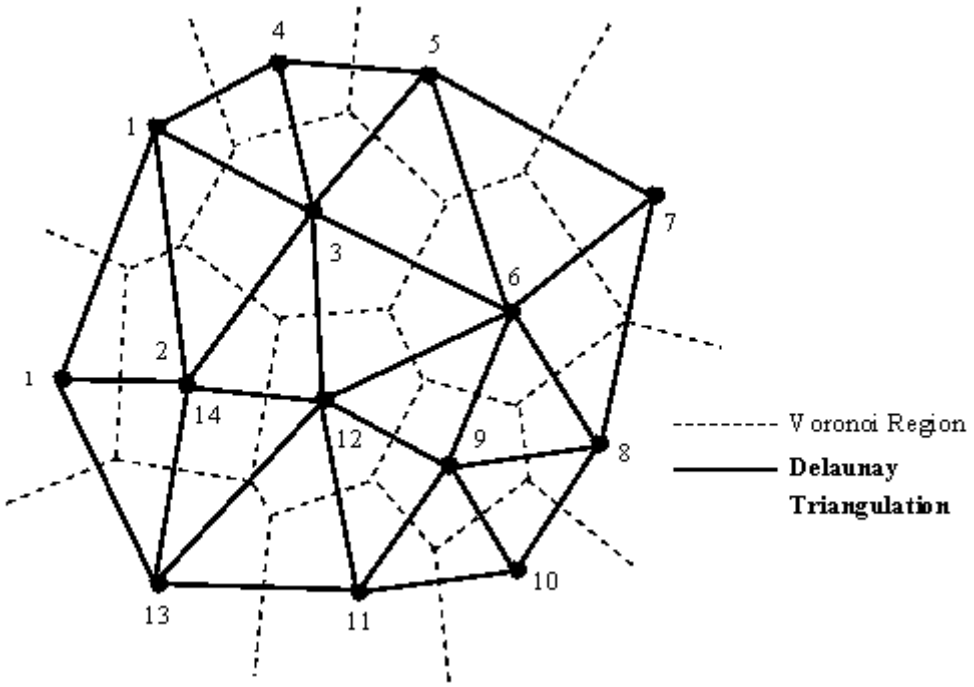

Figure 3.1.2 Delaunay triangulation

For some mesh free methods such as the element free Galerkin methods (EFG), a background mesh is need to be used in integration of the system matrices. However, the shape of the background mesh is not strict, provided that accuracy in the integrations is adequate.

In this study, MSC.Patran/Nastran software program is used to have background meshes for generating the nodes. Figure 3.1 presents a sample background mesh that can be used for an analysis.

Figure 3.1.3 shows both background mesh and nodes added to it. The nodes are created at the center and the three vertices of the triangular element.

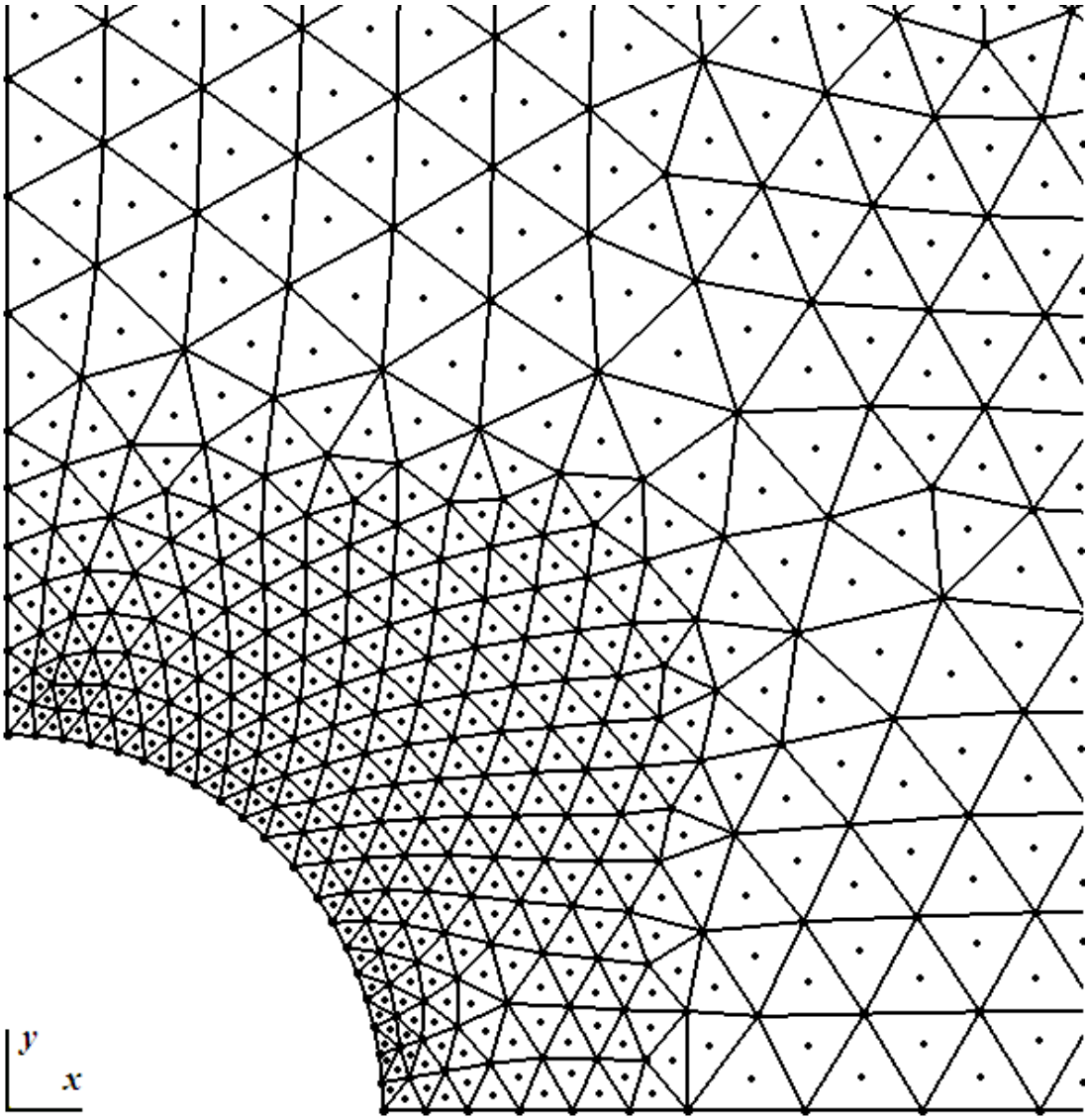

Figure 3.1.3 Node distribution on a background mesh

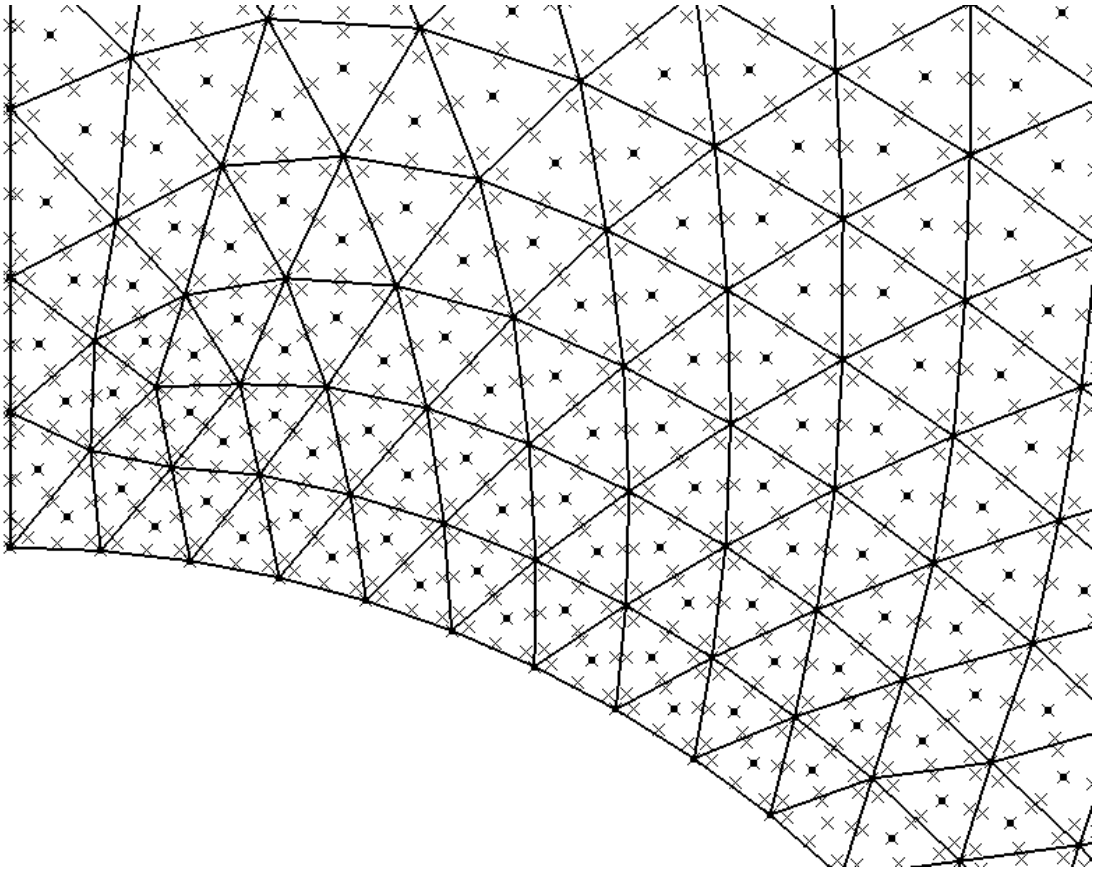

Figure 3.1.4 Node and integration point distribution on a background mesh

3.2. Shape Functions

The construction of the shape function has been the main and the most important issue for the mesh free methods while in the finite element analysis methods the shape functions are based on elements thus can be computed directly and satisfy the Kronecker delta function property.

First of all, in mesh free methods, a shape function must satisfy a condition called “partition of unity”. This condition is required in a shape function in order to be able to make any rigid motion of the problem domain. Secondly, there are other conditions that a shape function can satisfy preferably such as “linear field reproduction” or “Kronecker delta function property”. Linear field reproduction condition is required for a shape function to pass the standard patch test. The patch test often used in testing finite elements, is a simple indicator of the quality of a finite

element, developed by Bruce Irons [26-27]. If the finite element solution is same as the exact solution, it can be said that the elements pass the patch test. Passing the patch test is not compulsory for a mesh free shape function because a shape function which does not pass this test can still be used if it provides a converged solution. Nevertheless, many finite elements methods cannot pass the patch test yet they are used in finite element packages. Next, the Kronoker delta function condition is also preferable for mesh free methods shape functions since this condition simplifies to put the boundary conditions into effect.

In mesh free methods, the shape functions are based on arbitrarily distributed nodes in a domain without any relation between them. This makes it harder to construct the shape function. One of the tough issues in the area of mesh free methods is to generate more effective methods for creating the shape functions. For this purpose, a method should satisfy some basic requirements;

- Arbitrary nodal distribution: the nodes are flexible to be distributed without a relation between them.
- Stability: the algorithm must be stable. The algorithm that can be proven not to magnify approximation errors is called numerically stable algorithm. In mesh free methods, this errors or uncertainties can be due to the arbitrarily distributed nodes. Thus, the stability of the algorithm should be checked.
- Consistency: a certain order of consistency should be satisfied since it is fundamental for the convergence of the results when the spaces between nodes are decreased. Consistency can be described as the capability of the method to reproduce the lowest order fields of the complete polynomials at any node in the problem domain. Namely, a method reproduces polynomial up to n^{th} order, then the method can be said to have nth order consistency.
- Efficiency: the efficiency of the algorithm should be in the same order of complexity with of FEM.

- Compact support: the field variable interpolation domain (termed the support domain or influence domain (ID)) should be small compared to whole problem domain in order to avoid irredeemable cost of the procedure causing from expensive construction of the shape function.
- Delta function property: the shape function preferably should satisfy the Kronecker delta function. This requirement also saves money for the program since it facilitates to impose the boundary conditions.
- Compatibility: again, it is preferable to be compatible for the field approximation all around the problem domain. A compatible shape function requires that the approximation is continuous on the boundaries between sub-domains. Both consistency and compatibility affect the accuracy and convergence of the numerical results.

If a shape function of a mesh free method possesses all the characteristics above, the method would have very accurate results. In order to have a good shape function, there are different ways of generating the function as introduced in the literature so far; smoothed particle hydrodynamics (SPH) method, reproducing kernel particle method (RKPM), general kernel reproduction (GKR) method, moving least squares (MLS) methods, point interpolation methods (polynomial or radial) (PIM), partition of unity methods (PoUFE or hp-clouds) etc..

If the mostly used functions, which are MLS, PIM and SPH, are compared; MLS shape functions are both consistent and compatible while the PIM shape functions are only consistent but not compatible. On the contrary, the SPH shape functions are compatible but not consistent.

3.3. Formulation

Consider a plane stress problem where,

$$D = \frac{E}{(1-\nu^2)}\begin{bmatrix} 1 & \nu & 0 \\ \nu & 1 & 0 \\ 0 & 0 & \frac{1-\nu}{2} \end{bmatrix} \quad (3.1)$$

$$\varepsilon = \begin{bmatrix} \varepsilon_x \\ \varepsilon_y \\ \gamma_{xy} \end{bmatrix} \quad (3.2)$$

$$\sigma = \begin{bmatrix} \sigma_x \\ \sigma_y \\ \sigma_{xy} \end{bmatrix} \quad (3.3)$$

$$\sigma = D\varepsilon \quad (3.4)$$

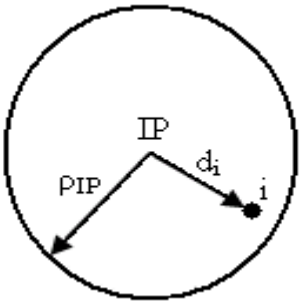

Figure 3.3.1 Representation of an Influence Domain (ID)

Let there be M_{IP} integration points (IP) and M nodes in the domain. Note that ($M_{IP} \geq$ 3 or 4M) must be satisfied. Each IP has an influence domain of radius ρ_{IP}. Consider an IP at point (x, y). Let there be N nodes in the influence domain of this IP. Let the distance of the i^{th} node from IP is d_i. The weight function and its derivatives are defined as follow:

$$d_i = \sqrt{(x_i - x)^2 + (y_i - y)^2} \quad (3.5)$$

$$s_i = \frac{d_i}{\rho_{IP}} \quad (3.6)$$

$$w_i = 1 - 6{s_i}^2 + 8{s_i}^3 - 3{s_i}^4 \quad (3.7)$$

$$\frac{\partial w_i}{\partial x} = \frac{12}{\rho_{IP}}(s_i - 2{s_i}^2 + {s_i}^3)(x_i - x) \quad (3.8)$$

$$\frac{\partial w_i}{\partial y} = \frac{12}{\rho_{IP}}(s_i - 2{s_i}^2 + {s_i}^3)(y_i - y) \quad (3.9)$$

Assume displacement as,

$$u = [1 \quad x \quad y \quad \cdots] \begin{bmatrix} \alpha_{u1} \\ \alpha_{u2} \\ \alpha_{u3} \\ \vdots \end{bmatrix} \quad (3.10)$$

$$u = p\alpha_u \quad (3.11)$$

$$v = [1 \quad x \quad y \quad \cdots] \begin{bmatrix} \alpha_{v1} \\ \alpha_{v2} \\ \alpha_{v3} \\ \vdots \end{bmatrix} \quad (3.12)$$

$$v = p\alpha_v \quad (3.13)$$

Define the error function for u as,

$$J_u = \sum_i^N w_i(p_i\alpha_i - u_i)^2 \quad (3.14)$$

$$\frac{\partial J_u}{\partial \alpha_u} = 0 \quad (3.15)$$

$$\sum_i^N w_i {p_i}^T(p_i\alpha_u - u_i) = 0 \quad (3.16)$$

This gives $A\alpha_u = RU$ where, *(3.17)*

$$A = \sum_i^N w_i \, p_i{}^T p_i \qquad (3.18)$$

$$R = [w_1 p_1{}^T \quad w_2 p_2{}^T \quad \cdots \quad w_N p_N{}^T] \qquad (3.19)$$

$$U = [u_1 \quad u_2 \quad \cdots \quad u_N] \qquad (3.20)$$

Then,

$$\alpha_u = A^{-1} R U \qquad (3.21)$$

Define,

$$C = A^{-1} R \qquad (3.22)$$

Then,

$$u = pCU \qquad (3.23)$$

Let,

$$\Phi = pC \qquad (3.24)$$

Then,

$$u = \Phi U = [\phi_1 \quad \phi_2 \quad \cdots \quad \phi_N] \begin{bmatrix} u_1 \\ u_2 \\ \vdots \\ u_N \end{bmatrix} \qquad (3.25)$$

where u_1 is the nodal displacement parameter vector in u direction at node 1.

Similarly,

$$v = pCV \tag{3.26}$$

And

$$v = \Phi V = [\phi_1 \quad \phi_2 \quad \dots \quad \phi_N] \begin{bmatrix} v_1 \\ v_2 \\ \vdots \\ v_N \end{bmatrix} \tag{3.27}$$

Then,

$$\delta = \begin{bmatrix} u \\ v \end{bmatrix} = \begin{bmatrix} \phi_1 & 0 \\ 0 & \phi_1 \end{bmatrix} \begin{bmatrix} u_1 \\ v_1 \end{bmatrix} + \begin{bmatrix} \phi_1 & 0 \\ 0 & \phi_1 \end{bmatrix} \begin{bmatrix} u_1 \\ v_1 \end{bmatrix} + \cdots + \begin{bmatrix} \phi_N & 0 \\ 0 & \phi_N \end{bmatrix} \begin{bmatrix} u_N \\ v_N \end{bmatrix} \tag{3.28}$$

Let,

$$\psi_i = \begin{bmatrix} \phi_i & 0 \\ 0 & \phi_i \end{bmatrix} \tag{3.29}$$

And

$$\delta_i = \begin{bmatrix} u_i \\ v_i \end{bmatrix} \tag{3.30}$$

Then,

$$\delta = \sum_i^N \psi_i \delta_i \tag{3.31}$$

$$\varepsilon = \begin{bmatrix} \varepsilon_x \\ \varepsilon_y \\ \gamma_{xy} \end{bmatrix} = \begin{bmatrix} \partial/\partial x & 0 \\ 0 & \partial/\partial y \\ \partial/\partial y & \partial/\partial x \end{bmatrix} \delta = \sum_i^N \begin{bmatrix} \partial\phi_i/\partial x & 0 \\ 0 & \partial\phi_i/\partial y \\ \partial\phi_i/\partial y & \partial\phi_i/\partial x \end{bmatrix} \delta_i \tag{3.32}$$

Let,

$$B_i = \begin{bmatrix} \partial\phi_i/\partial x & 0 \\ 0 & \partial\phi_i/\partial y \\ \partial\phi_i/\partial y & \partial\phi_i/\partial x \end{bmatrix} \quad (3.33)$$

Then,

$$\varepsilon = \sum_i^N B_i \delta_i \quad (3.34)$$

Note that,

$$\frac{\partial \Phi}{\partial x} = \begin{bmatrix} \frac{\partial \phi_1}{\partial x} & \frac{\partial \phi_2}{\partial x} & \dots & \frac{\partial \phi_N}{\partial x} \end{bmatrix} \quad (3.35)$$

$$\frac{\partial \Phi}{\partial y} = \begin{bmatrix} \frac{\partial \phi_1}{\partial y} & \frac{\partial \phi_2}{\partial y} & \dots & \frac{\partial \phi_N}{\partial y} \end{bmatrix} \quad (3.36)$$

where,

$$\frac{\partial \Phi}{\partial x} = \frac{\partial p}{\partial x} C + p \frac{\partial C}{\partial x} \quad (3.37)$$

$$\frac{\partial \Phi}{\partial y} = \frac{\partial p}{\partial y} C + p \frac{\partial C}{\partial y} \quad (3.38)$$

$$\frac{\partial p}{\partial y} = [0 \quad 1 \quad 0 \quad \dots] \quad (3.39)$$

$$\frac{\partial p}{\partial x} = [0 \quad 0 \quad 1 \quad \dots] \quad (3.40)$$

$$\frac{\partial C}{\partial x} = A^{-1}\left(\frac{\partial R}{\partial x} - \frac{\partial A}{\partial x} C\right) \quad (3.41)$$

$$\frac{\partial C}{\partial y} = A^{-1}\left(\frac{\partial R}{\partial y} - \frac{\partial A}{\partial y} C\right) \quad (3.42)$$

$$\frac{\partial A}{\partial x} = \sum_i^N \frac{\partial w_i}{\partial x} {p_i}^T p_i \qquad (3.43)$$

$$\frac{\partial A}{\partial y} = \sum_i^N \frac{\partial w_i}{\partial y} {p_i}^T p_i \qquad (3.44)$$

$$\frac{\partial R}{\partial x} = \left[\frac{\partial w_1}{\partial x} {p_1}^T \quad \frac{\partial w_2}{\partial x} {p_2}^T \quad \dots \quad \frac{\partial w_N}{\partial x} {p_N}^T\right] \qquad (3.45)$$

$$\frac{\partial R}{\partial y} = \left[\frac{\partial w_1}{\partial y} {p_1}^T \quad \frac{\partial w_2}{\partial y} {p_2}^T \quad \dots \quad \frac{\partial w_N}{\partial y} {p_N}^T\right] \qquad (3.46)$$

Consider the functional strain energy,

$$\pi = \frac{1}{2} \int \varepsilon^T D \, \varepsilon \, d\, V \qquad (3.47)$$

Substituting we get,

$$\pi = \frac{1}{2} \int \left(\sum_i^N B_i \delta_i\right)^T D \left(\sum_j^N B_j \delta_j\right) d\, V \qquad (3.48)$$

Then,

$$\pi = \frac{1}{2} \sum_i^M \sum_j^M {\delta_i}^T \left(\int {B_i}^T D B_j \, dV\right) \delta_j \qquad (3.49)$$

Let define the nodal stiffness matrix K_{ij} as the basic component of assembling the global stiffness matrix of the system.

$$K_{ij} = \int {B_i}^T D B_j \, dV \qquad (3.50)$$

Then,

$$\pi = \frac{1}{2} \sum_i^M \sum_j^M {\delta_i}^T K_{ij} \delta_j \qquad (3.51)$$

$$\frac{\partial \pi}{\partial \delta_i} = 0 \qquad (3.52)$$

$$\sum_i^M \sum_j^M K_{ij}\delta_j = \sum_i^M f_i \qquad (3.53)$$

$$K\Delta = F \qquad (3.54)$$

This gives,

$$\Delta = K^{-1}F \qquad (3.55)$$

This is the displacement parameter vector for the entire body. Then for each IP, the displacement parameter vectors U and V can be extracted from Δ.

Using the expressions $u = pCU$ (Equation 3.23) and $v = pCV$ (Equation 3.26), the displacements of any point can be calculated by considering the nearest IP to that point.

The stresses can be calculated as,

$$\sigma = D\varepsilon \qquad (3.57)$$

CHAPTER 4

NUMERICAL EXAMPLES

In this chapter, EFG method is used for some standard plane stress problems. The results are compared with analytical and FEM results. The parameters in the EFG method are the background mesh density, the number of nodes and the number of Gauss integration points. Generally, the finer background mesh provides the more accurate results. However, the density should be optimized considering CPU time, modeling cost and accuracy. On the other hand, increasing number of Gauss integration points give higher accuracy, but it is important not to have a too coarse background mesh when the number of integration points is very large. In this work, by using different densities of background mesh and different numbers of integration points, the displacement and stress distribution of the problem are found using EFG method and the results are compared with analytical and FEM results.

4.1. Cantilever Beam under Parabolic End Load

A cantilever beam subjected to a parabolic end load is shown in Figure 4.1.1.

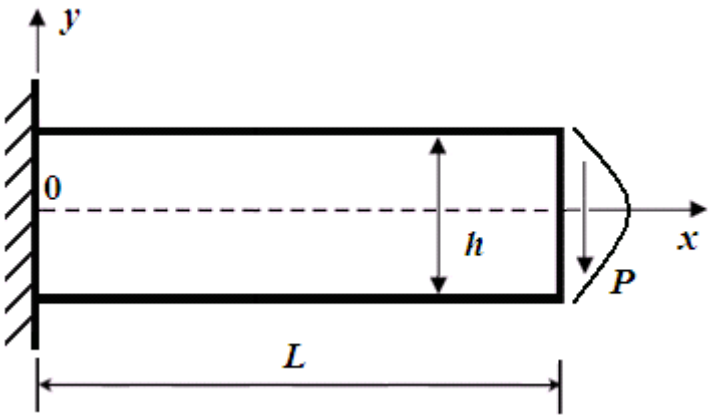

Figure 4.1.1 A cantilever beam subjected to parabolic end loading

The exact solution is given by Timoshenko and Goodier [29]. According to that the displacement in the x direction is,

$$u = -\frac{P}{6EI}\left[(6L - 3x)x + (2 + v)\left[y^2 - \frac{h^2}{4}\right]\right]y \qquad (4.2)$$

where,

$$I = \frac{h^3}{12} \qquad (4.3)$$

The displacement in the y direction is,

$$v = \frac{P}{6EI}\left[(4 + 5v)\frac{h^2 x}{4} + (3L - x)x^2\right] \qquad (4.4)$$

The normal stress on the cross section of the beam is,

$$\sigma_x = -\frac{P(L-x)}{I}y \qquad (4.5)$$

The normal stress in the y direction is,

$$\sigma_y = 0 \qquad (4.6)$$

The shear stress on the cross section of the beam is,

$$\tau_{xy} = \frac{P}{2I}\left[\frac{h^2}{4} - y^2\right] \qquad (4.7)$$

The loading P is distributed in a form of parabola at the right end of the beam:

$$\text{Loading: } P(i) = 1000\left[\frac{y(i)^2 - hy(i)}{288000}\right] \text{ N} \qquad (4.8)$$

In this example, the properties for this cantilever beam are taken as follows:

Young's modulus: $E = 200000$ N/mm^2
Poisson's ratio: $v = 0.3$
Height of the beam: $h = 120mm$
Length of the beam: $L = 480$ mm

For the first run of the example, there are 128 elements in the background mesh. The nodes are defined at the center and vertices of each element and seven Gauss integration points are used for each element. The background mesh, nodes and integration points used in this run are shown in Figure 4.1.2, Figure 4.1.3 and Figure 4.1.4 respectively;

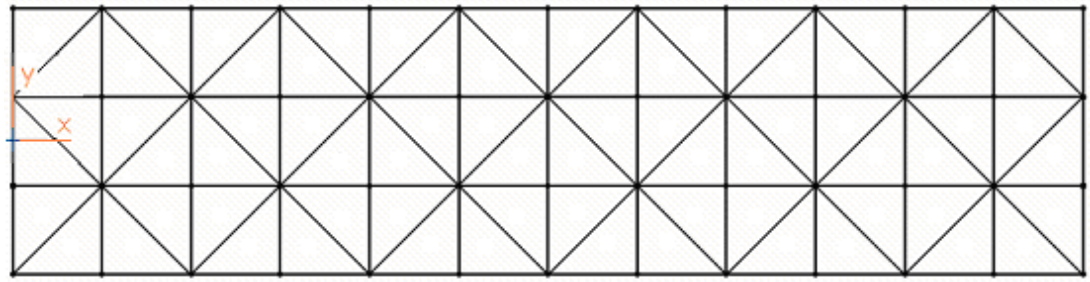

Figure 4.1.2 The background mesh

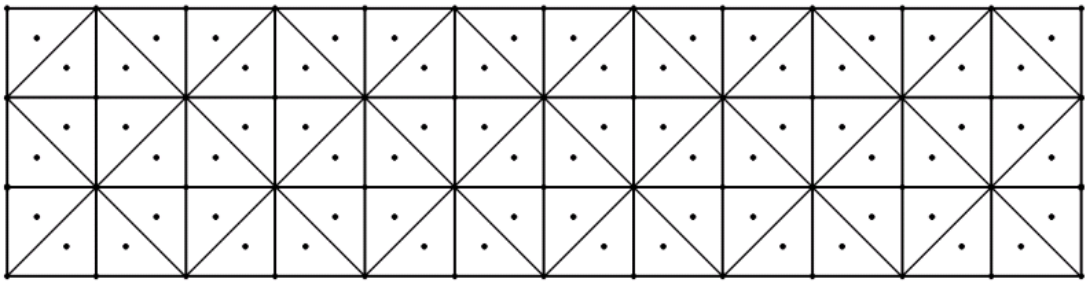

Figure 4.1.3 Node distribution on the background mesh

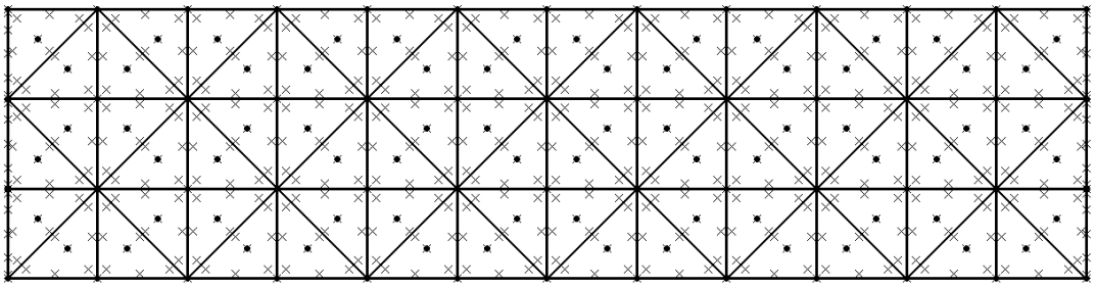

Figure 4.1.4 Node and integration point distribution on the background mesh

Table 4.1.1 and Figure 4.1.5 show the displacement results in x direction calculated by EFG program, finite element method and analytical method;

Table 4.1.1 Comparison of the displacements in x direction

x	y	u Analytic	u EFG	Error %
0	-60	0.000	0.000	0.000
0	-30	0.000	0.000	0.000
0	0	0.000	0.000	0.000
0	30	0.000	0.000	0.000
0	60	0.000	0.000	0.000
240	-60	-0.180	-0.179	0.469
240	-30	-0.089	-0.088	0.873
240	0	0.000	0.000	0.000
240	30	0.089	0.089	0.006
240	60	0.180	0.180	0.074
480	-60	-0.240	-0.239	0.215
480	-30	-0.119	-0.118	0.384
480	0	0.000	0.000	0.000
480	30	0.119	0.119	0.227
480	60	0.240	0.240	0.081

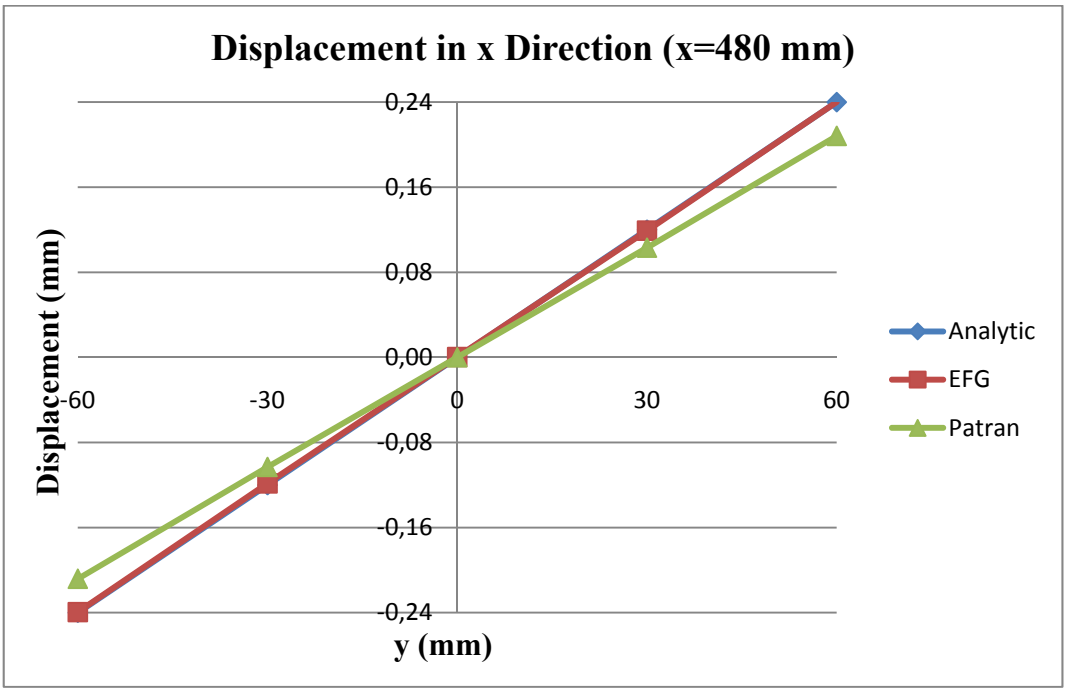

Figure 4.1.5 Graphical comparison of displacements in x direction

Table 4.1.2 and Figure 4.1.6 show the displacement results in y direction calculated by EFG program, finite element method and analytical method;

Table 4.1.2 Comparison of the displacements in y direction

x	y	v Analytic	v EFG	Error %
0	-60	0.000	0.000	0.000
0	-30	0.000	0.000	0.000
0	0	0.000	0.000	0.000
0	30	0.000	0.000	0.000
0	60	0.000	0.000	0.000
240	-60	-0.428	-0.424	0.776
240	-30	-0.428	-0.421	1.631
240	0	-0.428	-0.419	1.891
240	30	-0.428	-0.420	1.639
240	60	-0.428	-0.424	0.776
480	-60	-1.335	-1.326	0.679
480	-30	-1.335	-1.326	0.670
480	0	-1.335	-1.326	0.678
480	30	-1.335	-1.326	0.669
480	60	-1.335	-1.326	0.679

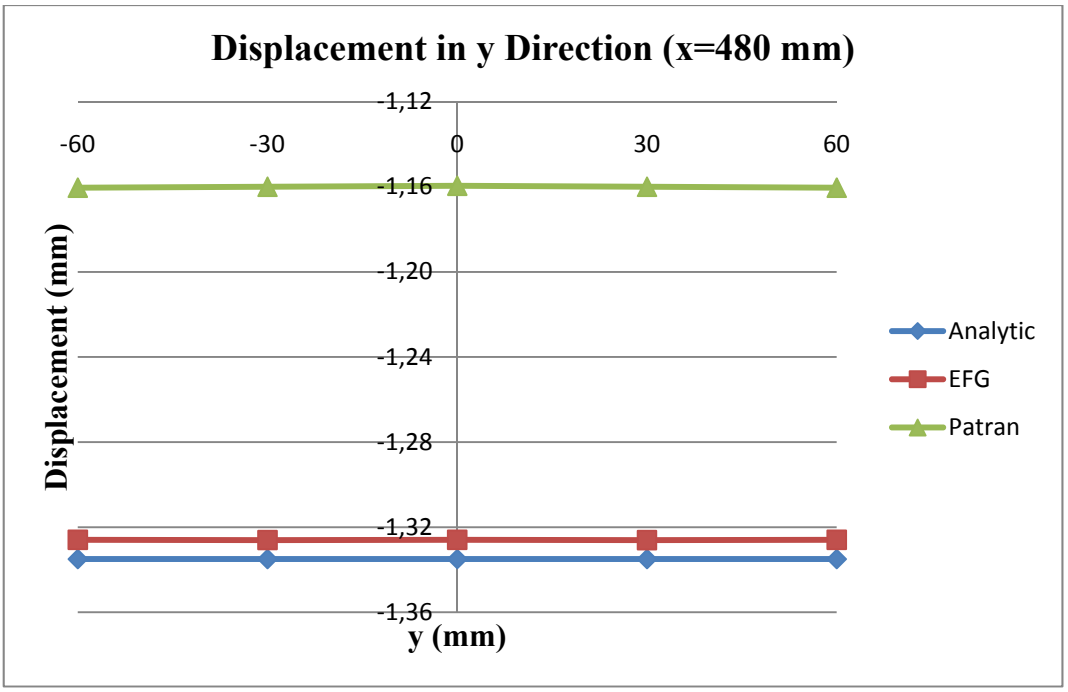

Figure 4.1.6 Graphical comparison of displacements in y direction

Table 4.1.3, Figure 4.1.7 and Figure 4.1.8 show the σ_x results calculated by EFG program, finite element method and analytical method;

Table 4.1.3 Comparison of the σ_x results

x	y	σx Analytic	σx EFG	Error %
0	-60	-200.000	-191.932	4.034
0	-30	-100.000	-95.868	4.132
0	0	0.000	3.078	100.000
0	30	100.000	103.965	3.814
0	60	200.000	203.506	1.723
240	-60	-100.000	-98.581	1.419
240	-30	-50.000	-59.000	15.255
240	0	0.000	-0.487	100.000
240	30	50.000	56.827	12.014
240	60	100.000	98.582	1.418
480	-60	0.000	-0.955	100.000
480	-30	0.000	0.912	100.000
480	0	0.000	0.095	100.000
480	30	0.000	-0.756	100.000
480	60	0.000	0.955	100.000

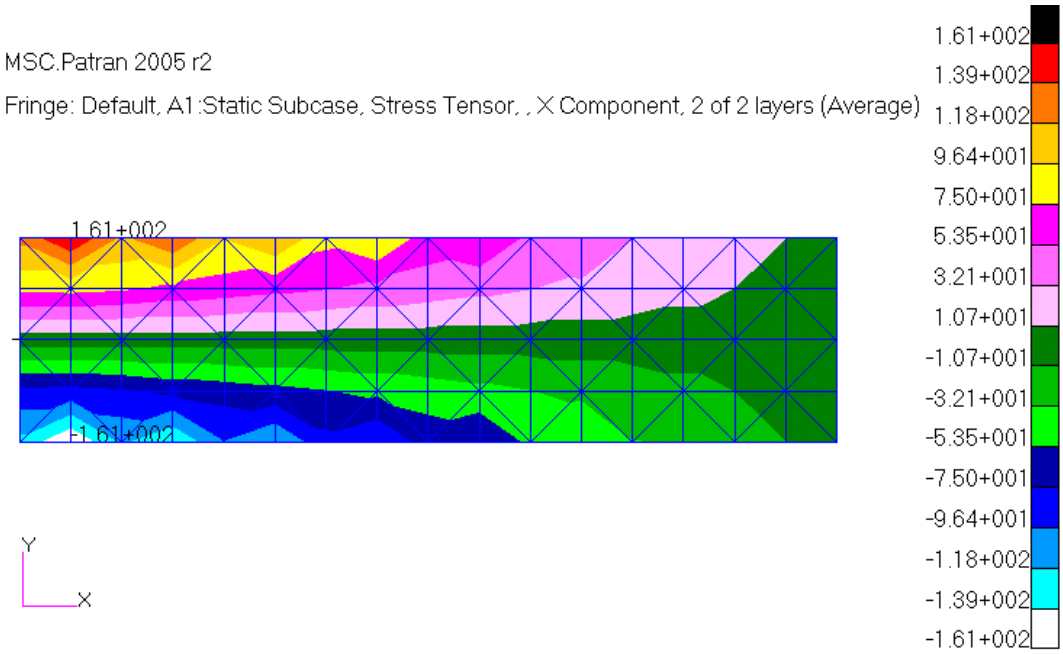

Figure 4.1.7 σ_x distribution obtained by Patran/Nastran

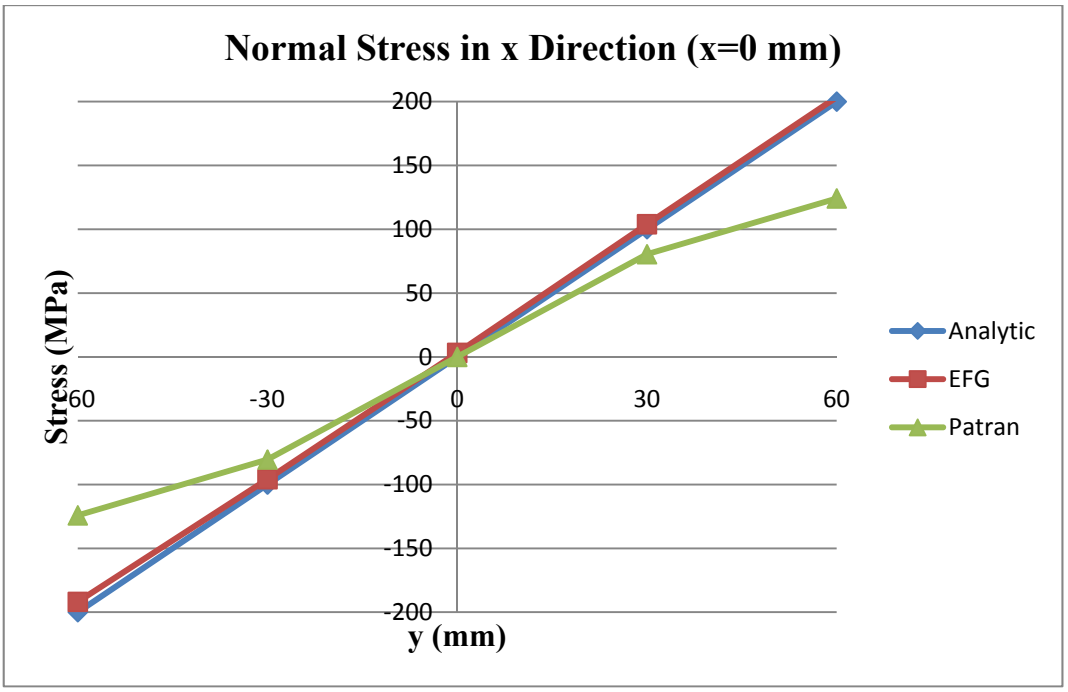

Figure 4.1.8 Graphical comparison of σ_x results

Table 4.1.4, Figure 4.1.9 and Figure 4.1.10 show the σ_{xy} results calculated by EFG program, finite element method and analytical method;

Table 4.1.4 Comparison of the σ_{xy} results

x	y	σxy Analytic	σxy EFG	Error %
0	-60	0.000	-13.420	100.000
0	-30	-9.375	-6.768	27.811
0	0	-12.500	-8.342	33.261
0	30	-9.375	-9.556	1.898
0	60	0.000	-17.095	100.000
240	-60	0.000	0.000	0.000
240	-30	-9.375	-10.203	8.116
240	0	-12.500	-11.677	6.587
240	30	-9.375	-10.352	9.438
240	60	0.000	0.000	0.000
480	-60	0.000	-0.717	100.000
480	-30	-9.375	-10.487	10.604
480	0	-12.500	-12.434	0.530
480	30	-9.375	-10.691	12.313
480	60	0.000	-0.716	100.000

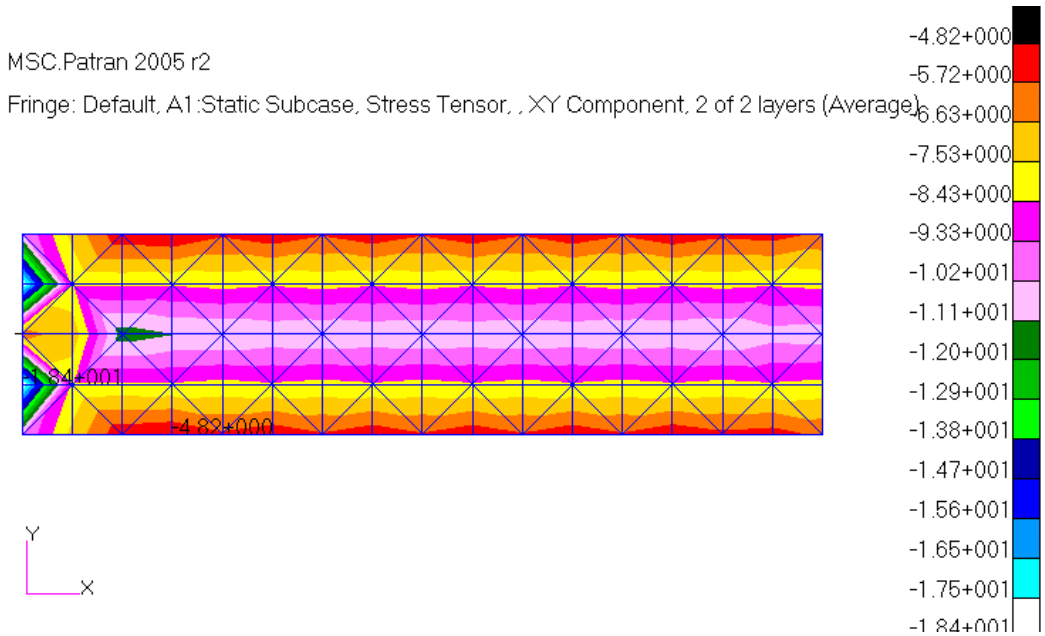

Figure 4.1.9 σ_{xy} distribution obtained by Patran/Nastran

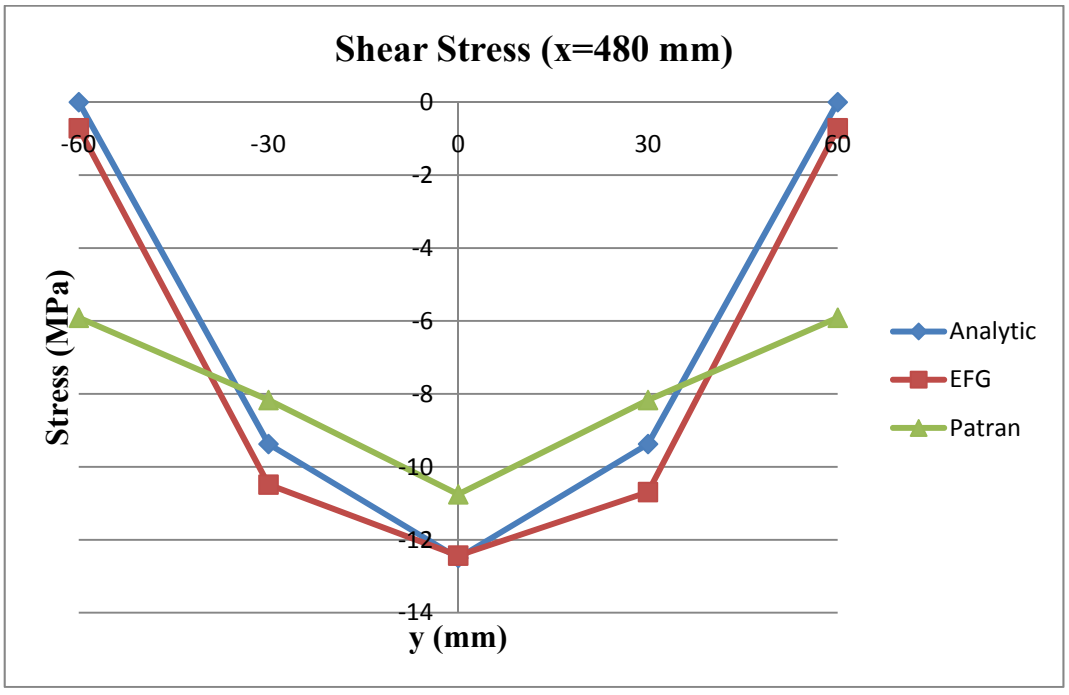

Figure 4.1.10 Graphical comparison of σ_{xy} results

For the second run, the same problem is modeled by a more refined background mesh which has 200 elements. The nodes are defined at the center and vertices of each element and seven Gauss integration points are used for each element. The

background mesh, nodes and integration points used in this run are shown in Figure 4.1.11, Figure 4.1.12 and Figure 4.1.13;

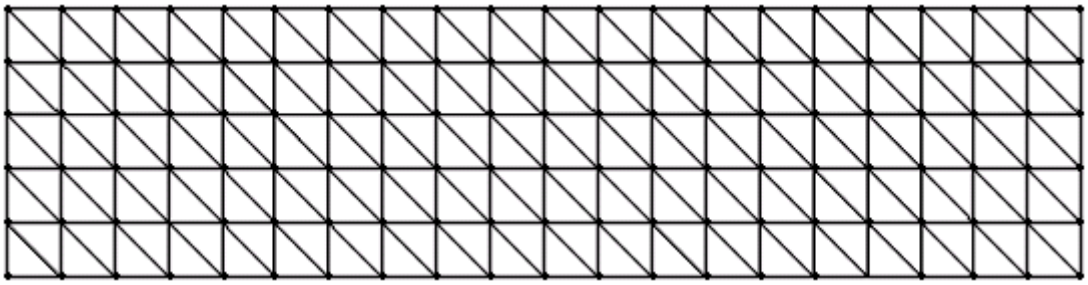

Figure 4.1.11 The background mesh

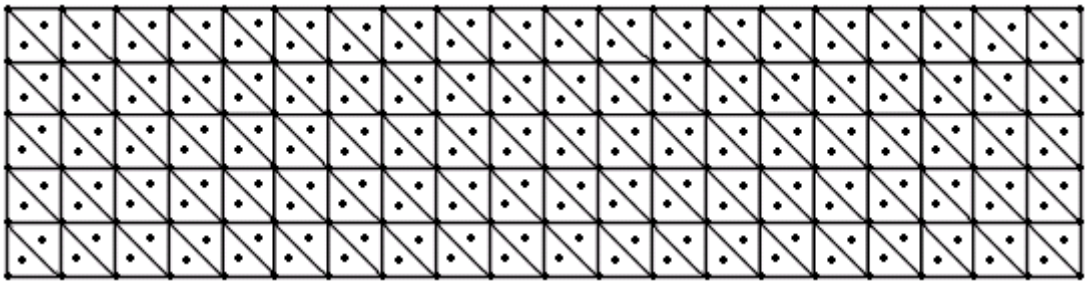

Figure 4.1.12 Node distribution on the background mesh

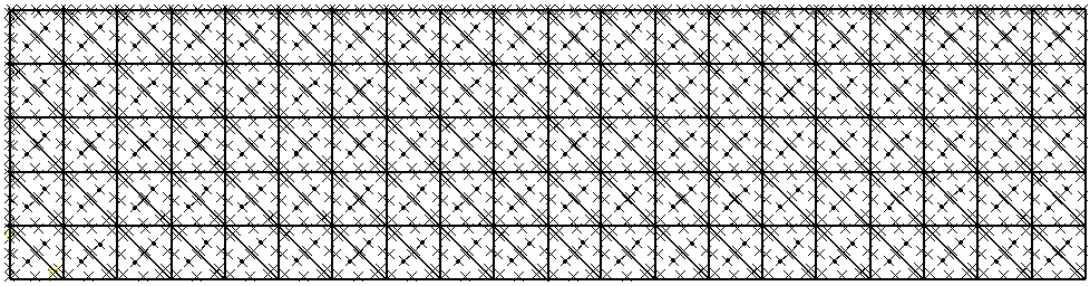

Figure 4.1.13 Node and integration point distribution on the background mesh

Table 4.1.5 and Figure 4.1.14 show the displacement results in x direction calculated by EFG program, finite element method and analytical method;

Table 4.1.5 Comparison of the displacements in x direction

x	y	u Analytic	u EFG	Error %
0	-60	0.000	0.000	0.000
0	-36	0.000	0.000	0.000
0	-12	0.000	0.000	0.000
0	12	0.000	0.000	0.000
0	36	0.000	0.000	0.000
0	60	0.000	0.000	0.000
240	-60	-0.180	-0.179	0.415
240	-36	-0.107	-0.106	0.442
240	-12	-0.035	-0.035	0.226
240	12	0.035	0.035	0.725
240	36	0.107	0.106	0.683
240	60	0.180	0.179	0.573
480	-60	-0.240	-0.239	0.290
480	-36	-0.143	-0.143	0.244
480	-12	-0.047	-0.047	0.183
480	12	0.047	0.047	0.592
480	36	0.143	0.142	0.446
480	60	0.240	0.239	0.405

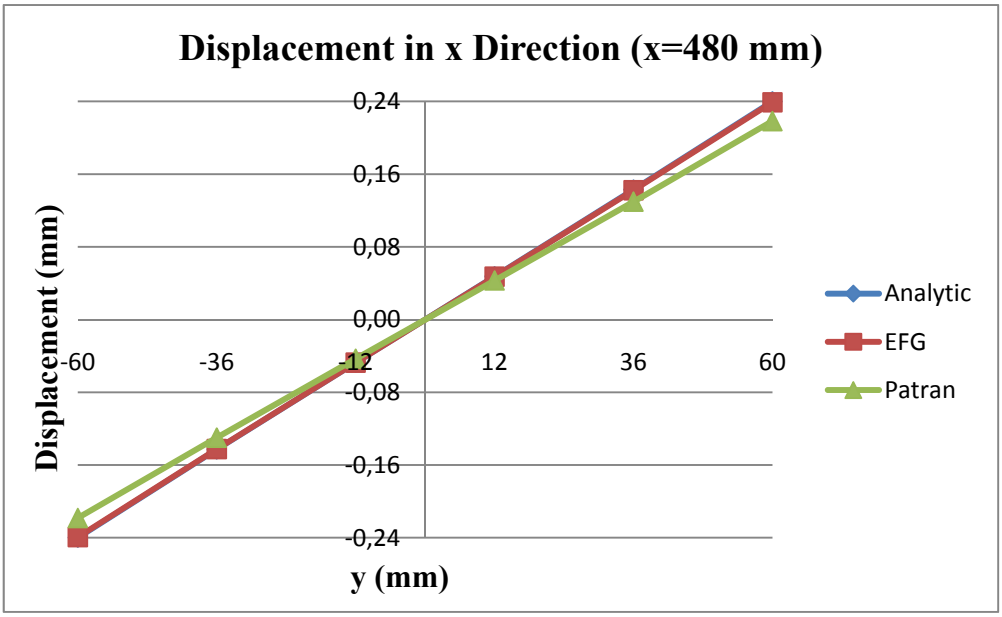

Figure 4.1.14 Graphical comparison of displacements in x direction

Table 4.1.6 and Figure 4.1.15 show the displacement results in y direction calculated by EFG program, finite element method and analytical method;

Table 4.1.6 Comparison of the displacements in y direction

x	y	v Analytic	v EFG	Error %
0	-60	0.000	0.000	0.000
0	-36	0.000	0.000	0.000
0	-12	0.000	0.000	0.000
0	12	0.000	0.000	0.000
0	36	0.000	0.000	0.000
0	60	0.000	0.000	0.000
240	-60	-0.428	-0.425	0.661
240	-36	-0.428	-0.422	1.337
240	-12	-0.428	-0.420	1.667
240	12	-0.428	-0.420	1.670
240	36	-0.428	-0.422	1.348
240	60	-0.428	-0.425	0.666
480	-60	-1.335	-1.324	0.796
480	-36	-1.335	-1.324	0.787
480	-12	-1.335	-1.324	0.789
480	12	-1.335	-1.325	0.787
480	36	-1.335	-1.324	0.789
480	60	-1.335	-1.324	0.790

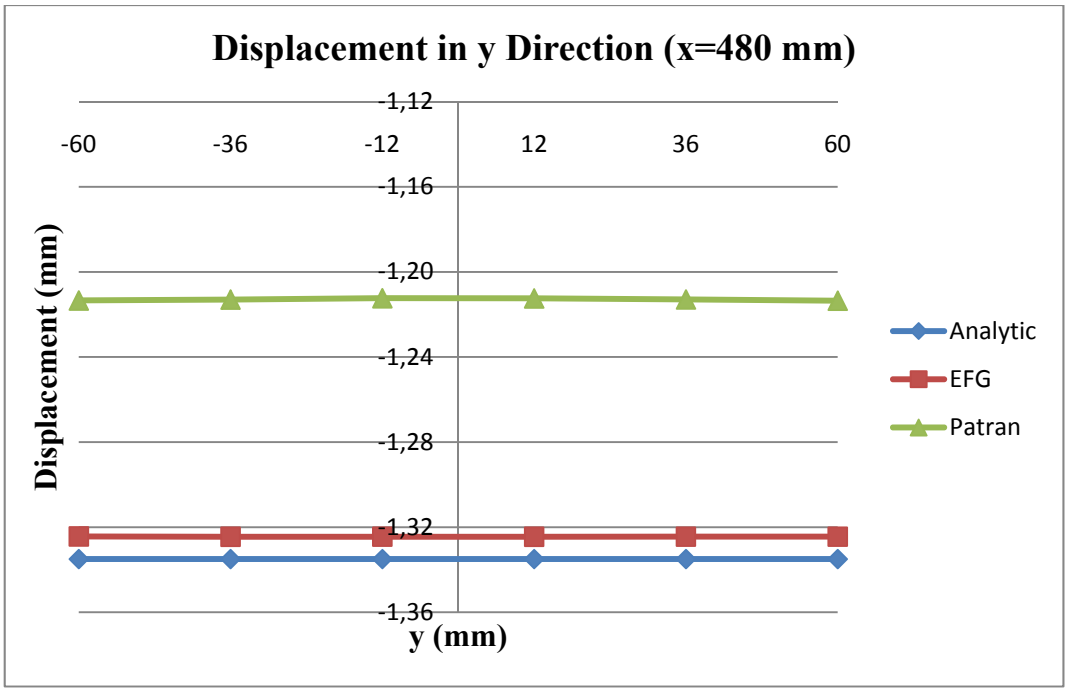

Figure 4.1.15 Graphical comparison of displacements in y direction

Table 4.1.7, Figure 4.1.16 and Figure 4.1.17 show the σ_x results calculated by EFG program, finite element method and analytical method;

Table 4.1.7 Comparison of the σ_x results

x	y	σx Analytic	σx EFG	Error %
0	-60	-200.000	-200.255	0.127
0	-36	-120.000	-127.873	6.157
0	-12	-40.000	-47.187	15.231
0	12	40.000	42.820	6.586
0	36	120.000	127.443	5.840
0	60	200.000	205.936	2.882
240	-60	-100.000	-100.122	0.122
240	-36	-60.000	-60.797	1.310
240	-12	-20.000	-17.515	12.424
240	12	20.000	20.508	2.478
240	36	60.000	59.477	0.872
240	60	100.000	99.616	0.384
480	-60	0.000	-0.836	100.000
480	-36	0.000	-1.104	100.000
480	-12	0.000	0.352	100.000
480	12	0.000	-0.684	100.000
480	36	0.000	-1.307	100.000
480	60	0.000	-0.039	100.000

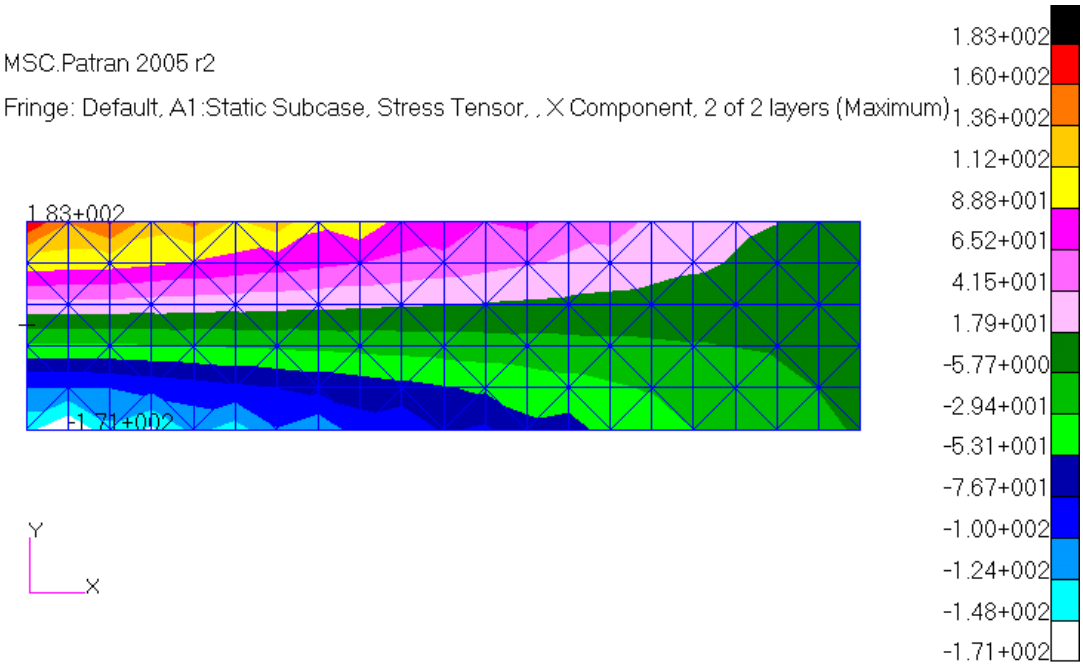

Figure 4.1.16 σ_x distribution obtained by Patran/Nastran

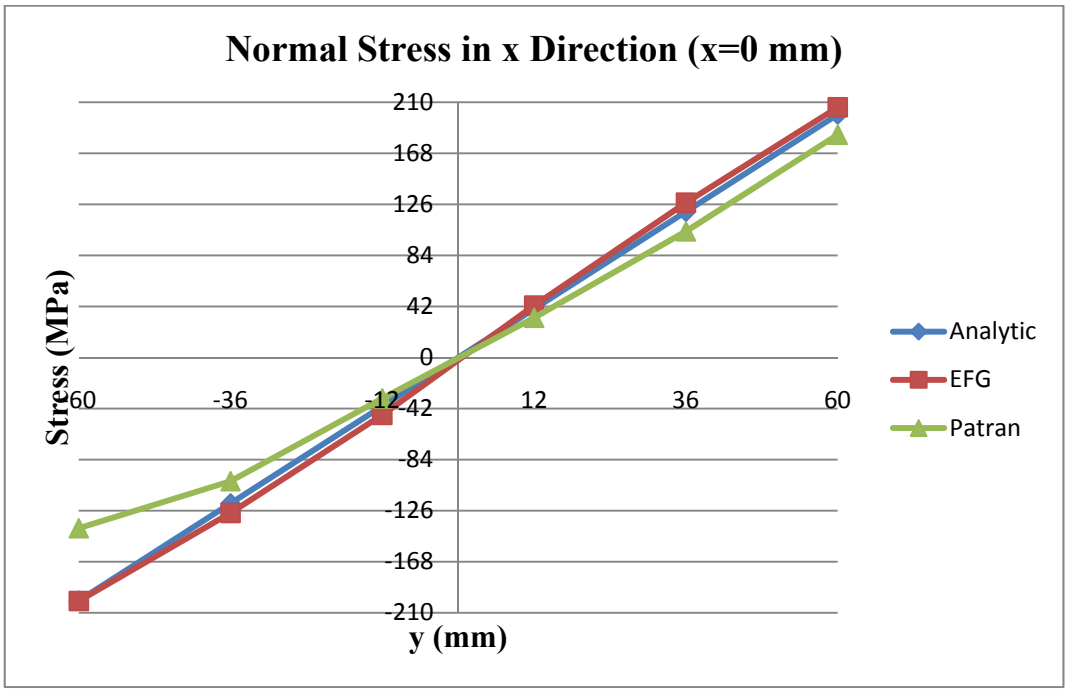

Figure 4.1.17 Graphical comparison of σ_x results

Table 4.1.8, Figure 4.1.18 and Figure 4.1.19 show the σ_{xy} results calculated by EFG program, finite element method and analytical method;

Table 4.1.8 Comparison of the σ_{xy} results

x	y	σxy Analytic	σxy EFG	Error %
0	-60	0.000	-16.464	100.000
0	-36	-8.000	-9.750	17.948
0	-12	-12.000	-3.157	73.694
0	12	-12.000	-0.861	92.828
0	36	-8.000	-3.083	61.463
0	60	0.000	-6.495	100.000
240	-60	0.000	-2.406	100.000
240	-36	-8.000	-8.299	3.607
240	-12	-12.000	-11.340	5.501
240	12	-12.000	-11.276	6.037
240	36	-8.000	-7.195	10.060
240	60	0.000	1.820	100.000
480	-60	0.000	-1.042	100.000
480	-36	-8.000	-9.178	12.839
480	-12	-12.000	-11.466	4.447
480	12	-12.000	-12.235	1.919
480	36	-8.000	-8.240	2.918
480	60	0.000	-0.985	100.000

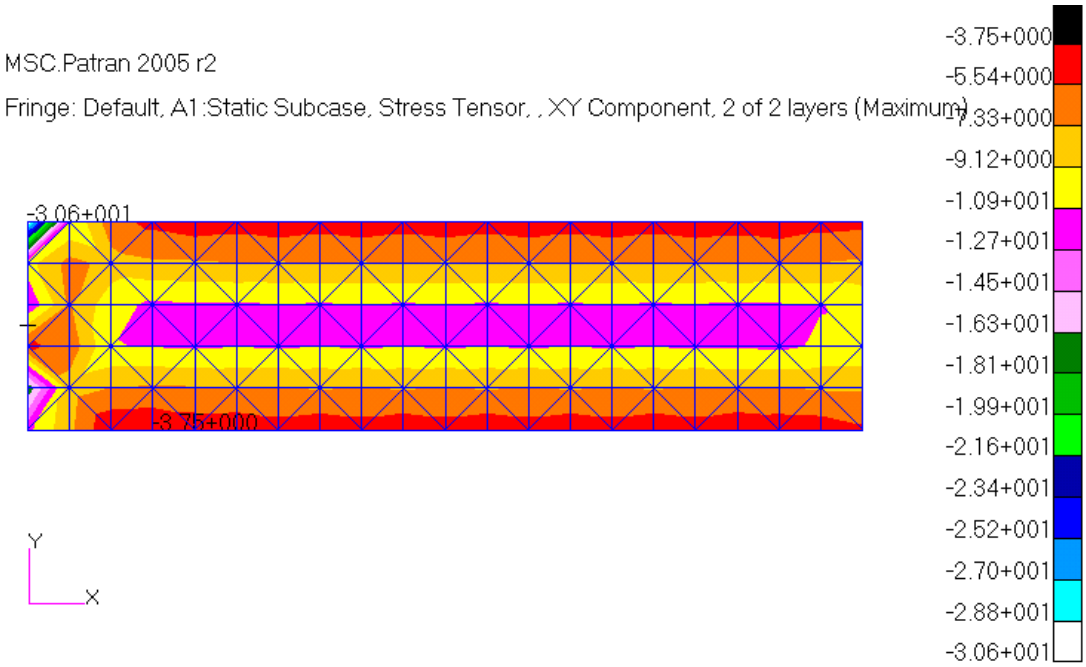

Figure 4.1.18 σ_{xy} distribution obtained by Patran/Nastran

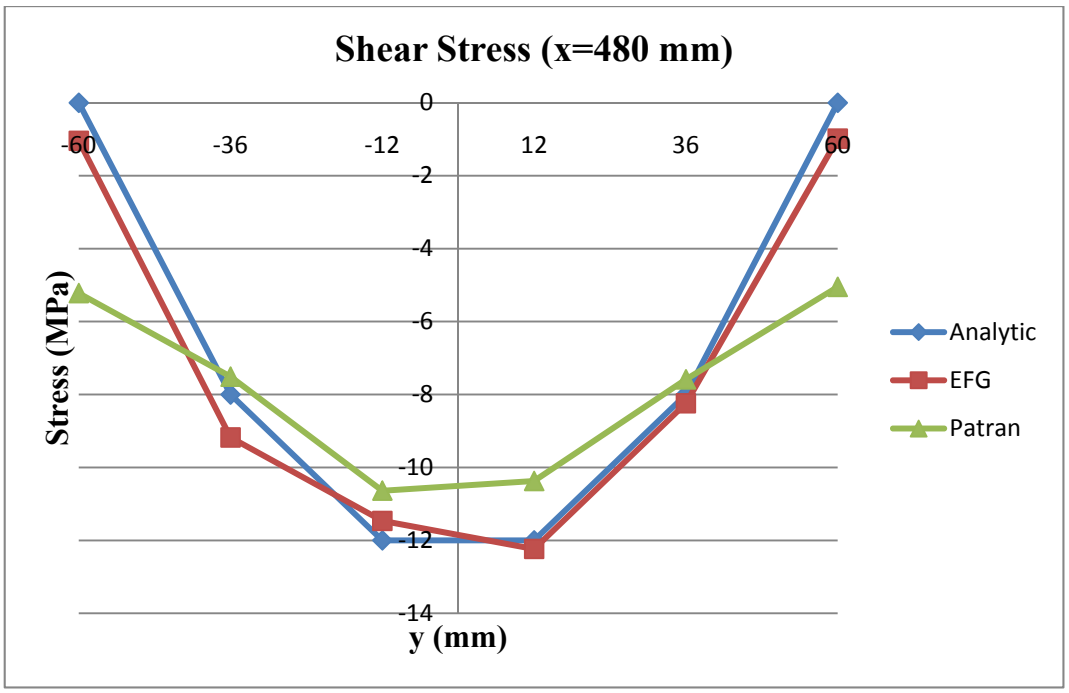

Figure 4.1.19 Graphical comparison of σ_{xy} results

For the third run, the same problem is solved by using the previous background mesh but increasing the number of integration points. There are 200 elements in the background mesh. The nodes are defined at the center and vertices of each element and thirteen Gauss integration points are used for each element.

Table 4.1.9 and Figure 4.1.20 show the displacement results in x direction calculated by EFG program, finite element method and analytical method;

Table 4.1.9 Comparison of the displacements in x direction

x	y	u Analytic	u EFG	Error %
0	-60	0.000	0.000	0.000
0	-36	0.000	0.000	0.000
0	-12	0.000	0.000	0.000
0	12	0.000	0.000	0.000
0	36	0.000	0.000	0.000
0	60	0.000	0.000	0.000
240	-60	-0.180	-0.177	1.780
240	-36	-0.107	-0.105	1.696
240	-12	-0.035	-0.035	2.164
240	12	0.035	0.035	1.323
240	36	0.107	0.105	1.750
240	60	0.180	0.177	1.678
480	-60	-0.240	-0.237	1.273
480	-36	-0.143	-0.141	1.282
480	-12	-0.047	-0.047	1.477
480	12	0.047	0.047	1.077
480	36	0.143	0.141	1.173
480	60	0.240	0.237	1.203

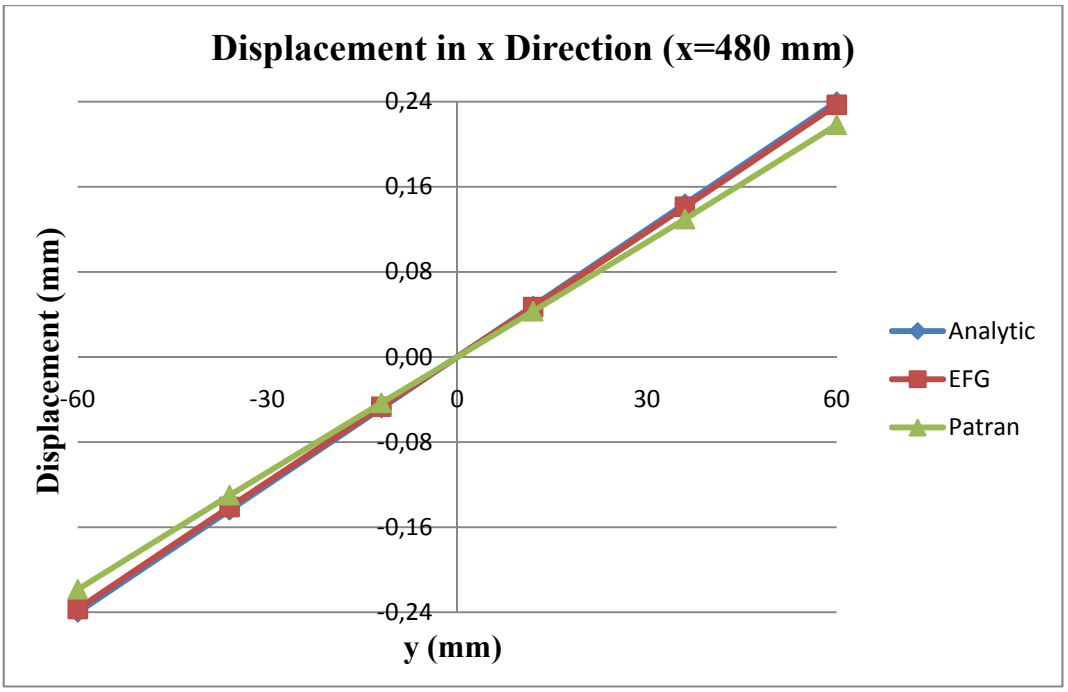

Figure 4.1.20 Graphical comparison of displacements in x direction

Table 4.1.10 and Figure 4.1.21 show the displacement results in y direction calculated by EFG program, finite element method and analytical method;

Table 4.1.10 Comparison of the displacements in y direction

x	y	v Analytic	v EFG	Error %
0	-60	0.000	0.000	0.000
0	-36	0.000	0.000	0.000
0	-12	0.000	0.000	0.000
0	12	0.000	0.000	0.000
0	36	0.000	0.000	0.000
0	60	0.000	0.000	0.000
240	-60	-0.428	-0.417	2.540
240	-36	-0.428	-0.414	3.217
240	-12	-0.428	-0.412	3.549
240	12	-0.428	-0.412	3.553
240	36	-0.428	-0.414	3.221
240	60	-0.428	-0.417	2.545
480	-60	-1.335	-1.308	2.054
480	-36	-1.335	-1.308	2.052
480	-12	-1.335	-1.308	2.049
480	12	-1.335	-1.308	2.048
480	36	-1.335	-1.308	2.048
480	60	-1.335	-1.308	2.051

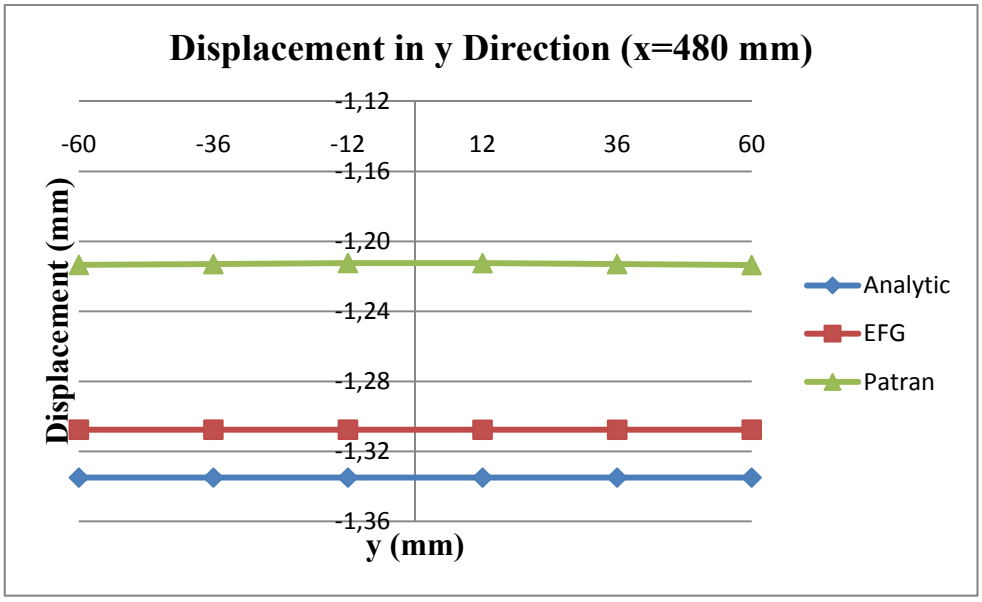

Figure 4.1.21 Graphical comparison of displacements in y direction

Table 4.1.11, Figure 4.1.22 and Figure 4.1.23 show the σ_x results calculated by EFG program, finite element method and analytical method;

Table 4.1.11 Comparison of the σ_x results

x	y	σx Analytic	σx EFG	Error %
0	-60	-200.000	-189.250	5.375
0	-36	-120.000	-112.662	6.115
0	-12	-40.000	-36.074	9.814
0	12	40.000	40.514	1.268
0	36	120.000	117.102	2.415
0	60	200.000	193.690	3.155
240	-60	-100.000	-99.909	0.091
240	-36	-60.000	-60.250	0.415
240	-12	-20.000	-19.516	2.418
240	12	20.000	19.241	3.797
240	36	60.000	62.954	4.692
240	60	100.000	99.359	0.641
480	-60	0.000	-0.908	100.000
480	-36	0.000	-1.311	100.000
480	-12	0.000	1.208	100.000
480	12	0.000	-1.360	100.000
480	36	0.000	-0.283	100.000
480	60	0.000	0.426	100.000

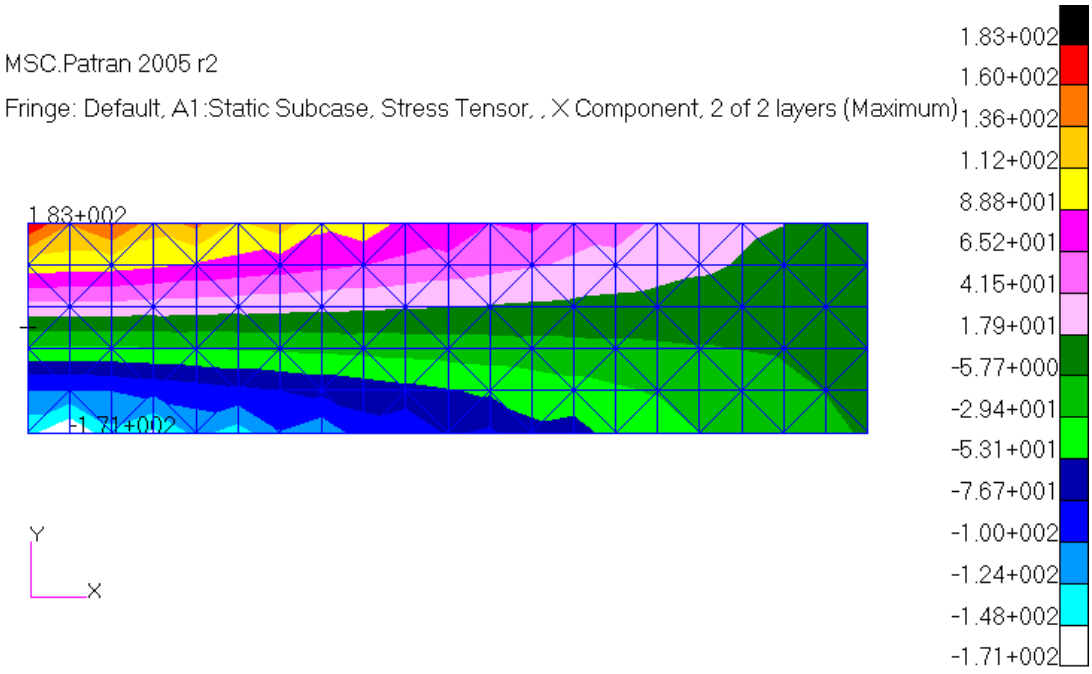

Figure 4.1.22 σ_x distribution obtained by Patran/Nastran

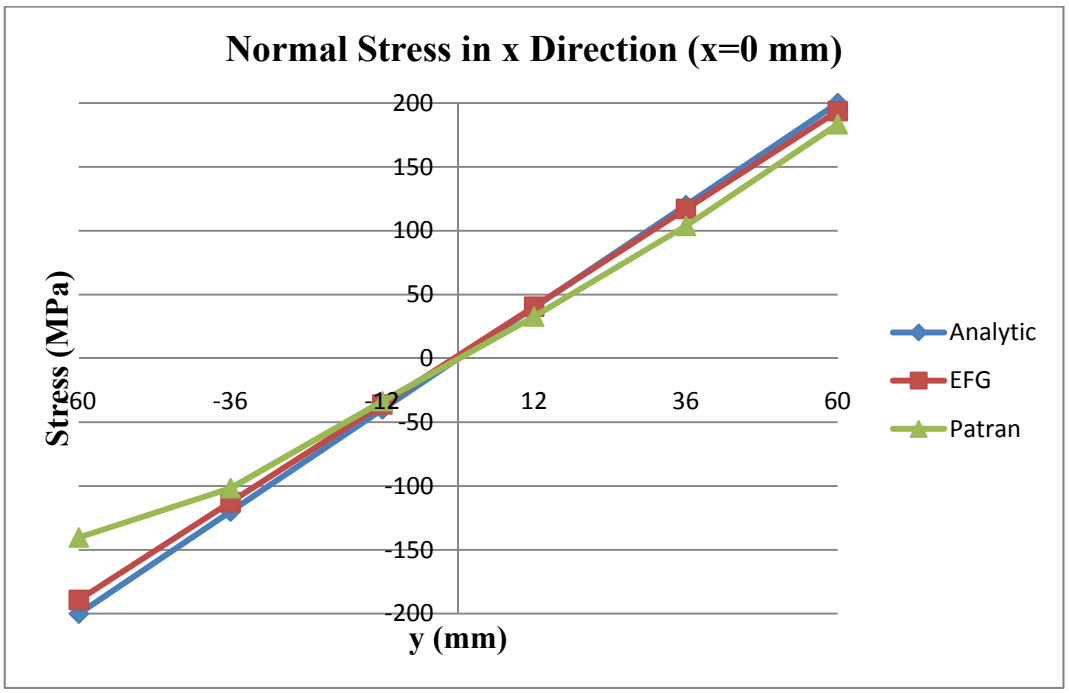

Figure 4.1.23 Graphical comparison of σ_x results

Table 4.1.12, Figure 4.1.24 and Figure 4.1.25 show the σ_{xy} results calculated by EFG program, finite element method and analytical method;

Table 4.1.12 Comparison of the σ_{xy} results

x	y	σxy Analytic	σxy EFG	Error %
0	-60	0.000	-3.152	100.000
0	-36	-8.000	-3.232	59.595
0	-12	-12.000	-3.312	72.397
0	12	-12.000	-3.392	71.731
0	36	-8.000	-3.472	56.598
0	60	0.000	-3.552	100.000
240	-60	0.000	-1.275	100.000
240	-36	-8.000	-8.411	4.883
240	-12	-12.000	-12.663	5.233
240	12	-12.000	-11.557	3.688
240	36	-8.000	-7.088	11.398
240	60	0.000	0.386	100.000
480	-60	0.000	-1.020	100.000
480	-36	-8.000	-8.690	7.943
480	-12	-12.000	-12.897	6.955
480	12	-12.000	-13.154	8.776
480	36	-8.000	-8.096	1.180
480	60	0.000	-0.877	100.000

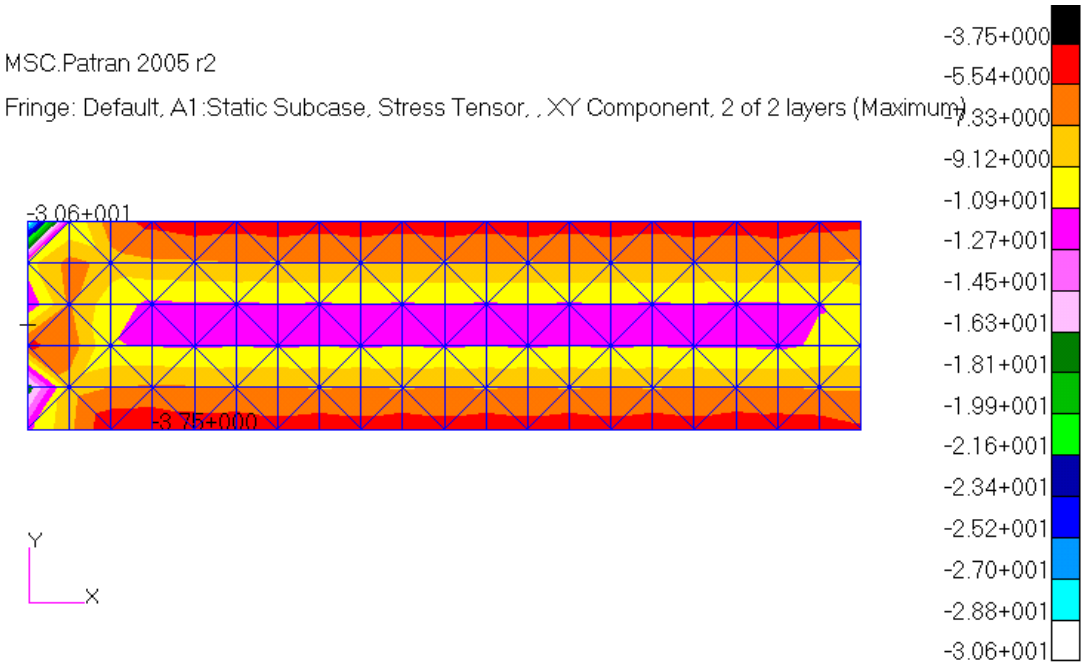

Figure 4.1.24 σ_{xy} distribution obtained by Patran/Nastran

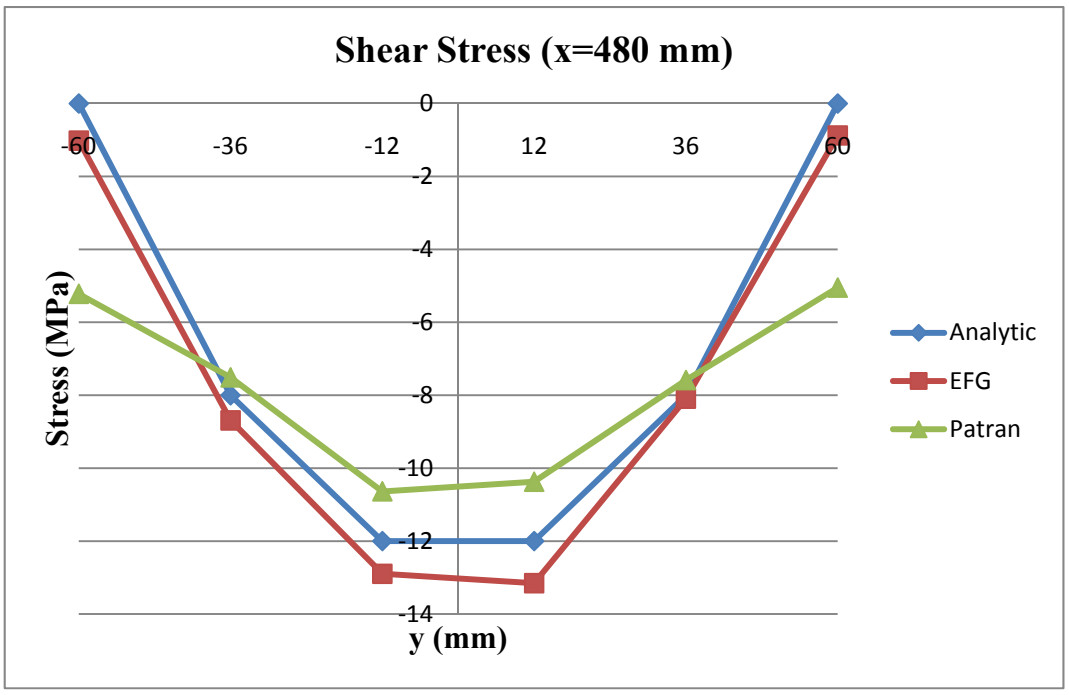

Figure 4.1.25 Graphical comparison of σ_{xy} results

The results obtained from the different EFG solutions are compared. Table 4.1.13 and Figure 4.1.26 show the displacement results in x direction calculated by analytical method and EFG program runs 1, 2 and 3;

Table 4.1.13 Comparison of the displacements in x direction

x	y	u Analytic	u EFG run 1	u EFG run 2	u EFG run 3
480	-60	-0.240	-0.239	-0.239	-0.237
480	-36	-0.143	-0.142	-0.143	-0.141
480	-30	-0.120	-0.118	-0.119	-0.117
480	-12	-0.047	-0.047	-0.047	-0.047
480	0	0.000	0.000	0.000	0.000
480	12	0.047	0.048	0.047	0.047
480	30	0.120	0.119	0.118	0.118
480	60	0.240	0.240	0.239	0.237

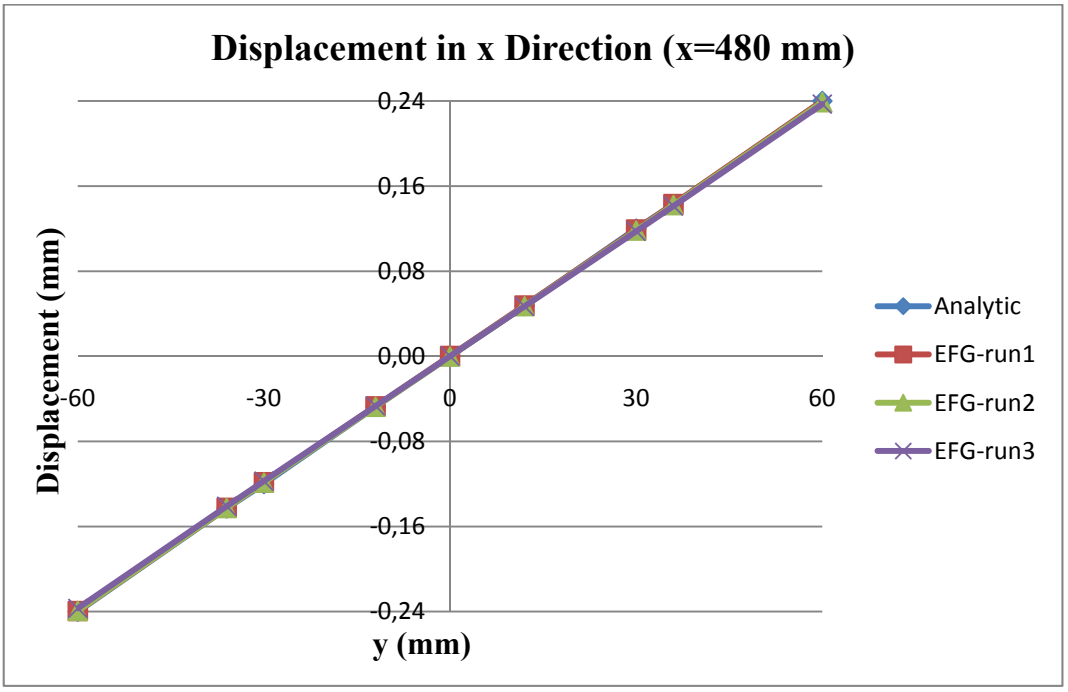

Figure 4.1.26 Graphical comparison of displacements in x direction

Table 4.1.14 and Figure 4.1.27 show the displacement results in y direction calculated by analytical method and EFG program runs 1, 2 and 3;

Table 4.1.14 Comparison of the displacements in y direction

x	y	v Analytic	v EFG run 1	v EFG run 2	v EFG run 3
480	-60	-1.335	-1.326	-1.324	-1.308
480	-36	-1.335	-1.326	-1.324	-1.308
480	-30	-1.335	-1.326	-1.324	-1.308
480	-12	-1.335	-1.326	-1.324	-1.308
480	0	-1.335	-1.326	-1.324	-1.308
480	12	-1.335	-1.326	-1.324	-1.308
480	30	-1.335	-1.326	-1.324	-1.308
480	36	-1.335	-1.326	-1.324	-1.308
480	60	-1.335	-1.326	-1.324	-1.308

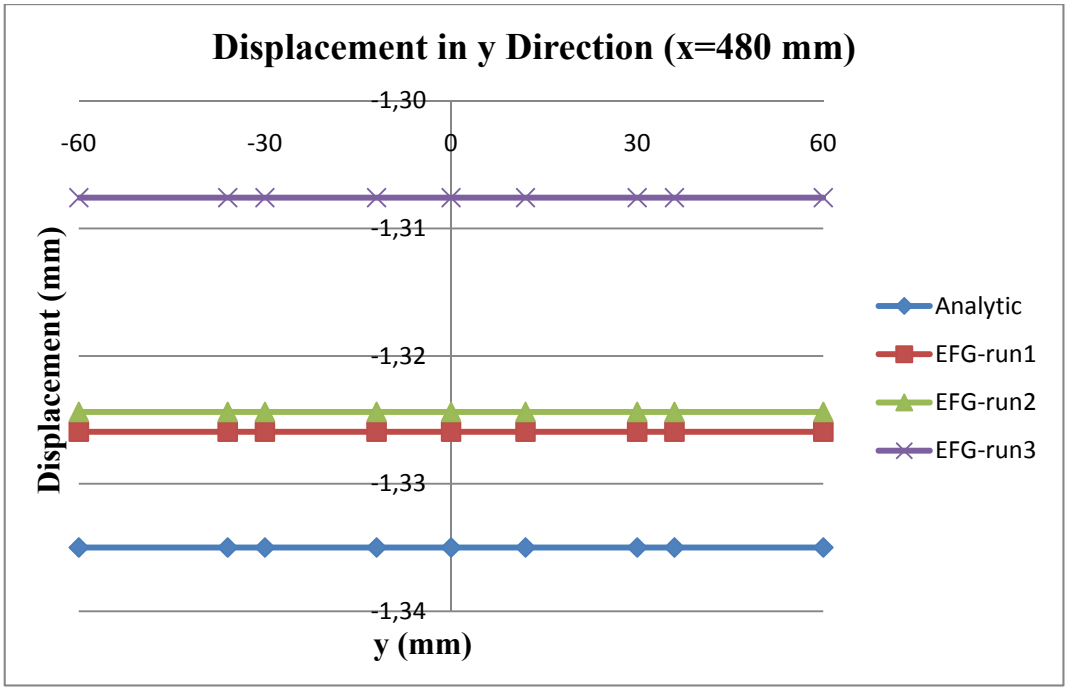

Figure 4.1.27 Graphical comparison of displacements in y direction

Table 4.1.15 and Figure 4.1.28 show the σ_x results calculated by analytic method and EFG program runs 1, 2 and 3;

Table 4.1.15 Comparison of the σ_x results

x	y	σx Analytic	σx EFG run 1	σx EFG run 2	σx EFG run 3
0	-60	-200.000	-191.932	-200.255	-189.250
0	-36	-120.000	-115.232	-127.873	-112.662
0	-30	-100.000	-95.868	-109.729	-93.515
0	-12	-40.000	-37.903	-47.187	-36.074
0	0	0.000	3.078	-2.683	2.220
0	12	40.000	44.907	42.820	40.514
0	30	100.000	103.965	107.819	97.955
0	36	120.000	123.749	127.443	117.102
0	60	200.000	203.506	205.936	193.690

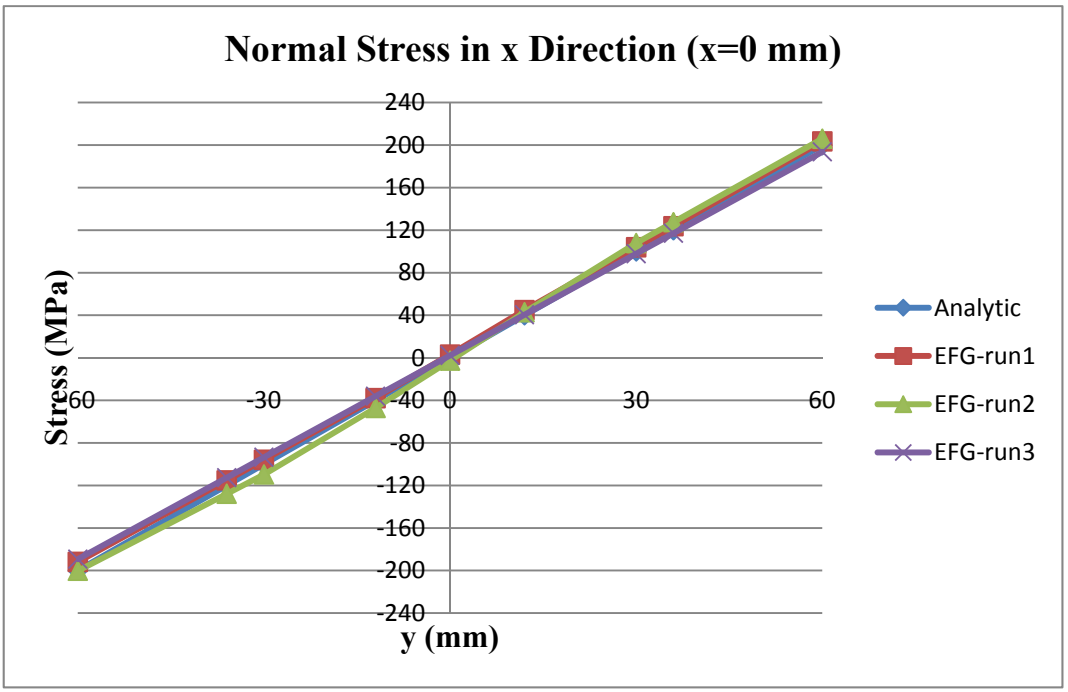

Figure 4.1.28 Graphical comparison of σ_x results

Table 4.1.16 and Figure 4.1.29 show the σ_{xy} results calculated by analytical method and EFG program runs 1, 2 and 3;

Table 4.1.16 Comparison of the σ_{xy} results

x	y	σxy Analytic	σxy EFG run1	σxy EFG run2	σxy EFG run3
480	-60	0.000	-0.717	-1.042	-1.020
480	-36	-8.000	-8.846	-9.178	-8.690
480	-30	-9.375	-10.487	-10.897	-10.336
480	-12	-12.000	-13.311	-11.466	-12.897
480	0	-12.500	-12.434	-12.716	-14.193
480	12	-12.000	-13.324	-12.235	-13.154
480	30	-9.375	-10.691	-9.619	-9.795
480	36	-8.000	-8.849	-8.240	-8.096
480	60	0.000	-0.716	-0.985	-0.877

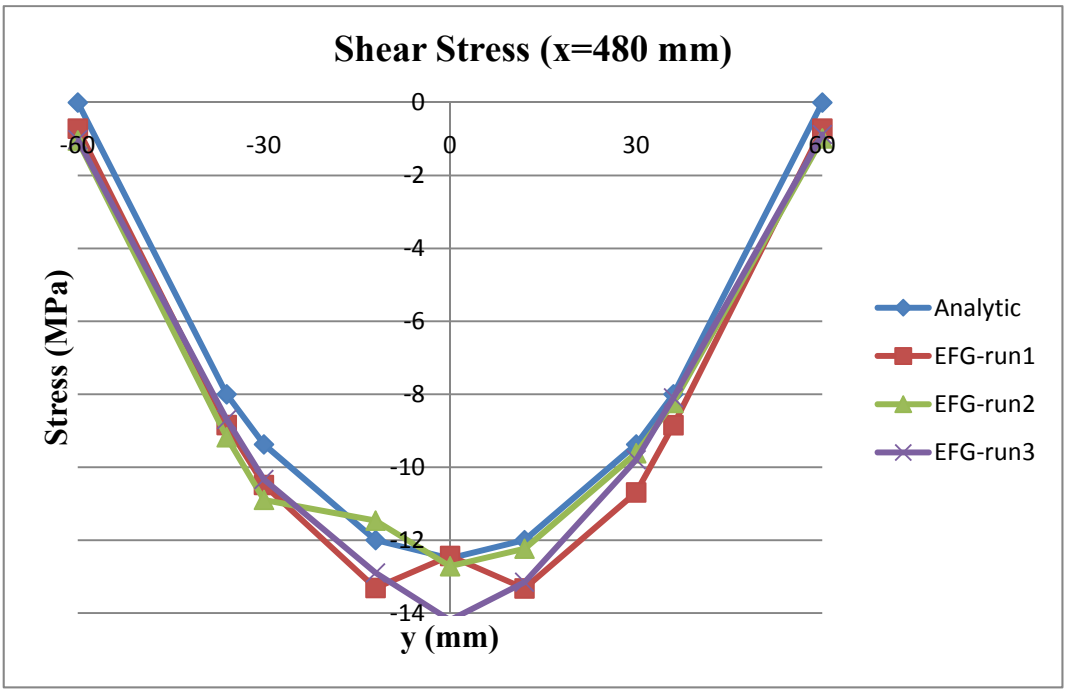

Figure 4.1.29 Graphical comparison of σ_{xy} results

4.2. Cantilever Beam under Uniform Transverse Load

A cantilever beam subjected to uniform transverse load is shown in Figure 4.2.1.

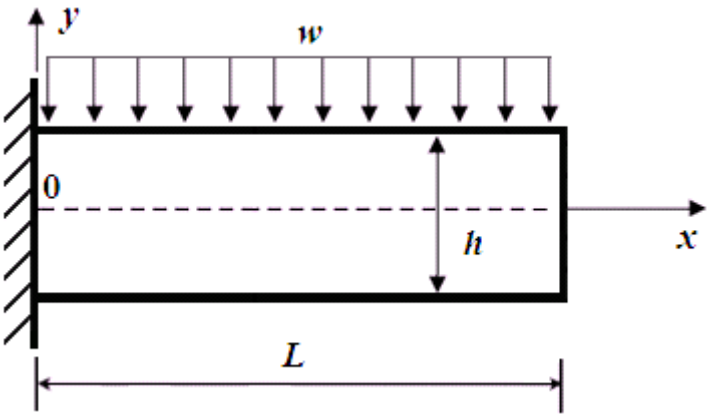

Figure 4.2.1 A cantilever beam subjected to uniform transverse loading

The exact solutions are,

$$v = \frac{w}{24EI}(x^4 - 4Lx^3 + 6L^2x^2) \qquad (4.10)$$

$$\sigma_x = -\frac{wy}{2I}(L - x)^2 \qquad (4.11)$$

$$\sigma_{xy} = \frac{w}{I}(L - x)(yh - \frac{3h^2}{8} - \frac{y^2}{2}) \qquad (4.12)$$

In this example, the properties for this cantilever beam are taken as follows:

The uniform distributed transverse loading: $w = -1$ N/mm
Young's modulus: $E = 200000$ N/mm^2
Poisson's ratio: $v = 0.3$
Height of the beam: $h = 120$ mm
Length of the beam: $L = 480$ mm

For the first run of the example, there are 128 elements in the background mesh. The nodes are defined at the center and vertices of each element and seven Gauss

integration points are used for each element. The background mesh, nodes and integration points used in this run are same with the first run of previous example and shown in Figure 4.1.2, Figure 4.1.3 and Figure 4.1.4 respectively.

Table 4.2.1 and Figure 4.2.2 show the displacement results in y direction calculated by EFG program, finite element method and analytical method;

Table 4.2.1 Comparison of the displacements in y direction

x	y	v Analytic	v EFG	Error %
0	-60	0.000	0.000	0.000
0	-30	0.000	0.000	0.000
0	0	0.000	0.000	0.000
0	30	0.000	0.000	0.000
0	60	0.000	0.000	0.000
240	-60	-0.082	-0.091	9.893
240	-30	-0.082	-0.090	9.464
240	0	-0.082	-0.090	9.377
240	30	-0.082	-0.090	9.615
240	60	-0.082	-0.091	10.192
480	-60	-0.230	-0.242	4.802
480	-30	-0.230	-0.242	4.804
480	0	-0.230	-0.242	4.818
480	30	-0.230	-0.242	4.863
480	60	-0.230	-0.242	4.923

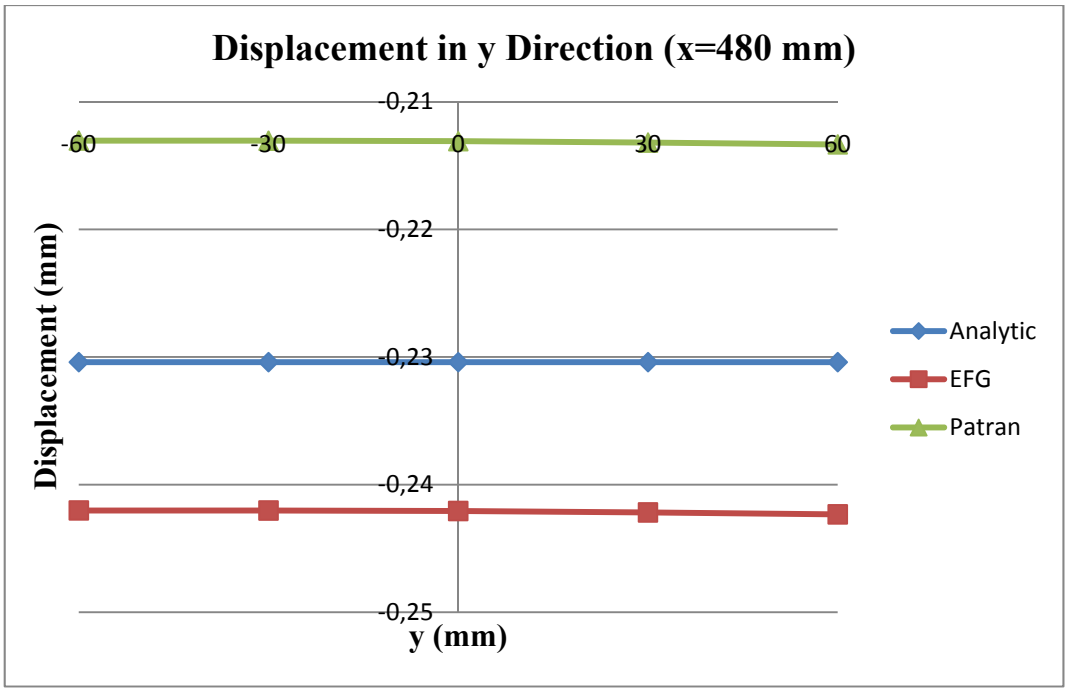

Figure 4.2.2 Graphical comparison of displacements in y direction

Table 4.2.2, Figure 4.2.3 and Figure 4.2.4 show the σ_x results calculated by EFG program, finite element method and analytical method;

Table 4.2.2 Comparison of the σ_x results

x	y	σx Analytic	σx EFG	Error %
0	-60	-48.000	-44.663	6.952
0	-30	-24.000	-22.534	6.107
0	0	0.000	0.727	100.000
0	30	24.000	24.459	1.878
0	60	48.000	47.720	0.584
240	-60	-12.000	-11.649	2.929
240	-30	-6.000	-7.121	15.738
240	0	0.000	-0.074	100.000
240	30	6.000	6.878	12.761
240	60	12.000	11.499	4.175
480	-60	0.000	0.122	100.000
480	-30	0.000	0.025	100.000
480	0	0.000	0.027	100.000
480	30	0.000	-0.013	100.000
480	60	0.000	-0.063	100.000

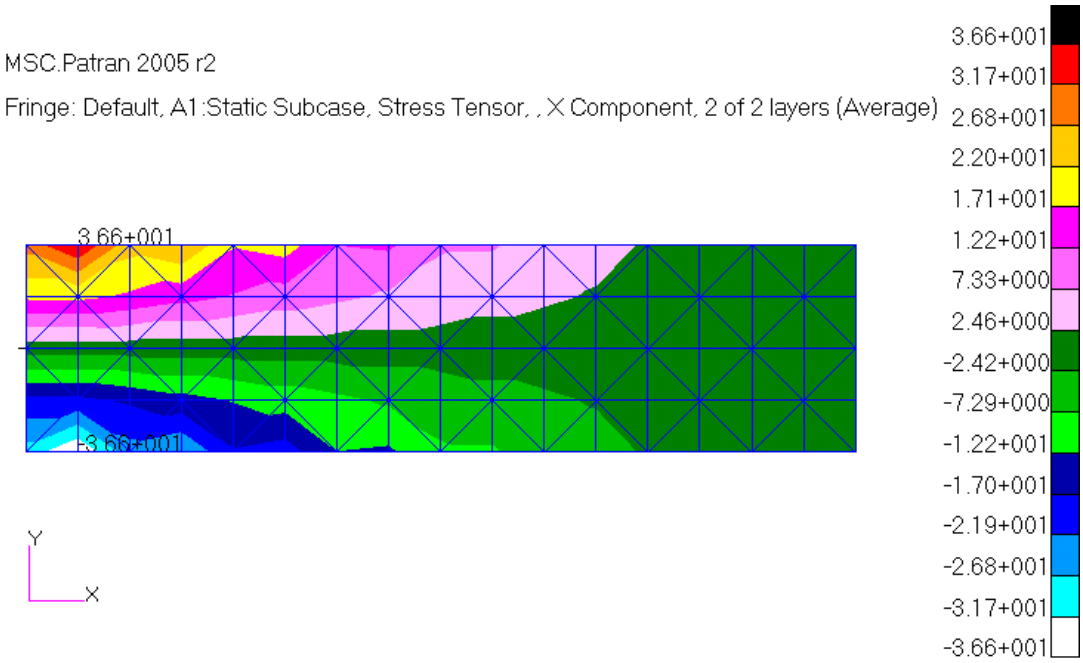

Figure 4.2.3 σ_x distribution obtained by Patran/Nastran

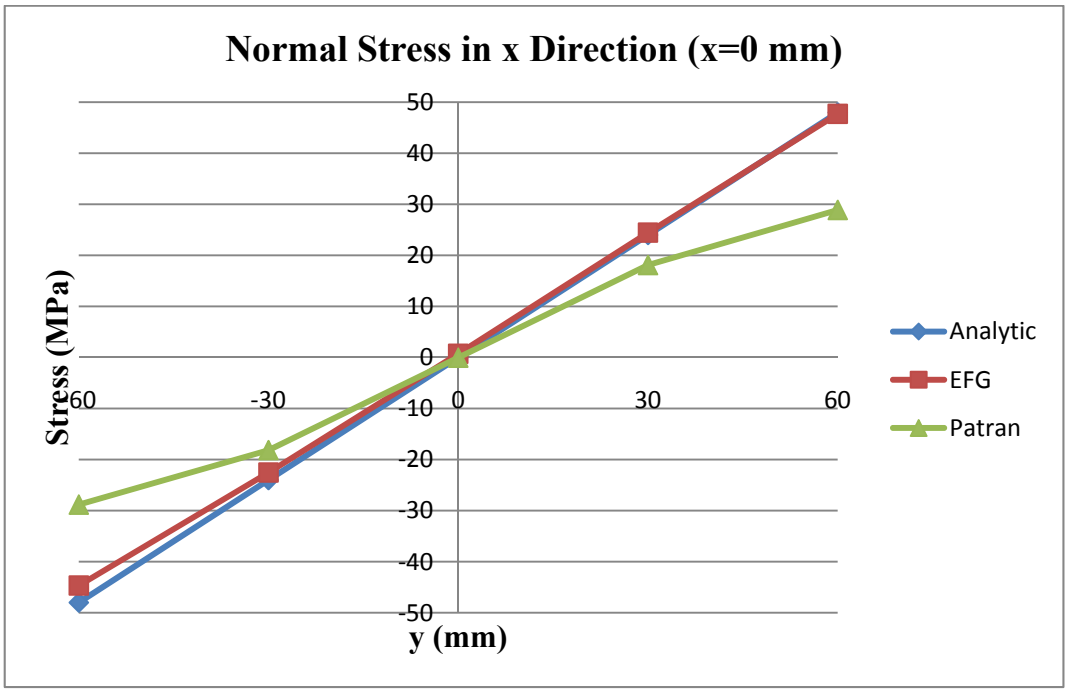

Figure 4.2.4 Graphical comparison of σ_x results

Table 4.2.3, Figure 4.2.5 and Figure 4.2.6 show the σ_{xy} results calculated by EFG program, finite element method and analytical method;

Table 4.2.3 Comparison of the σ_{xy} results

x	y	σxy Analytic	σxy EFG	Error %
0	-60	0.000	-4.755	100.000
0	-30	-4.500	-3.457	23.176
0	0	-6.000	-4.100	31.665
0	30	-4.500	-4.572	1.576
0	60	0.000	-6.481	100.000
240	-60	0.000	-0.025	100.000
240	-30	-2.250	-2.422	7.096
240	0	-3.000	-2.881	3.957
240	30	-2.250	-2.458	8.477
240	60	0.000	-0.080	100.000
480	-60	0.000	0.107	100.000
480	-30	0.000	-0.024	100.000
480	0	0.000	-0.018	100.000
480	30	0.000	-0.027	100.000
480	60	0.000	0.061	100.000

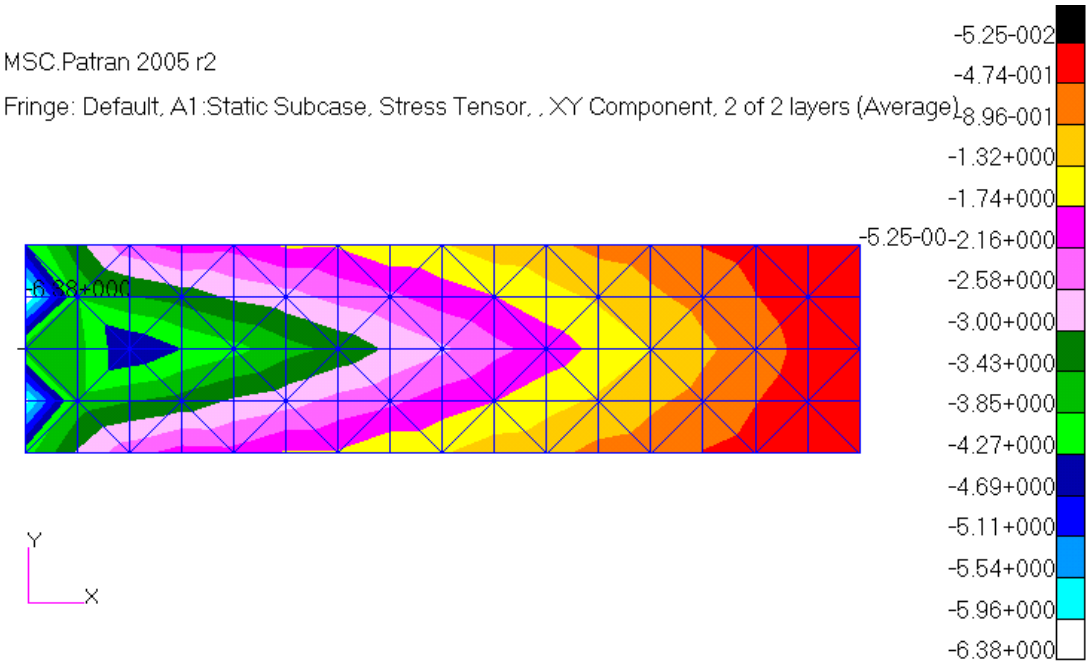

Figure 4.2.5 σ_{xy} distribution obtained by Patran/Nastran

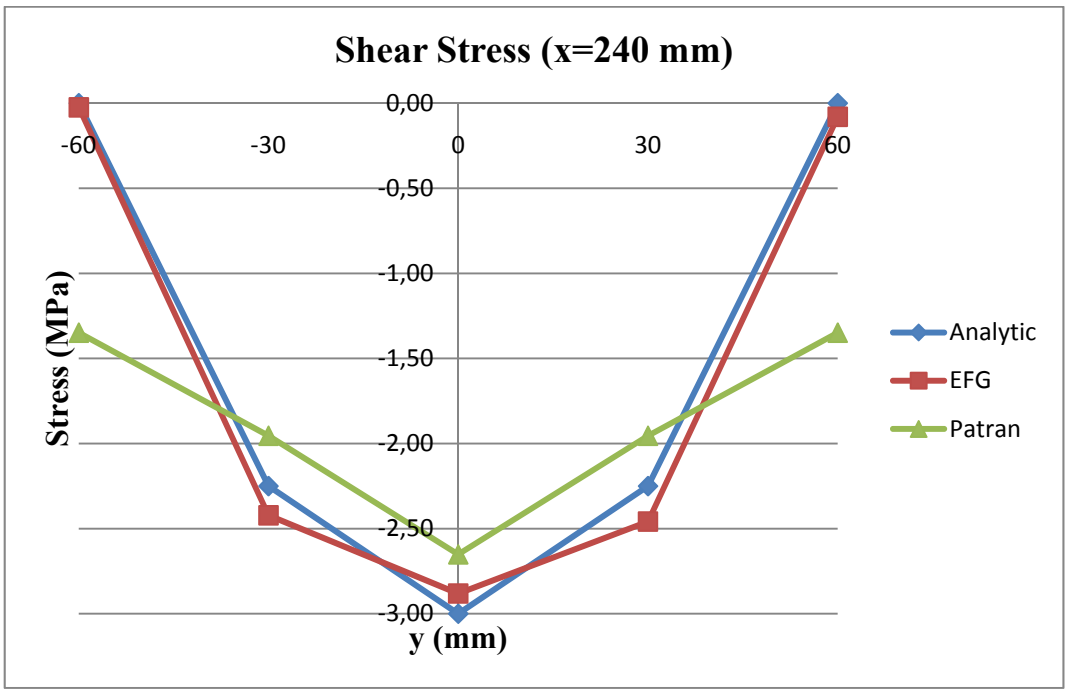

Figure 4.2.6 Graphical comparison of σ_{xy} results

For the second run, the same problem is modeled by a more refined background mesh which has 200 elements. The nodes are defined at the center and vertices of each element and seven Gauss integration points are used for each element. The background mesh, nodes and integration points used in this run are same with the second run of the previous example and shown in Figure 4.1.11, Figure 4.1.12 and Figure 4.1.13 respectively.

Table 4.2.4 and Figure 4.2.7 show the displacement results in y direction calculated by EFG program, finite element method and analytical method;

Table 4.2.4 Comparison of the displacements in y direction

x	y	v Analytic	v EFG	Error %
0	-60	0.000	0.000	0.000
0	-36	0.000	0.000	0.000
0	-12	0.000	0.000	0.000
0	12	0.000	0.000	0.000
0	36	0.000	0.000	0.000
0	60	0.000	0.000	0.000
240	-60	-0.082	-0.091	10.103
240	-36	-0.082	-0.090	9.766
240	-12	-0.082	-0.090	9.623
240	12	-0.082	-0.090	9.680
240	36	-0.082	-0.091	9.940
240	60	-0.082	-0.091	10.398
480	-60	-0.230	-0.242	4.817
480	-36	-0.230	-0.242	4.817
480	-12	-0.230	-0.242	4.822
480	12	-0.230	-0.242	4.845
480	36	-0.230	-0.242	4.887
480	60	-0.230	-0.242	4.939

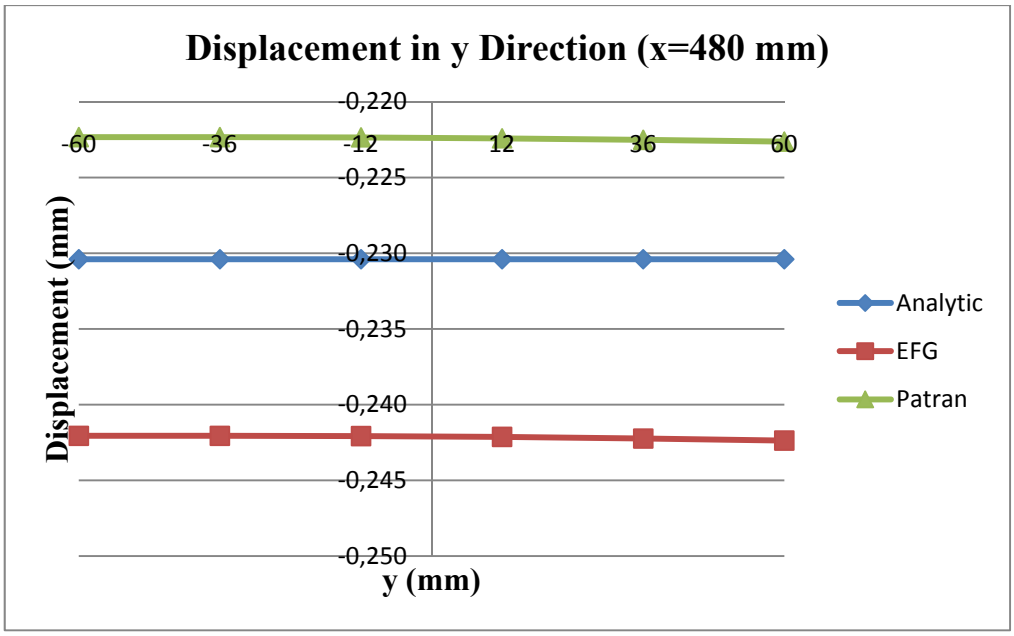

Figure 4.2.7 Graphical comparison of displacements in y direction

Table 4.2.5, Figure 4.2.8 and Figure 4.2.9 show the σ_x results calculated by EFG program, finite element method and analytical method;

Table 4.2.5 Comparison of the σ_x results

x	y	σx Analytic	σx EFG	Error %
0	-60	-48.000	-47.493	1.055
0	-36	-28.800	-30.577	5.811
0	-12	-9.600	-11.388	15.703
0	12	9.600	10.325	7.018
0	36	28.800	30.371	5.172
0	60	48.000	48.374	0.774
240	-60	-12.000	-11.859	1.176
240	-36	-7.200	-7.208	0.117
240	-12	-2.400	-2.049	14.642
240	12	2.400	2.596	7.560
240	36	7.200	7.209	0.120
240	60	12.000	11.678	2.684
480	-60	0.000	0.081	100.000
480	-36	0.000	-0.007	100.000
480	-12	0.000	-0.006	100.000
480	12	0.000	-0.003	100.000
480	36	0.000	-0.041	100.000
480	60	0.000	-0.020	100.000

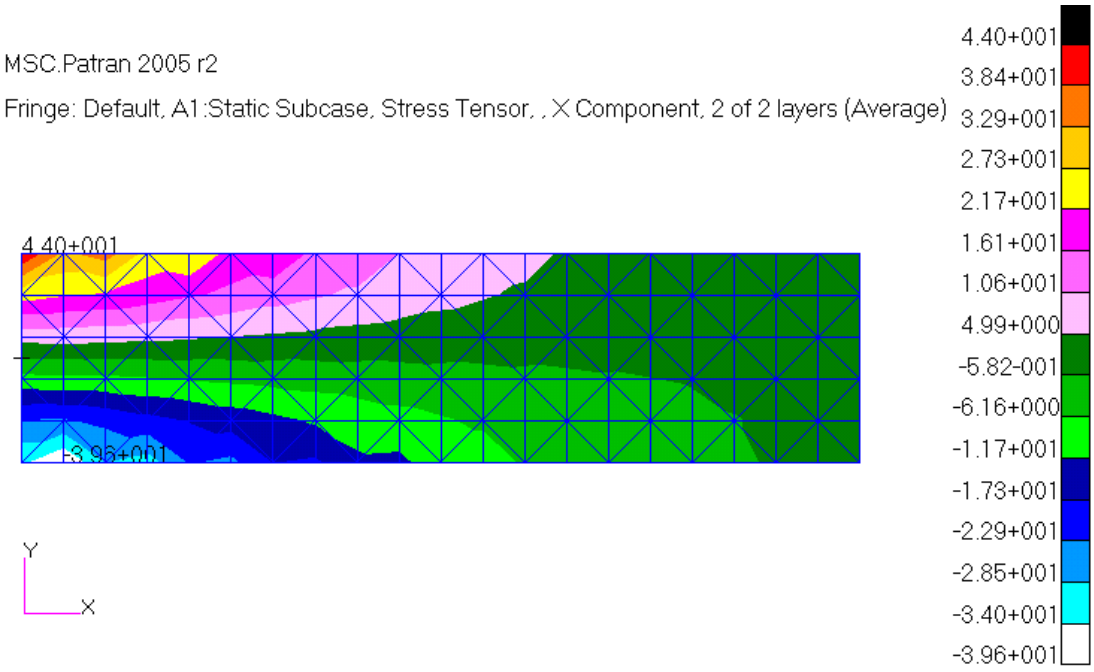

Figure 4.2.8 σ_x distribution obtained by Patran/Nastran

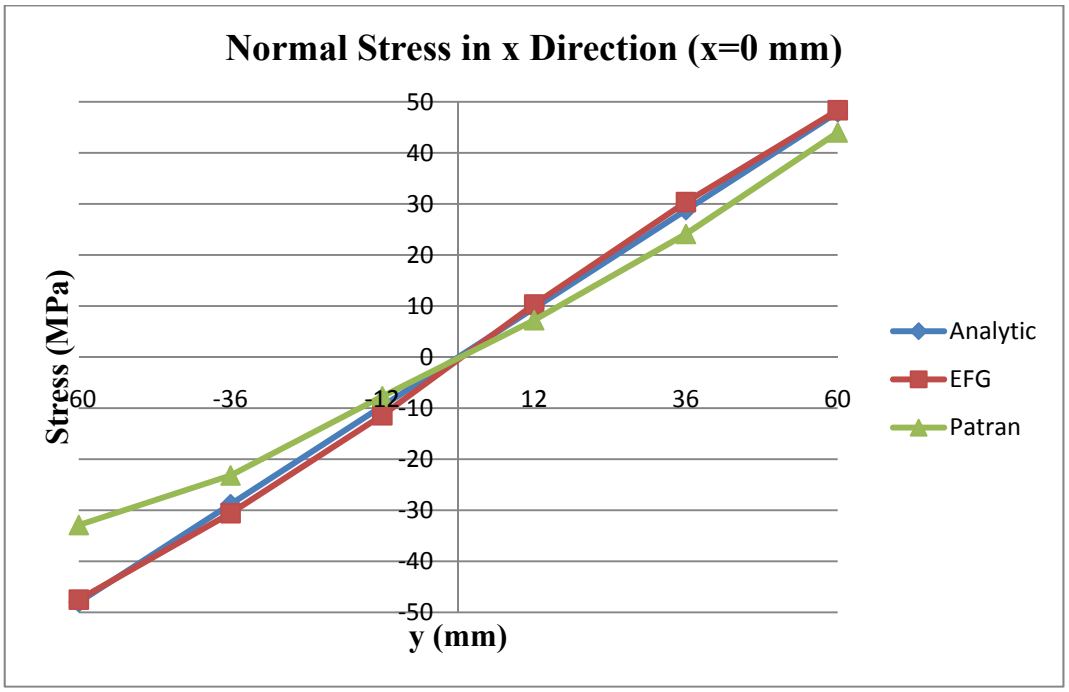

Figure 4.2.9 Graphical comparison of σ_x results

Table 4.2.6, Figure 4.2.10 and Figure 4.2.11 show the σ_{xy} results calculated by EFG program, finite element method and analytical method;

Table 4.2.6 Comparison of the σ_{xy} results

x	y	σxy Analytic	σxy EFG	Error %
0	-60	0.000	-5.429	100.000
0	-36	-3.840	-4.006	4.149
0	-12	-5.760	-2.543	55.849
0	12	-5.760	-2.131	63.004
0	36	-3.840	-2.772	27.800
0	60	0.000	-3.637	100.000
240	-60	0.000	-0.354	100.000
240	-36	-1.920	-1.961	2.066
240	-12	-2.880	-2.731	5.157
240	12	-2.880	-2.721	5.522
240	36	-1.920	-1.751	8.818
240	60	0.000	0.311	100.000
480	-60	0.000	0.048	100.000
480	-36	0.000	-0.023	100.000
480	-12	0.000	0.014	100.000
480	12	0.000	0.033	100.000
480	36	0.000	-0.049	100.000
480	60	0.000	-0.030	100.000

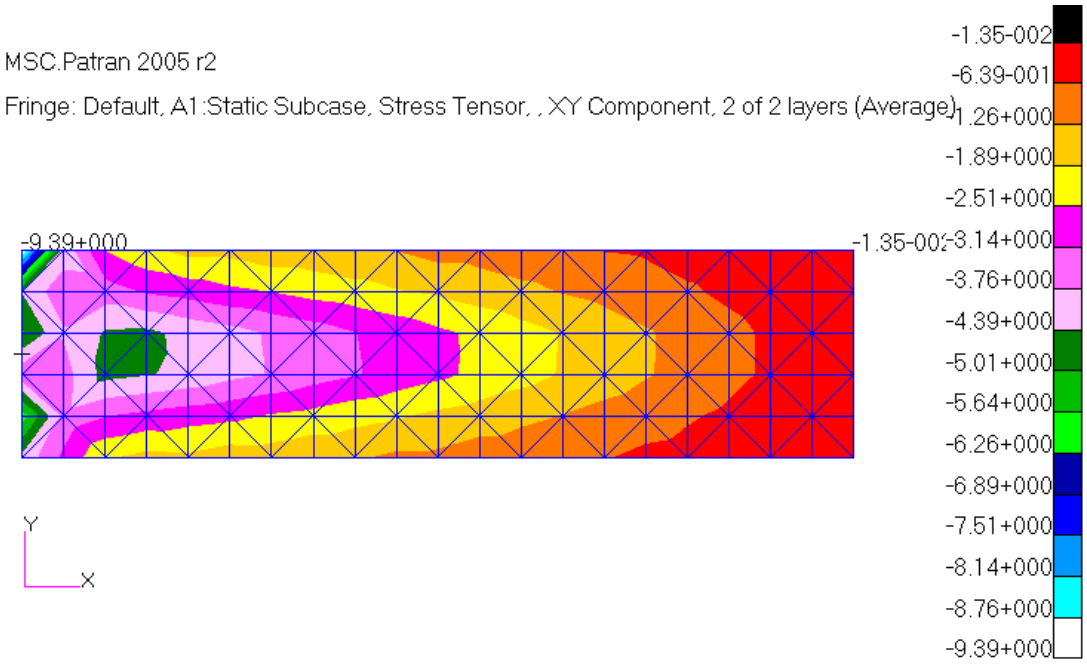

Figure 4.2.10 σ_{xy} distribution obtained by Patran/Nastran

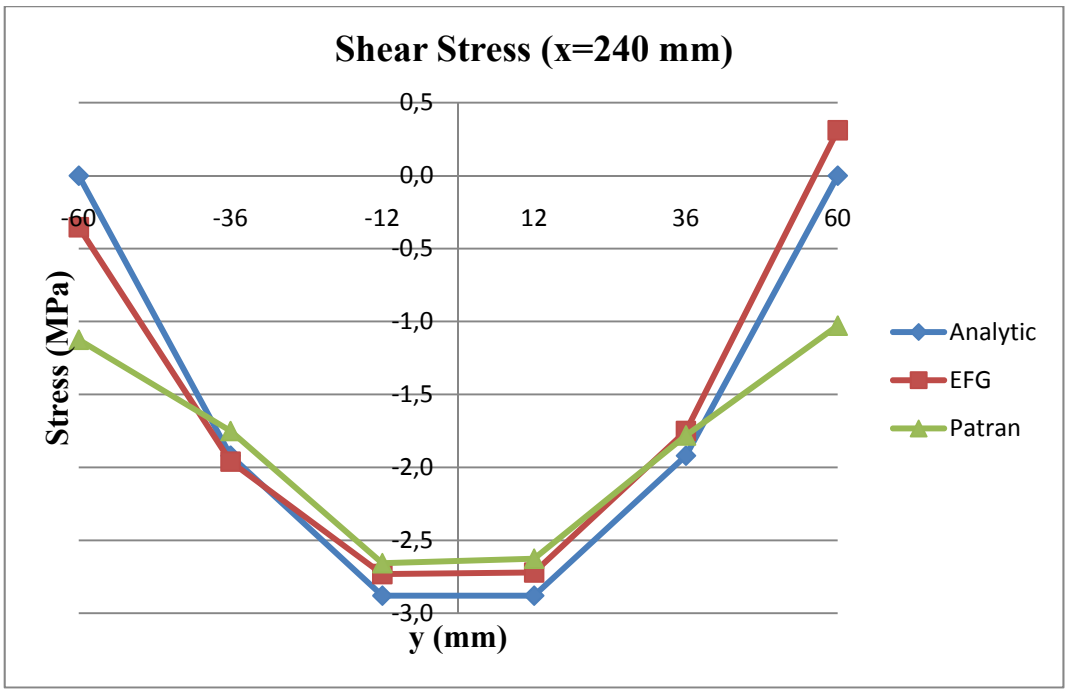

Figure 4.2.11 Graphical comparison of σ_{xy} results

For the third run, the same problem is solved by using the previous background mesh but increasing the number of integration points. There are 200 elements in the background mesh. The nodes are defined at the center and vertices of each element and thirteen Gauss integration points are used for each element.

Table 4.2.7 and Figure 4.2.12 show the displacement results in y direction calculated by EFG program, finite element method and analytical method;

Table 4.2.7 Comparison of the displacements in y direction

x	y	v Analytic	v EFG	Error %
0	-60	0.000	0.000	0.000
0	-36	0.000	0.000	0.000
0	-12	0.000	0.000	0.000
0	12	0.000	0.000	0.000
0	36	0.000	0.000	0.000
0	60	0.000	0.000	0.000
240	-60	-0.082	-0.089	8.182
240	-36	-0.082	-0.089	7.828
240	-12	-0.082	-0.088	7.674
240	12	-0.082	-0.088	7.733
240	36	-0.082	-0.089	8.011
240	60	-0.082	-0.089	8.485
480	-60	-0.230	-0.238	3.230
480	-36	-0.230	-0.238	3.230
480	-12	-0.230	-0.238	3.236
480	12	-0.230	-0.238	3.260
480	36	-0.230	-0.238	3.303
480	60	-0.230	-0.238	3.355

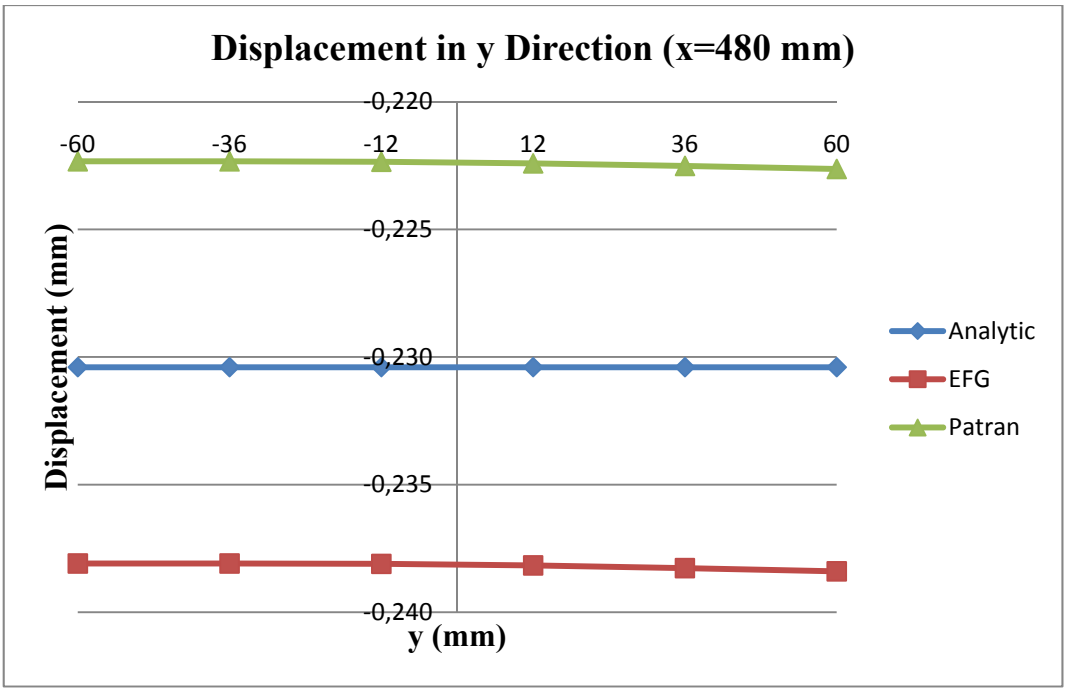

Figure 4.2.12 Graphical comparison of displacements in y direction

Table 4.2.8, Figure 4.2.13 and Figure 4.2.14 show the σ_x results calculated by EFG program, finite element method and analytical method;

Table 4.2.8 Comparison the σ_x results

x	y	σx Analytic	σx EFG	Error %
0	-60	-48.000	-43.539	9.294
0	-36	-28.800	-25.938	9.936
0	-12	-9.600	-8.338	13.146
0	12	9.600	9.262	3.517
0	36	28.800	26.863	6.726
0	60	48.000	44.463	7.368
240	-60	-12.000	-11.851	1.245
240	-36	-7.200	-7.324	1.692
240	-12	-2.400	-2.399	0.050
240	12	2.400	2.353	1.956
240	36	7.200	7.562	4.791
240	60	12.000	11.654	2.883
480	-60	0.000	0.087	100.000
480	-36	0.000	-0.007	100.000
480	-12	0.000	0.057	100.000
480	12	0.000	-0.060	100.000
480	36	0.000	0.025	100.000
480	60	0.000	-0.041	100.000

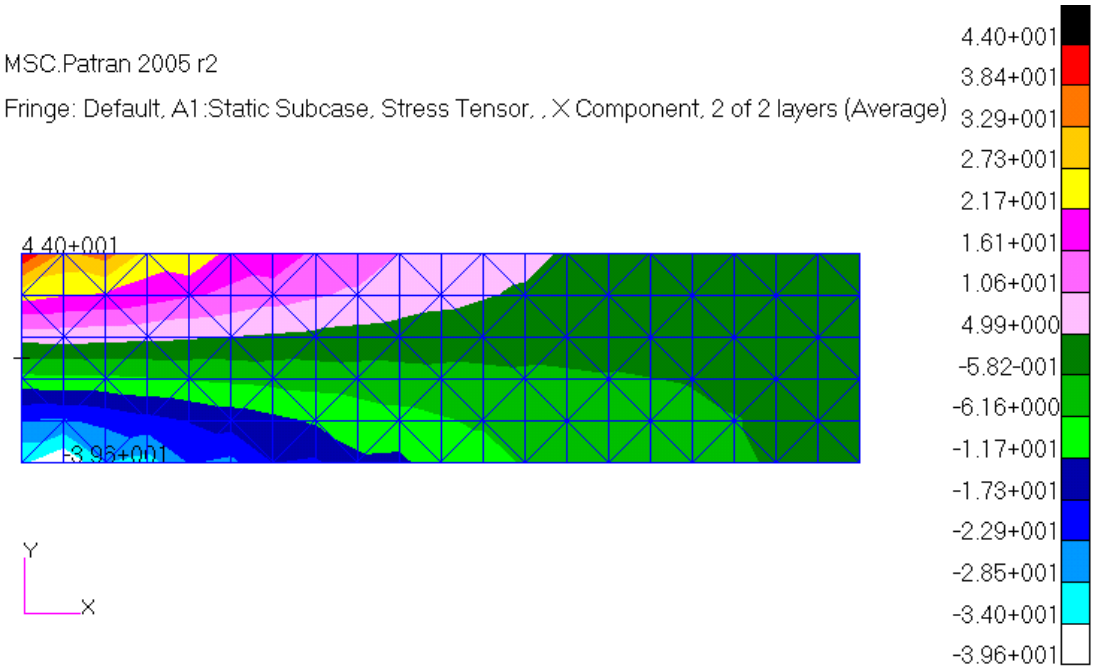

Figure 4.2.13 σ_x distribution obtained by Patran/Nastran

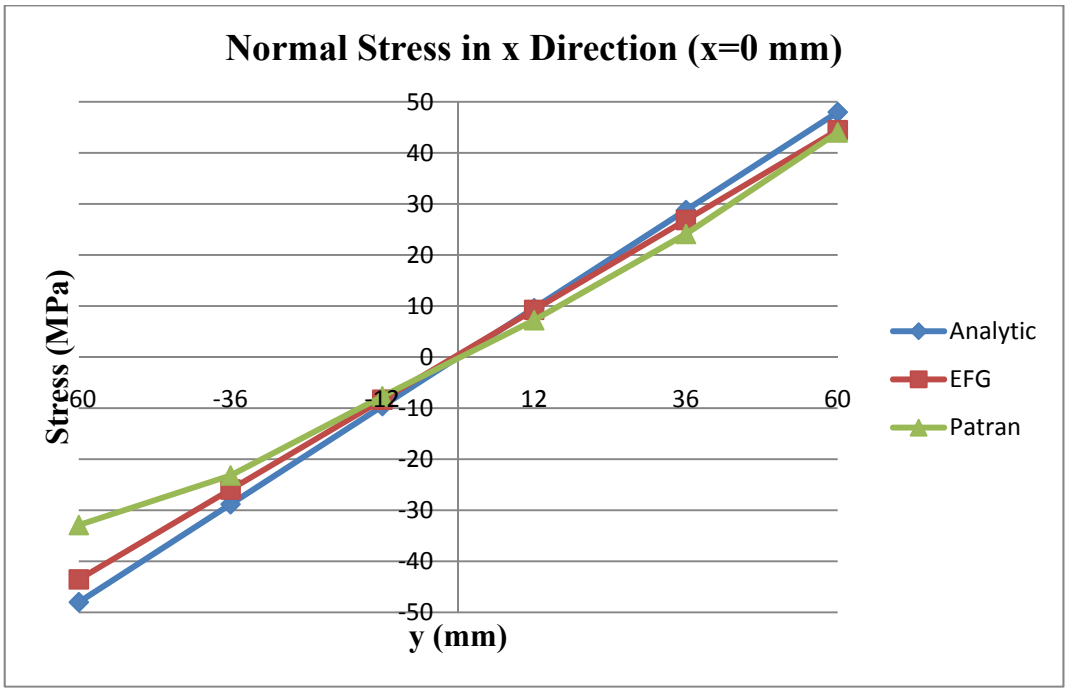

Figure 4.2.14 Graphical comparison of σ_x results

Table 4.2.9, Figure 4.2.15 and Figure 4.2.16 show the σ_{xy} results calculated by EFG program, finite element method and analytical method;

Table 4.2.9 Comparison of the σ_{xy} results

x	y	σxy Analytic	σxy EFG	Error %
0	-60	0.000	-2.493	100.000
0	-36	-3.840	-2.605	32.149
0	-12	-5.760	-2.718	52.813
0	12	-5.760	-2.831	50.859
0	36	-3.840	-2.943	23.359
0	60	0.000	-3.056	100.000
240	-60	0.000	-0.203	100.000
240	-36	-1.920	-1.972	2.619
240	-12	-2.880	-2.982	3.415
240	12	-2.880	-2.839	1.408
240	36	-1.920	-1.804	6.016
240	60	0.000	0.020	100.000
480	-60	0.000	0.059	100.000
480	-36	0.000	-0.009	100.000
480	-12	0.000	-0.005	100.000
480	12	0.000	-0.037	100.000
480	36	0.000	-0.044	100.000
480	60	0.000	0.023	100.000

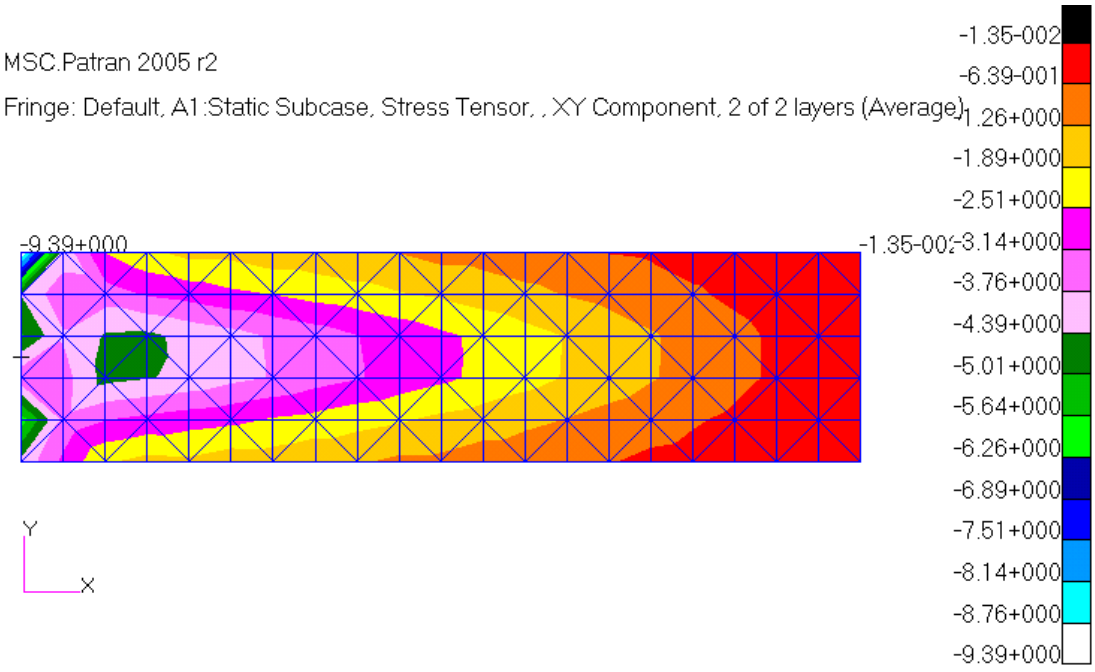

Figure 4.2.15 σ_{xy} distribution obtained by Patran/Nastran

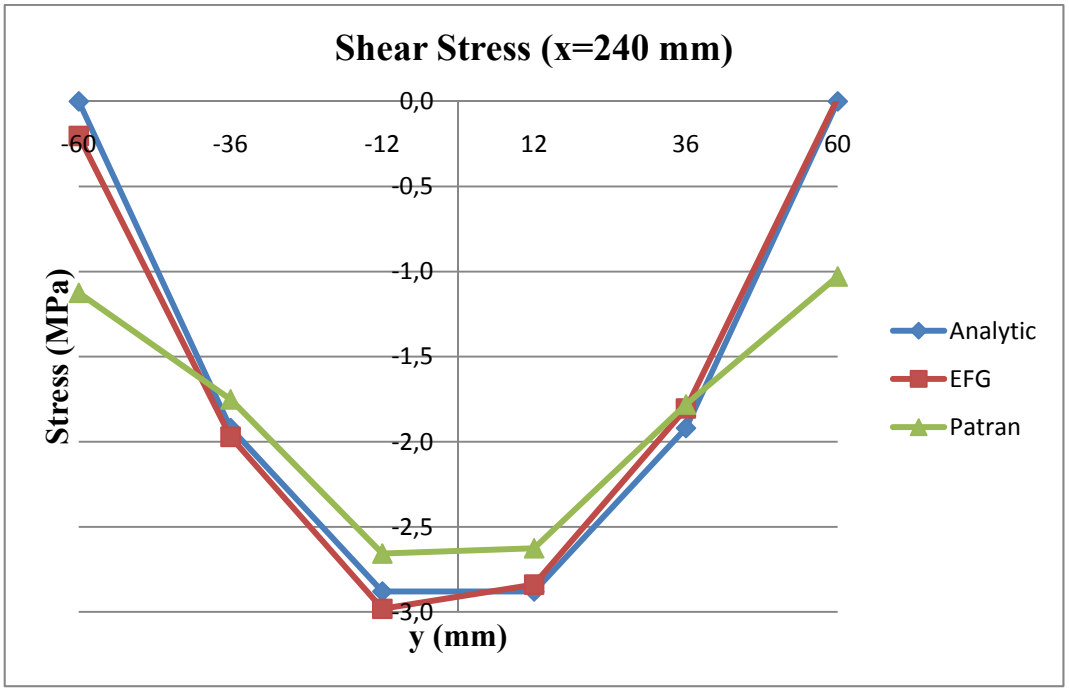

Figure 4.2.16 Graphical comparison of σ_{xy} results

The results obtained from the different EFG solutions are compared. Table 4.2.10 and Figure 4.2.17 show the displacement results in y direction calculated by analytical method and EFG program runs 1, 2 and 3;

Table 4.2.10 Comparison of the displacements in y direction

x	y	v Analytic	v EFG run 1	v EFG run 2	v EFG run 3
480	-60	-0.230	-0.242	-0.242	-0.238
480	-36	-0.230	-0.242	-0.242	-0.238
480	-30	-0.230	-0.242	-0.242	-0.238
480	-12	-0.230	-0.242	-0.242	-0.238
480	0	-0.230	-0.242	-0.242	-0.238
480	12	-0.230	-0.242	-0.242	-0.238
480	30	-0.230	-0.242	-0.242	-0.238
480	36	-0.230	-0.242	-0.242	-0.238
480	60	-0.230	-0.242	-0.242	-0.238

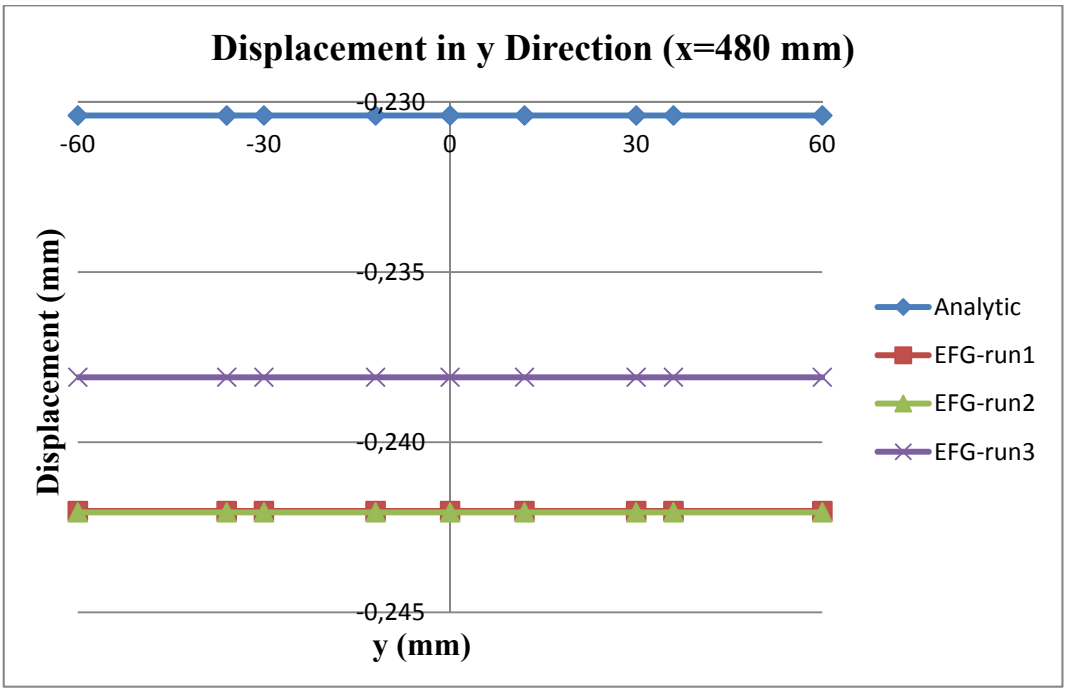

Figure 4.2.17 Graphical comparison of displacements in y direction

Table 4.2.11 and Figure 4.2.18 show the σ_x results calculated by analytic method and EFG program runs 1, 2 and 3;

Table 4.2.11 Comparison of the σ_x results

x	y	σx Analytic	σx EFG run 1	σx EFG run 2	σx EFG run 3
0	-60	-48.000	-44.663	-47.493	-43.539
0	-36	-28.800	-27.050	-30.577	-25.938
0	-30	-24.000	-22.534	-26.200	-21.538
0	-12	-9.600	-8.876	-11.388	-8.338
0	0	0.000	0.727	-0.621	0.462
0	12	9.600	10.555	10.325	9.262
0	30	24.000	24.459	25.807	22.463
0	36	28.800	29.139	30.371	26.863
0	60	48.000	47.720	48.374	44.463

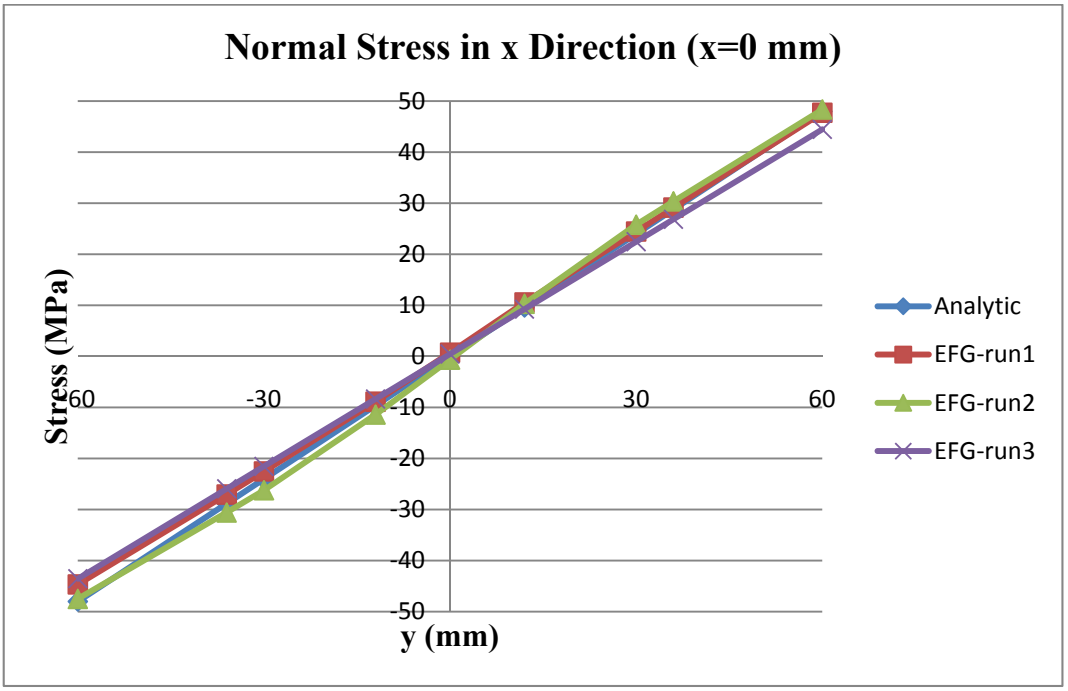

Figure 4.2.18 Graphical comparison of σ_x results

Table 4.2.12 and Figure 4.2.19 show the σ_{xy} results calculated by analytical method and EFG program runs 1, 2 and 3;

Table 4.2.12 Comparison of the σ_{xy} results

x	y	σxy Analytic	σxy EFG run 1	σxy EFG run 2	σxy EFG run 3
240	-60	0.000	-0.025	-0.354	-0.203
240	-36	-1.920	-2.086	-1.961	-1.972
240	-30	-2.250	-2.422	-2.488	-2.093
240	-12	-2.880	-2.880	-2.731	-2.982
240	0	-3.000	-2.881	-2.957	-3.047
240	12	-2.880	-2.887	-2.721	-2.839
240	30	-2.250	-2.458	-2.187	-2.311
240	36	-1.920	-2.092	-1.751	-1.804
240	60	0.000	-0.080	0.311	0.020

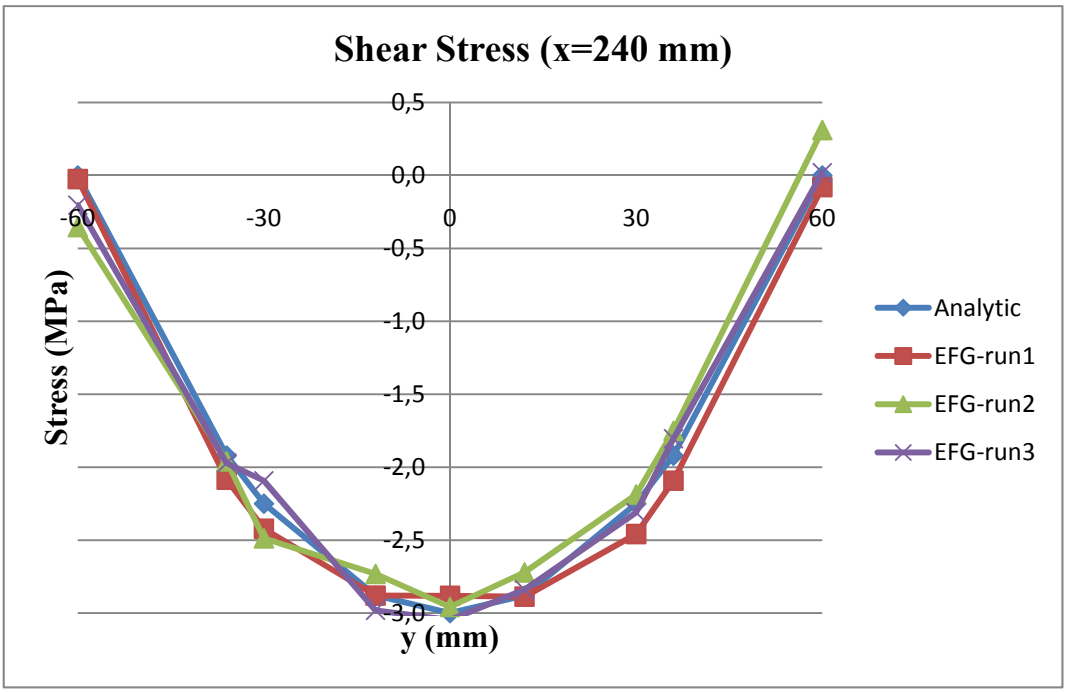

Figure 4.2.19 Graphical comparison of σ_{xy} results

4.3. A Square Plate with Hole under Uniform Distributed Load at both sides

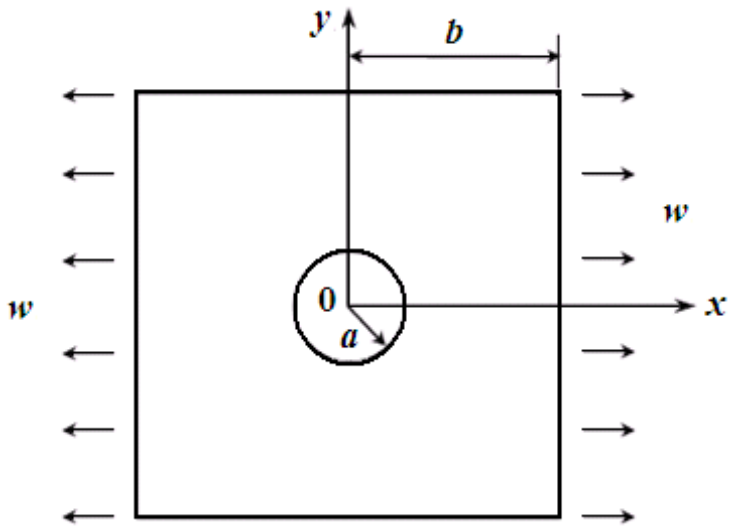

Figure 4.3.1 A square plate with hole subjected to uniform distributed side loading

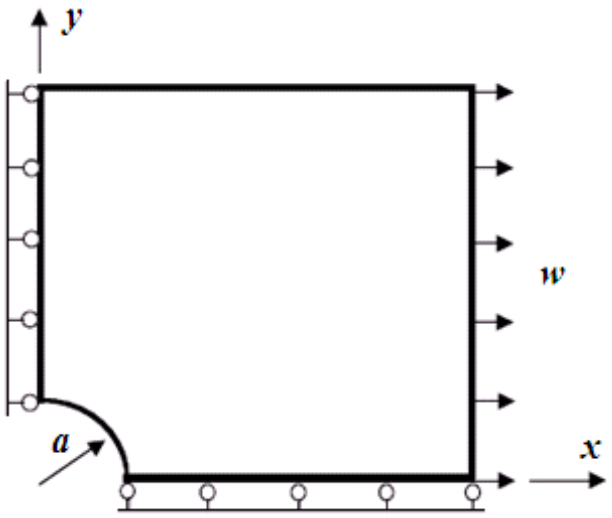

Figure 4.3.2 Geometry reduction and boundary condition application

In this example, the properties for this cantilever beam are taken as follows:

Loading: $w = 100$ N/mm

Young's modulus: $E = 200000$ N/mm^2

Poisson's ratio: $v = 0.3$

Height of the plate: $a = 100$ mm

Length of the plate: $b = 600$ mm

For the first run of the example, there are 750 elements in the background mesh. The nodes are defined at the center and vertices of each element and seven Gauss integration points are used for each element.

Table 4.3.1 and Figure 4.3.3 show the displacement results in x direction calculated by EFG program and finite element method;

Table 4.3.1 Comparison of the displacements in x direction

x	y	u EFG	u Patran	Error %
0	100	0.000	0.000	0.000
0	200	0.000	0.000	0.000
0	300	0.000	0.000	0.000
0	419	0.000	0.000	0.000
0	600	0.000	0.000	0.000
38	92	0.061	0.060	2.325
71	71	0.114	0.111	2.024
92	38	0.150	0.147	1.812
100	0	0.161	0.160	0.389
200	0	0.176	0.174	1.261
300	0	0.209	0.207	0.739
419	0	0.260	0.258	0.638
600	0	0.347	0.344	0.904
200	600	0.093	0.092	0.224
400	600	0.191	0.191	0.114
600	200	0.334	0.332	0.538
600	400	0.312	0.311	0.457
600	600	0.292	0.291	0.279

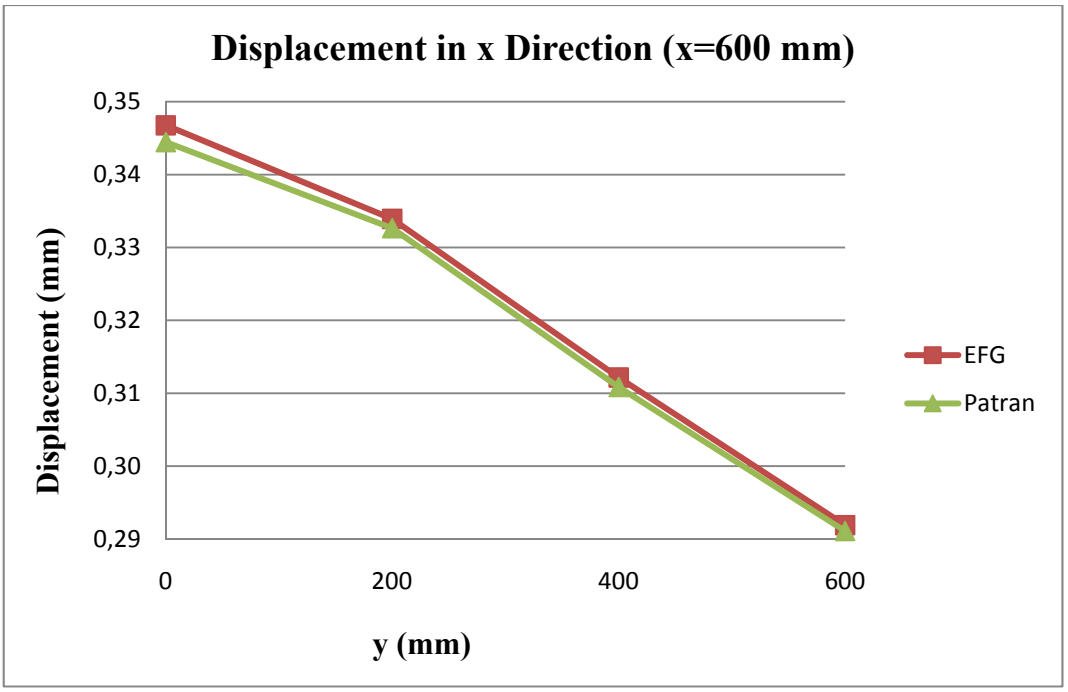

Figure 4.3.3 Graphical comparison of displacements in x direction

Table 4.3.2 and Figure 4.3.4 show the displacement results in y direction calculated by EFG program and finite element method;

Table 4.3.2 Comparison of the displacements in y direction

x	y	v EFG	v Patran	Error %
0	100	-0.059	-0.059	0.097
0	200	-0.070	-0.069	2.160
0	300	-0.078	-0.077	0.885
0	419	-0.092	-0.092	0.630
0	600	-0.117	-0.117	0.558
38	92	-0.055	-0.053	4.660
71	71	-0.042	-0.040	4.522
92	38	-0.022	-0.021	3.555
100	0	0.000	0.000	0.000
200	0	0.000	0.000	0.000
300	0	0.000	0.000	0.000
419	0	0.000	0.000	0.000
600	0	0.000	0.000	0.000
200	600	-0.108	-0.107	0.736
400	600	-0.090	-0.090	0.379
600	200	-0.015	-0.015	2.242
600	400	-0.040	-0.041	0.923
600	600	-0.071	-0.071	0.138

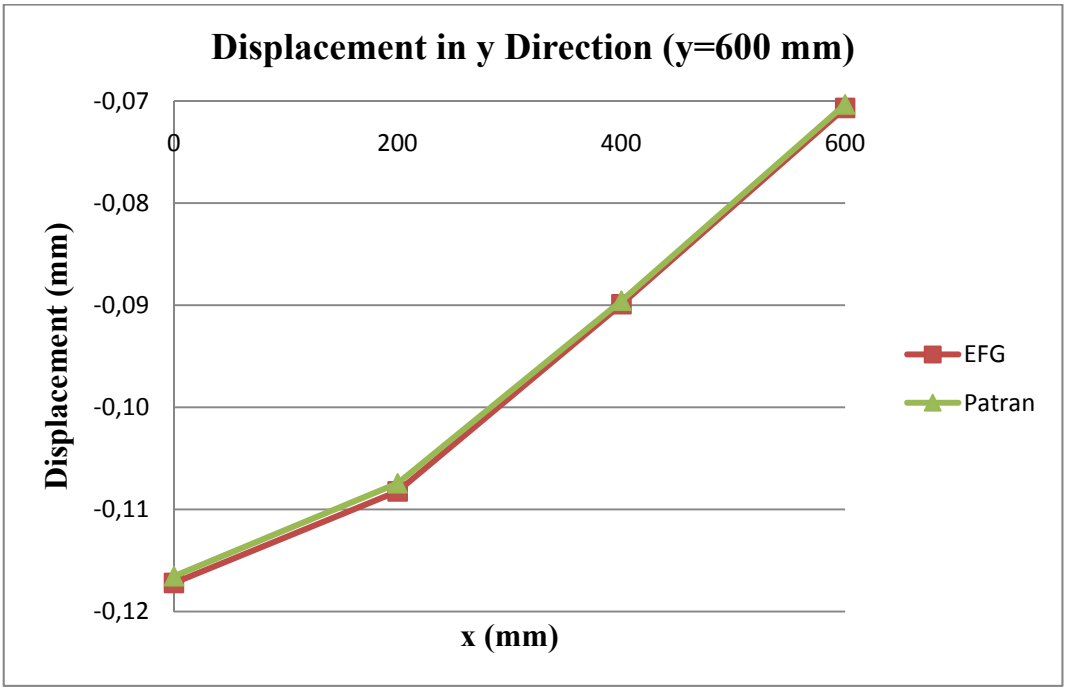

Figure 4.3.4 Graphical comparison of displacements in y direction

Table 4.3.3, Figure 4.3.5 and Figure 4.3.6 show the σ_x results calculated by EFG program and finite element method;

Table 4.3.3 Comparison of the σ_x results

x	y	σx EFG	σx Patran	Error %
0	100	308.088	273.014	11.384
0	200	137.120	129.397	5.632
0	300	108.702	110.265	1.417
0	419	107.067	102.708	4.071
0	600	107.937	90.674	15.993
38	92	232.062	212.423	8.463
71	71	61.277	93.460	34.436
92	38	-6.490	14.339	145.263
100	0	0.051	-1.611	103.185
200	0	54.016	49.824	7.761
300	0	80.108	80.662	0.687
419	0	93.836	93.196	0.682
600	0	115.063	99.471	13.551
200	600	92.170	96.440	4.428
400	600	99.740	100.052	0.312
600	200	115.387	100.012	13.325
600	400	95.312	100.091	4.774
600	600	100.863	99.974	0.882

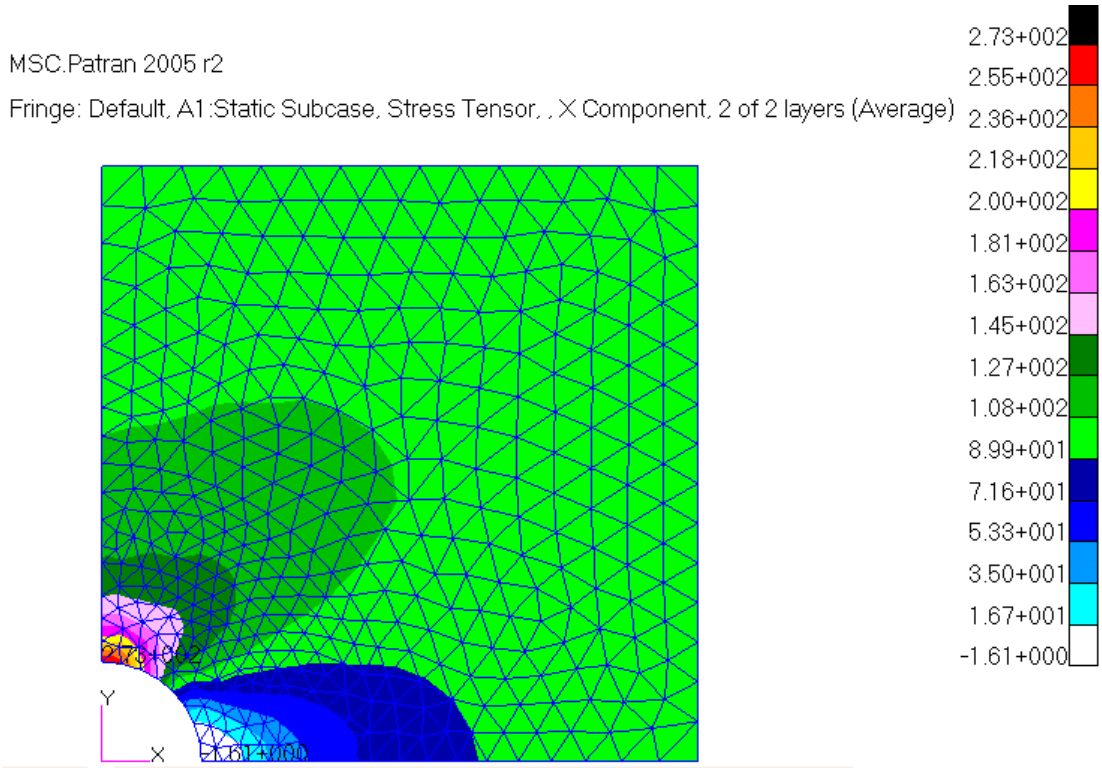

Figure 4.3.5 σ_x distribution obtained by Patran/Nastran

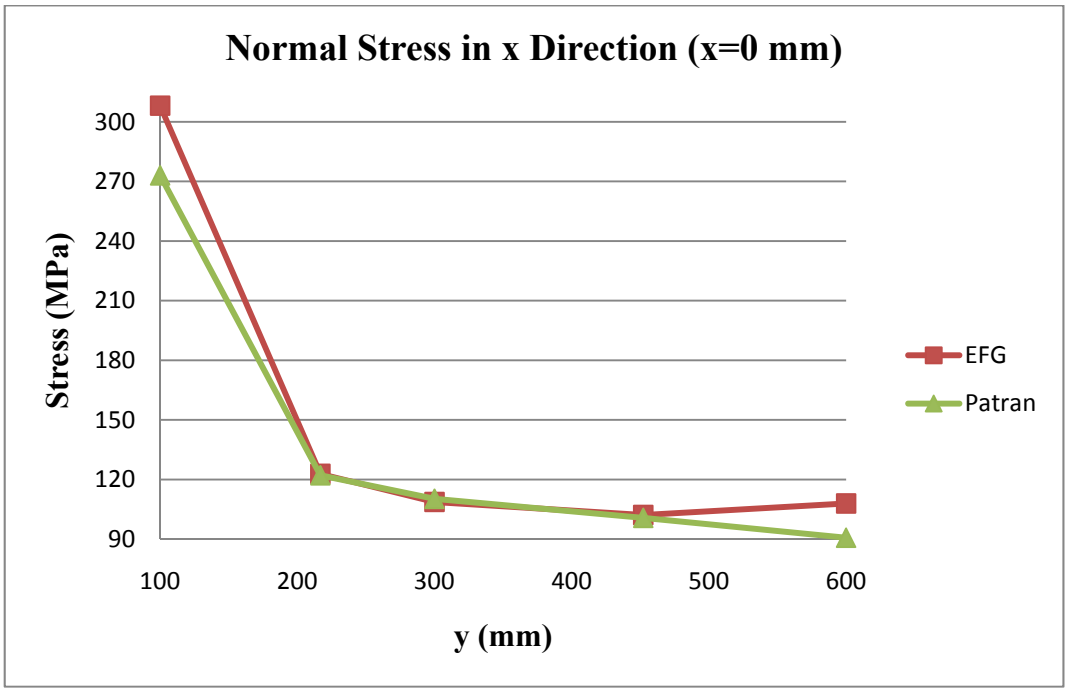

Figure 4.3.6 Graphical comparison of the σ_x results

Table 4.3.4, Figure 4.3.7 and Figure 4.3.8 show the σ_y results calculated by EFG program and finite element method;

Table 4.3.4 Comparison of the σ_y results

x	y	σy EFG	σy Patran	Error %
0	100	36.649	30.309	17.299
0	200	30.086	26.958	10.396
0	300	12.619	11.354	10.025
0	419	5.725	4.092	28.520
0	600	1.093	0.463	57.677
38	92	46.798	30.273	35.312
71	71	44.705	22.018	50.747
92	38	-55.246	-44.533	19.392
100	0	-78.871	-80.263	1.735
200	0	1.057	-0.800	175.757
300	0	4.848	2.804	42.155
419	0	5.694	5.551	2.517
600	0	23.295	17.551	24.655
200	600	0.050	-0.044	186.667
400	600	-0.046	-0.047	2.507
600	200	13.212	8.805	33.357
600	400	0.011	0.871	98.760
600	600	0.060	-0.026	143.730

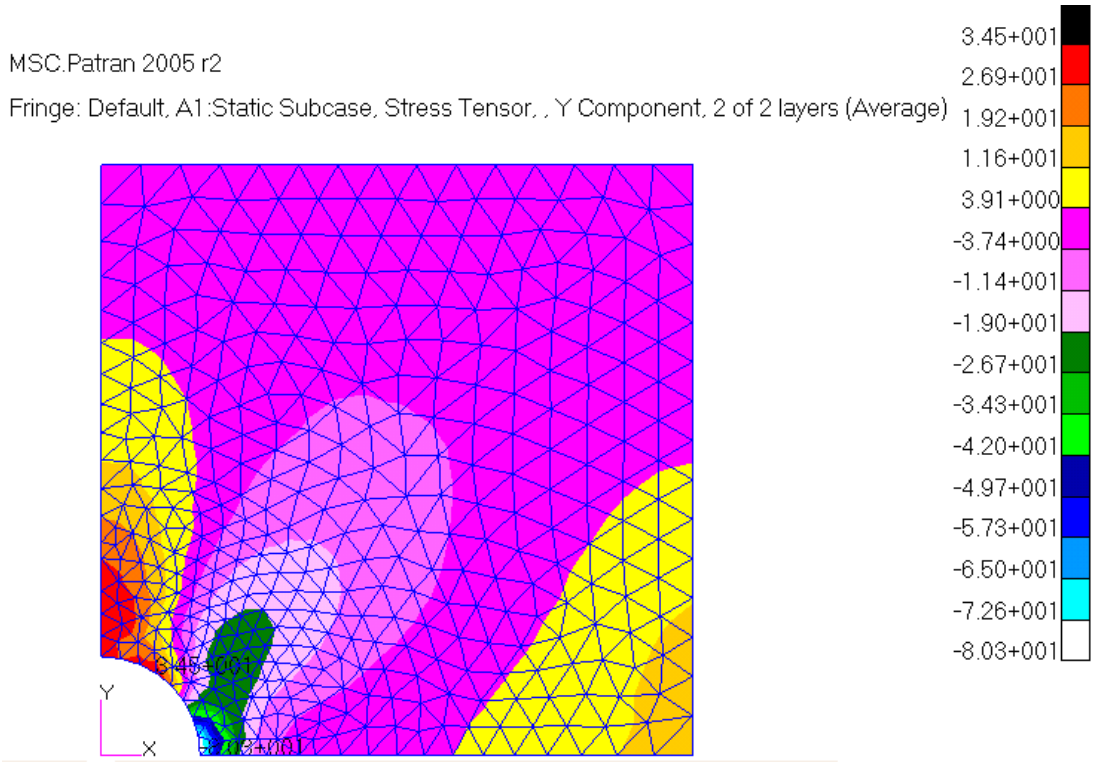

Figure 4.3.7 σ_y distribution obtained by Patran/Nastran

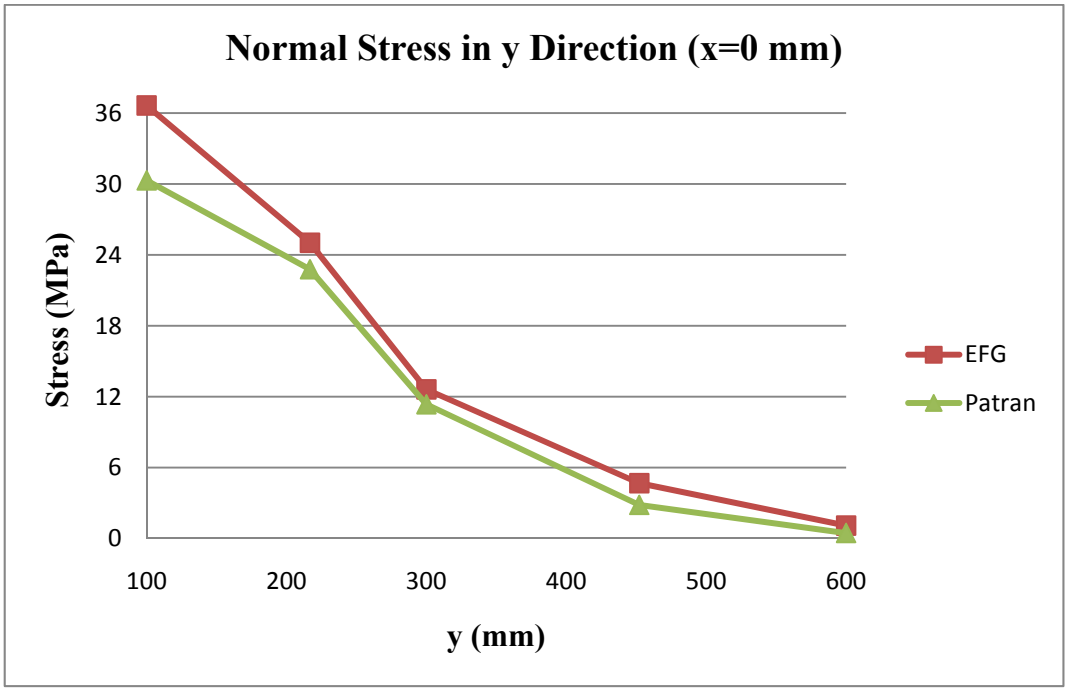

Figure 4.3.8 Graphical comparison of σ_y results

Table 4.3.5, Figure 4.3.9 and Figure 4.3.10 show the σ_{xy} results calculated by EFG program and finite element method;

Table 4.3.5 Comparison of the σ_{xy} results

x	y	σxy EFG	σxy Patran	Error %
0	100	-6.220	-13.622	54.339
0	200	0.136	2.207	93.837
0	300	-0.207	1.427	114.524
0	419	-0.340	0.820	141.509
0	600	0.840	0.470	44.054
38	92	-93.010	-53.167	42.837
71	71	-48.804	-44.783	8.240
92	38	21.435	-2.987	113.933
100	0	1.405	-1.245	188.575
200	0	-2.199	-4.377	49.767
300	0	2.157	-2.366	191.140
419	0	-4.737	-1.129	76.178
600	0	-5.134	-0.537	89.536
200	600	0.056	0.674	91.756
400	600	-0.915	0.043	104.651
600	200	0.011	-1.079	101.063
600	400	-0.439	-0.318	27.519
600	600	0.775	0.026	96.620

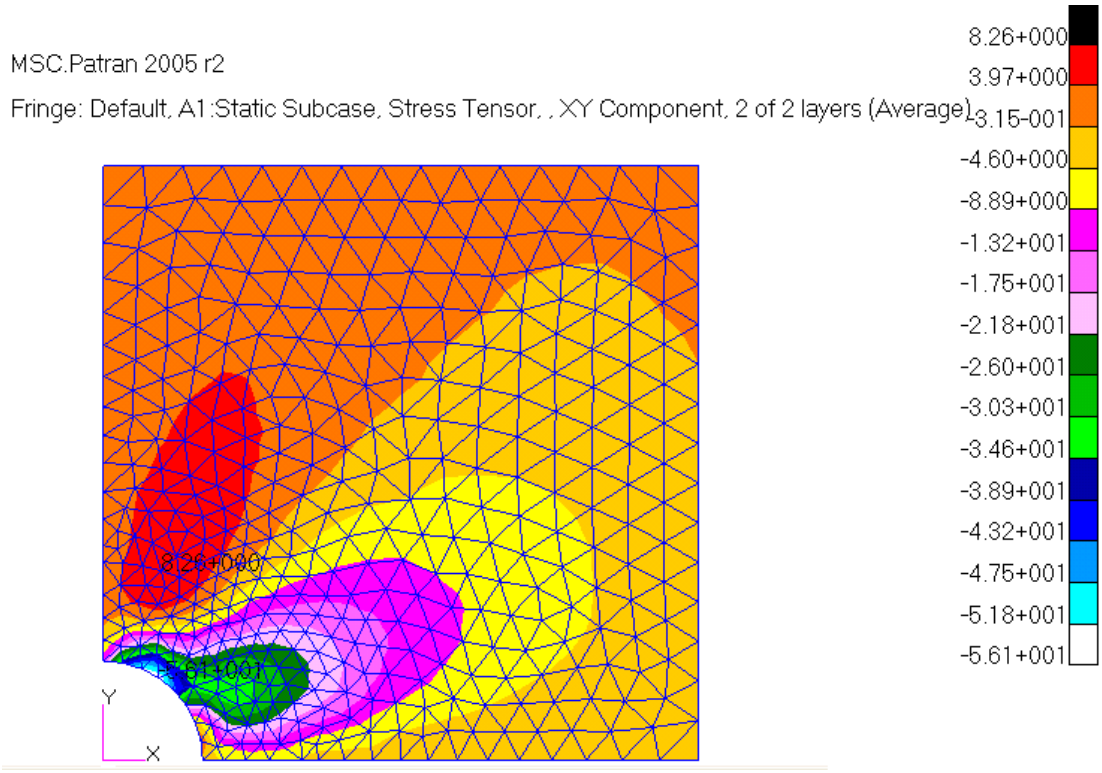

Figure 4.3.9 σ_{xy} distribution obtained by Patran/Nastran

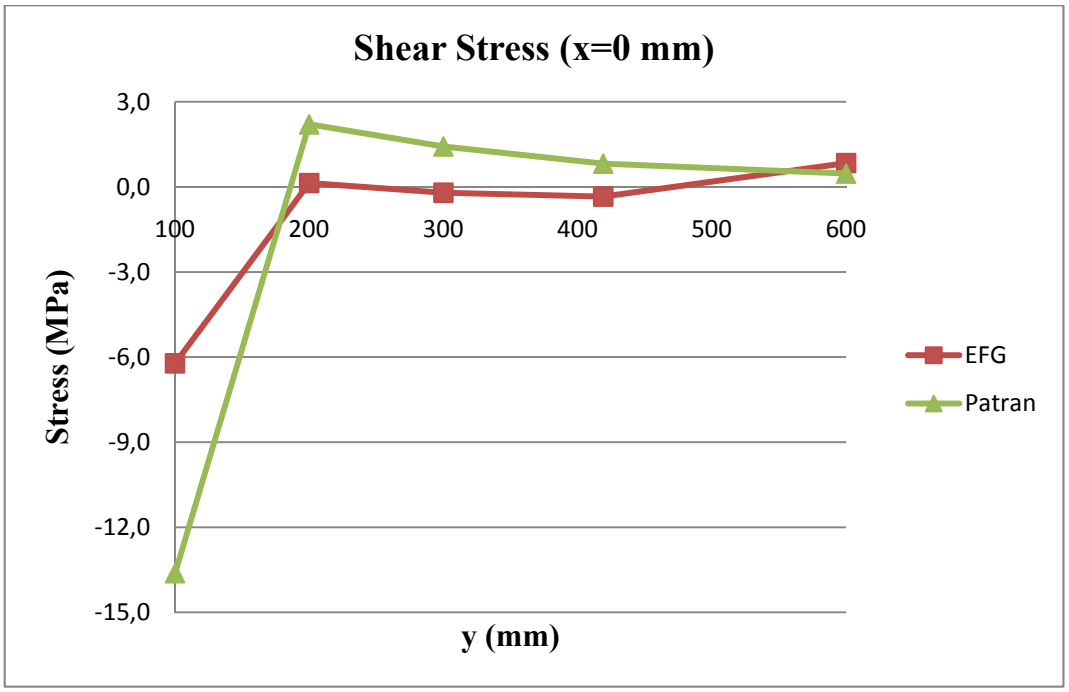

Figure 4.3.10 Graphical comparison of the σ_{xy} results

For the second run, the same problem is modeled by a more refined background mesh which has 1154 elements. The nodes are defined at the center and vertices of each element and seven Gauss integration points are used for each element. The background mesh, nodes and integration points used in this run are shown in Figure 4.3.11, Figure 4.3.12, Figure 4.3.13 and Figure 4.3.14;

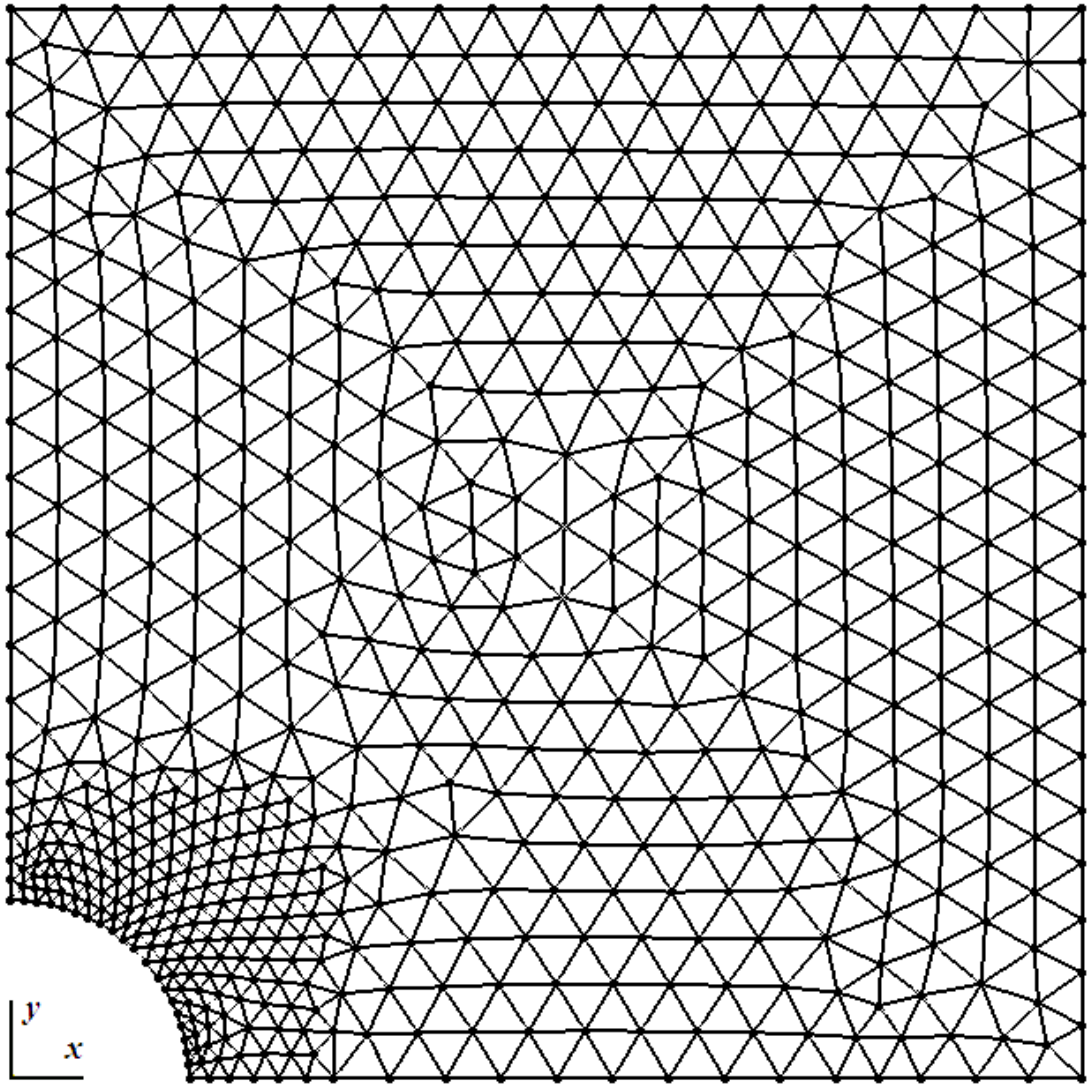

Figure 4.3.11 The background mesh distribution

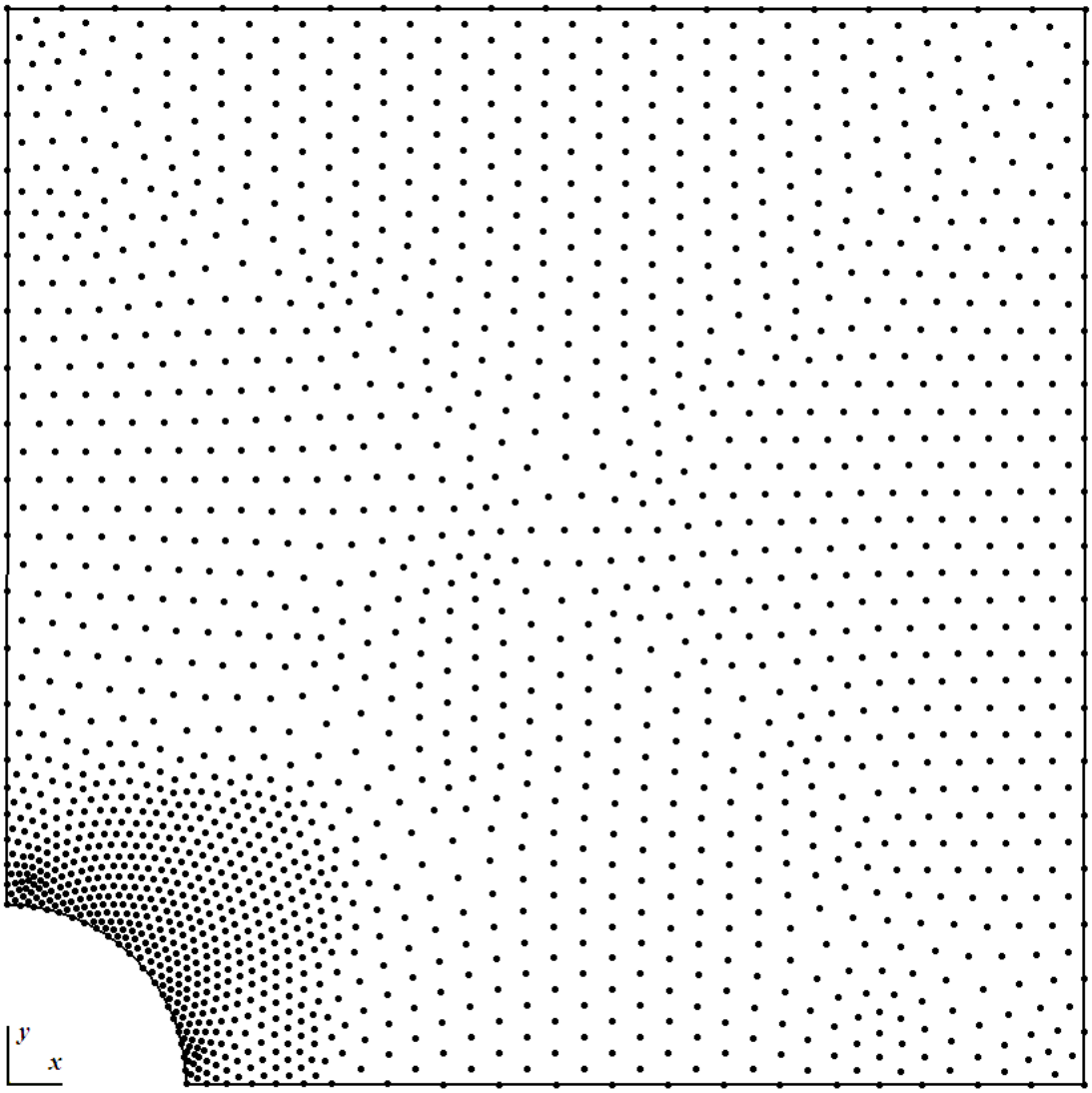

Figure 4.3.12 Node distribution in the problem domain

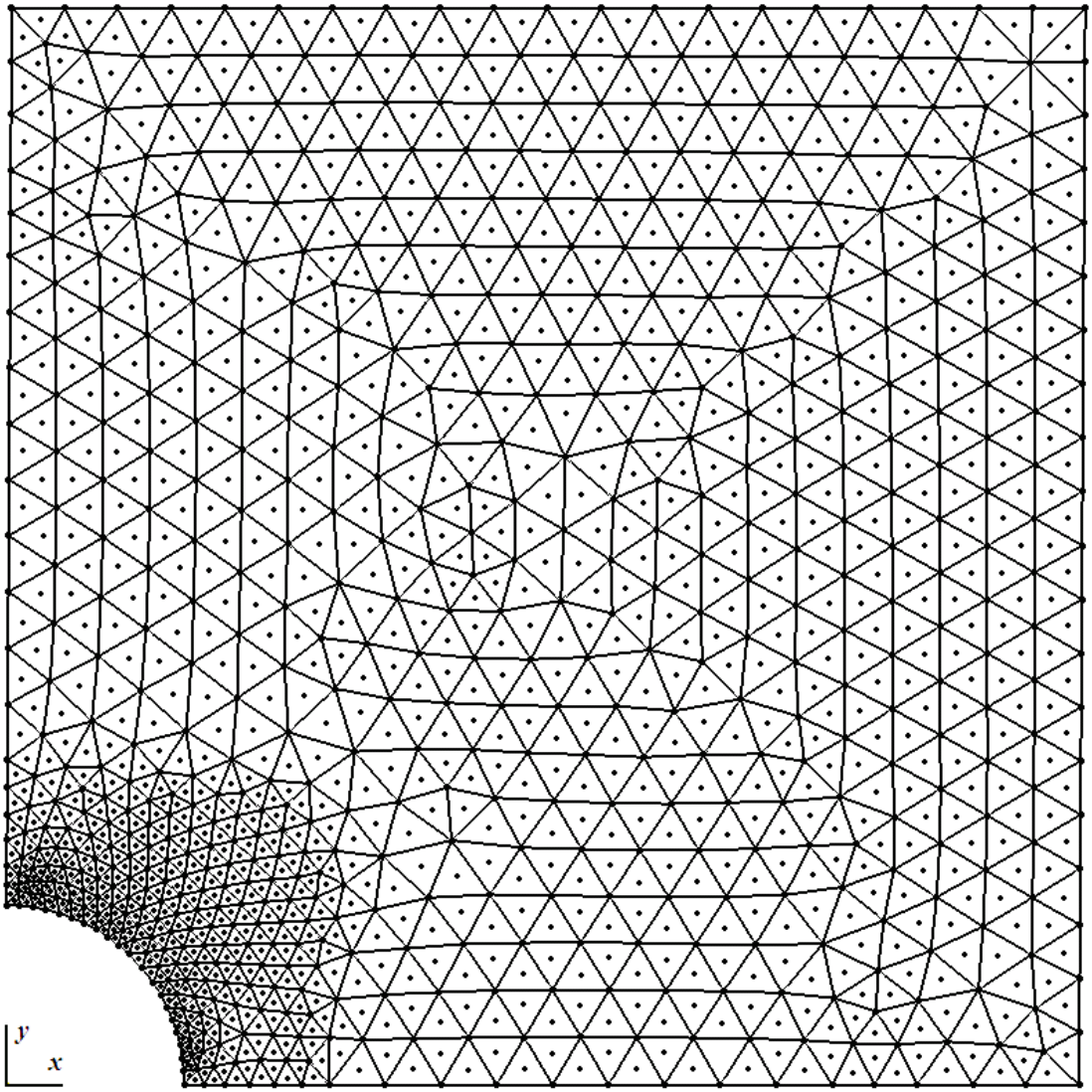

Figure 4.3.13 Node distribution on the background mesh

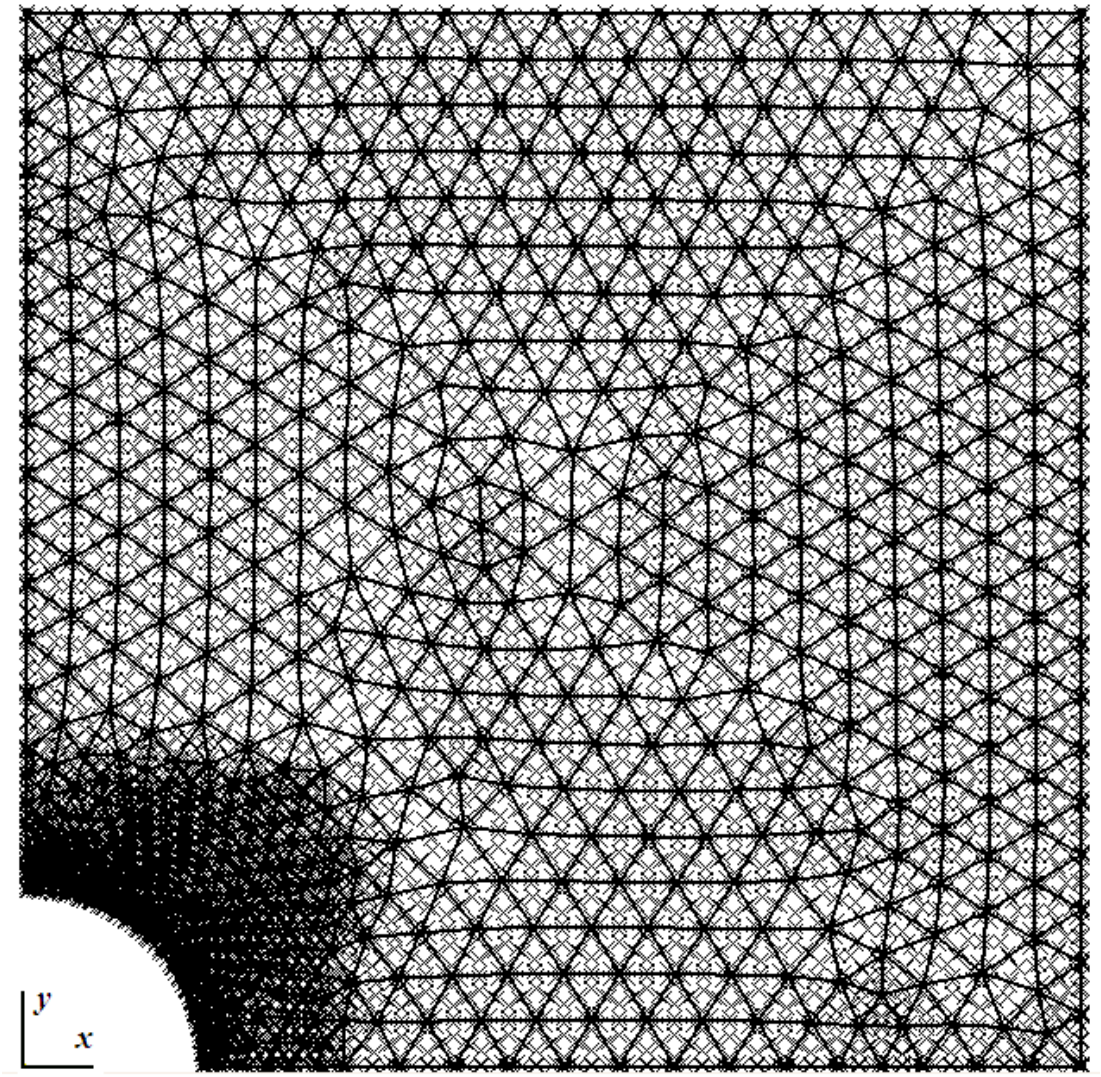

Figure 4.3.14 Node and integration point distribution on the background mesh

Table 4.3.6 and Figure 4.3.15 show the displacement results in x direction calculated by EFG program and finite element method;

Table 4.3.6 Comparison of the displacements in x direction

x	y	u EFG	u Patran	Error %
0	100	0.000	0.000	0.000
0	136	0.000	0.000	0.000
0	150	0.000	0.000	0.000
0	600	0.000	0.000	0.000
7	100	0.012	0.012	1.864
7	108	0.009	0.009	2.464
9	127	0.007	0.008	10.273
15	99	0.024	0.024	0.824
22	98	0.036	0.036	0.306
36	93	0.059	0.058	0.246
69	73	0.111	0.110	0.713
93	36	0.151	0.150	0.994
100	0	0.163	0.161	0.978
107	9	0.163	0.161	1.178
400	0	0.252	0.251	0.490
600	0	0.347	0.345	0.489
600	600	0.291	0.291	0.034

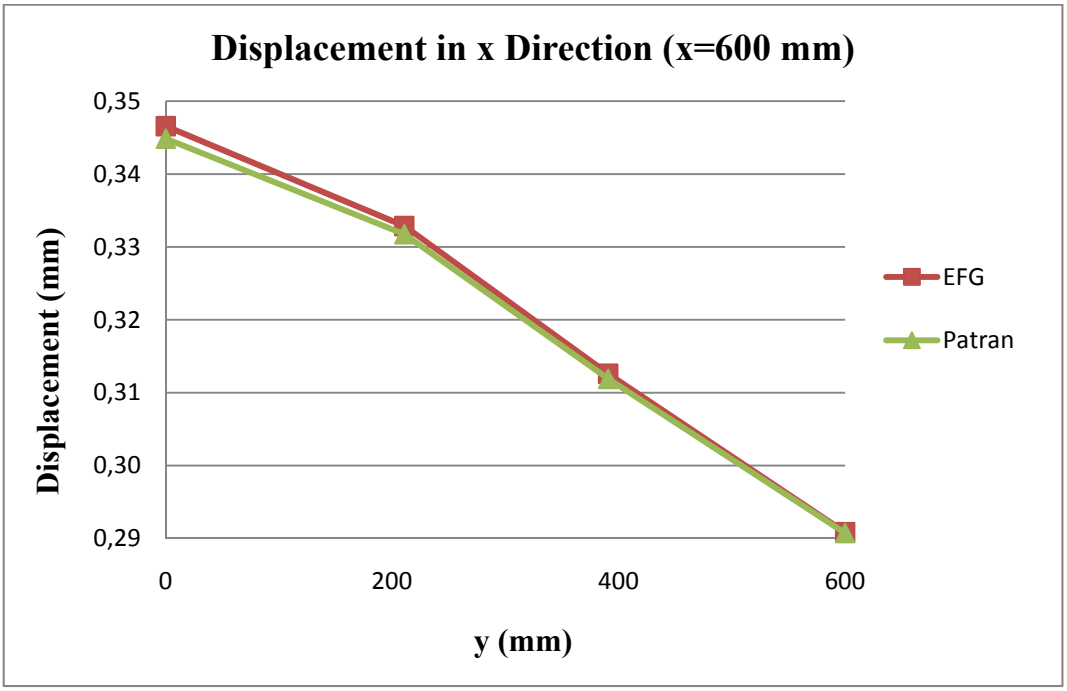

Figure 4.3.15 Graphical comparison of displacements in x direction

Table 4.3.7 and Figure 4.3.16 show the displacement results in y direction calculated by EFG program and finite element method;

Table 4.3.7 Comparison of the displacements in y direction

x	y	v EFG	v Patran	Error %
0	100	-0.061	-0.059	2.625
0	136	-0.068	-0.067	1.253
0	150	-0.068	-0.068	0.849
0	600	-0.118	-0.118	0.281
7	100	-0.060	-0.059	2.889
7	108	-0.064	-0.062	2.717
9	127	-0.067	-0.066	1.490
15	99	-0.060	-0.058	2.371
22	98	-0.059	-0.058	1.846
36	93	-0.056	-0.055	1.894
69	73	-0.044	-0.043	2.475
93	36	-0.022	-0.021	2.227
100	0	0.000	0.000	0.000
107	9	-0.004	-0.004	1.207
400	0	0.000	0.000	0.000
600	0	0.000	0.000	0.000
600	600	-0.070	-0.070	0.247

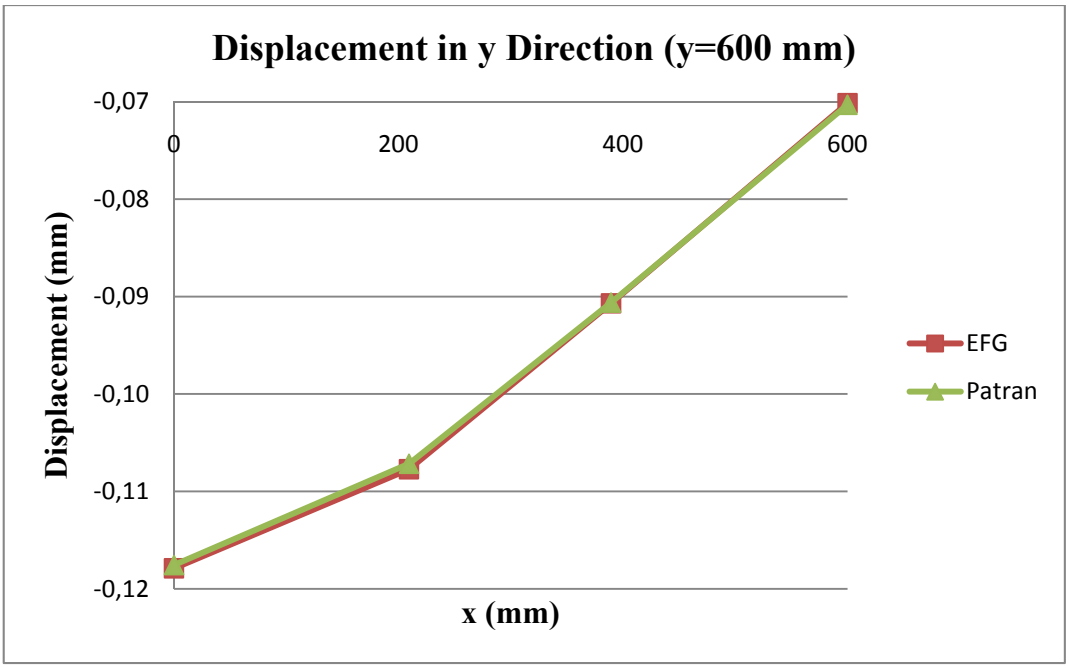

Figure 4.3.16 Graphical comparison of displacements in y direction

Table 4.3.8, Figure 4.3.17 and Figure 4.3.18 show the σ_x results calculated by EFG program and finite element method;

Table 4.3.8 Comparison of the σ_x results

x	y	σx EFG	σx Patran	Error %
0	100	288.623	296.044	2.506
0	136	170.358	184.966	7.898
0	150	149.669	163.198	8.290
0	600	87.434	90.801	3.709
7	100	317.162	303.290	4.374
7	108	240.912	270.965	11.091
9	127	161.576	198.814	18.730
15	99	312.711	292.198	6.560
22	98	284.121	274.073	3.537
36	93	231.082	226.493	1.986
69	73	46.500	76.158	38.942
93	36	-11.684	-0.888	92.402
100	0	-2.666	-6.361	58.091
107	9	-4.474	-3.278	26.728
400	0	91.782	91.537	0.267
600	0	101.341	99.833	1.488
600	600	104.392	99.993	4.214

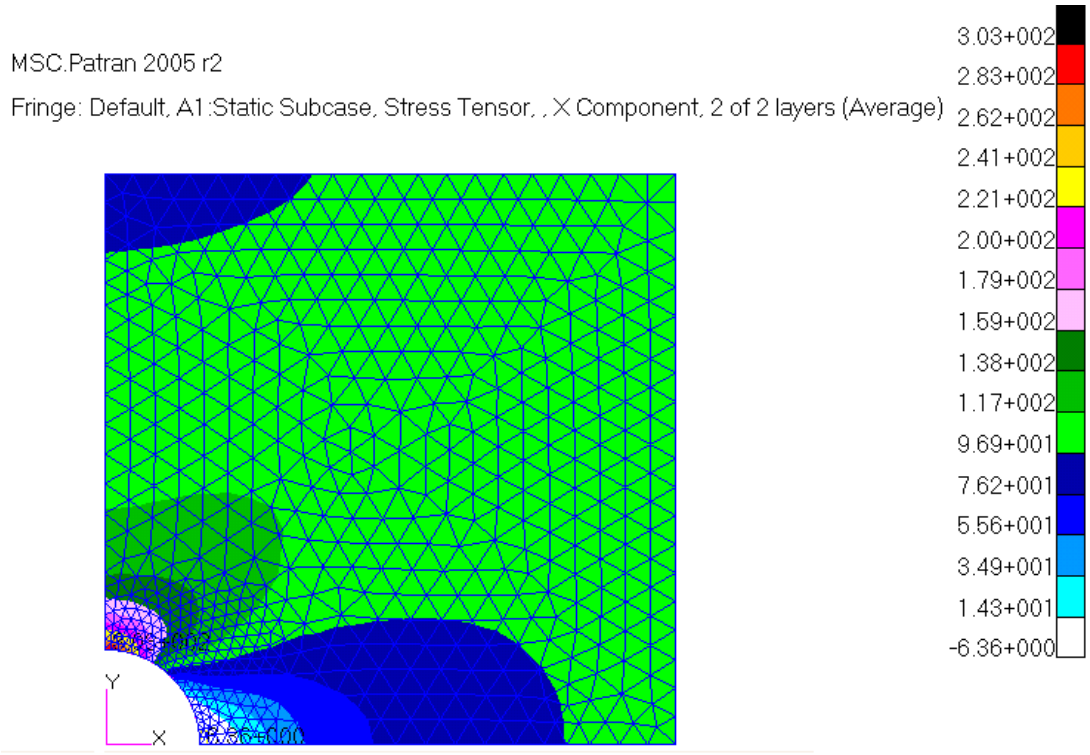

Figure 4.3.17 σx distribution obtained by Patran/Nastran

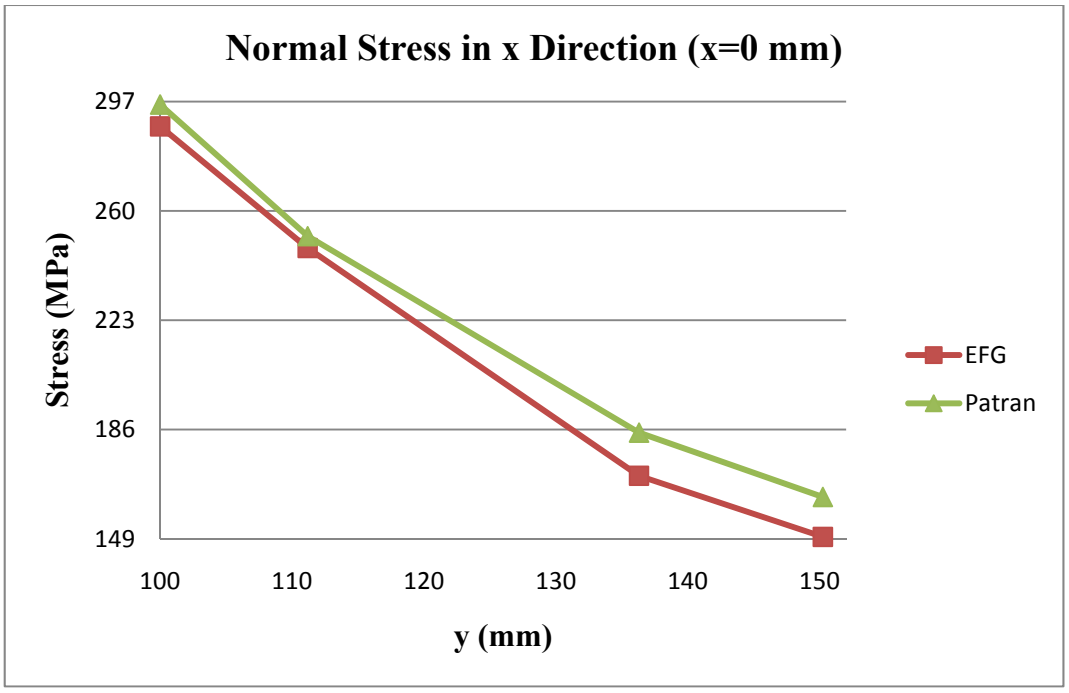

Figure 4.3.18 Graphical comparison of σ_x results

Table 4.3.9, Figure 4.3.19 and Figure 4.3.20 show the σ_y results calculated by EFG program and finite element method;

Table 4.3.9 Comparison of the σ_y results

x	y	σy EFG	σy Patran	Error %
0	100	-4.921	17.157	128.685
0	136	39.138	37.929	3.089
0	150	34.772	37.648	7.639
0	600	-0.314	0.121	138.473
7	100	6.912	14.645	52.803
7	108	22.016	20.073	8.824
9	127	32.786	36.190	9.407
15	99	13.177	17.706	25.577
22	98	10.843	23.480	53.819
36	93	35.076	36.343	3.487
69	73	59.125	38.058	35.632
93	36	-54.831	-52.861	3.592
100	0	-118.946	-98.600	17.105
107	9	-69.626	-82.446	15.550
400	0	6.908	4.948	28.369
600	0	18.198	17.617	3.193
600	600	-2.545	-0.006	99.776

Figure 4.3.19 σ_y distribution obtained by Patran/Nastran

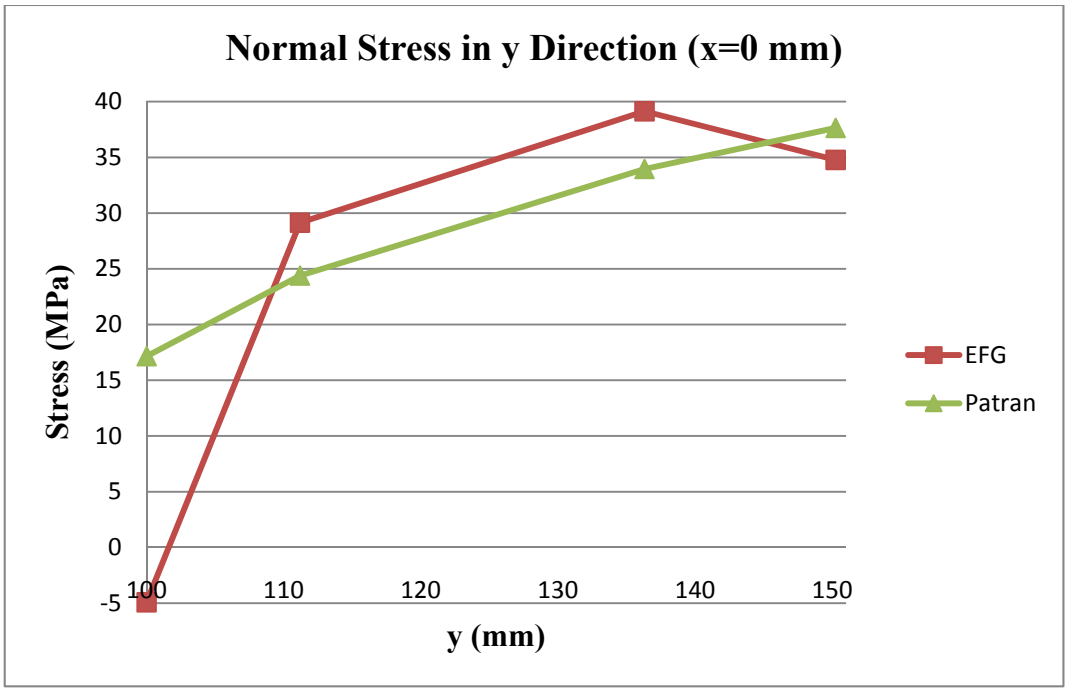

Figure 4.3.20 Graphical comparison of σ_y results

Table 4.3.10, Figure 4.3.21 and Figure 4.3.22 show the σ_{xy} results calculated by EFG program and finite element method;

Table 4.3.10 Comparison of the σ_{xy} results

x	y	σxy EFG	σxy Patran	Error %
0	100	-2.560	-6.967	63.253
0	136	-0.528	0.151	128.678
0	150	-3.013	1.484	149.240
0	600	-0.025	0.180	113.722
7	100	-31.573	-21.144	33.031
7	108	-31.333	-11.451	63.453
9	127	-11.086	-3.306	70.179
15	99	-49.999	-38.630	22.738
22	98	-61.570	-52.888	14.102
36	93	-88.430	-72.432	18.092
69	73	-61.406	-51.039	16.883
93	36	20.002	9.223	53.890
100	0	2.310	1.264	45.305
107	9	2.772	1.103	60.224
400	0	0.850	-1.144	174.345
600	0	-9.175	-0.238	97.411
600	600	2.330	0.023	99.007

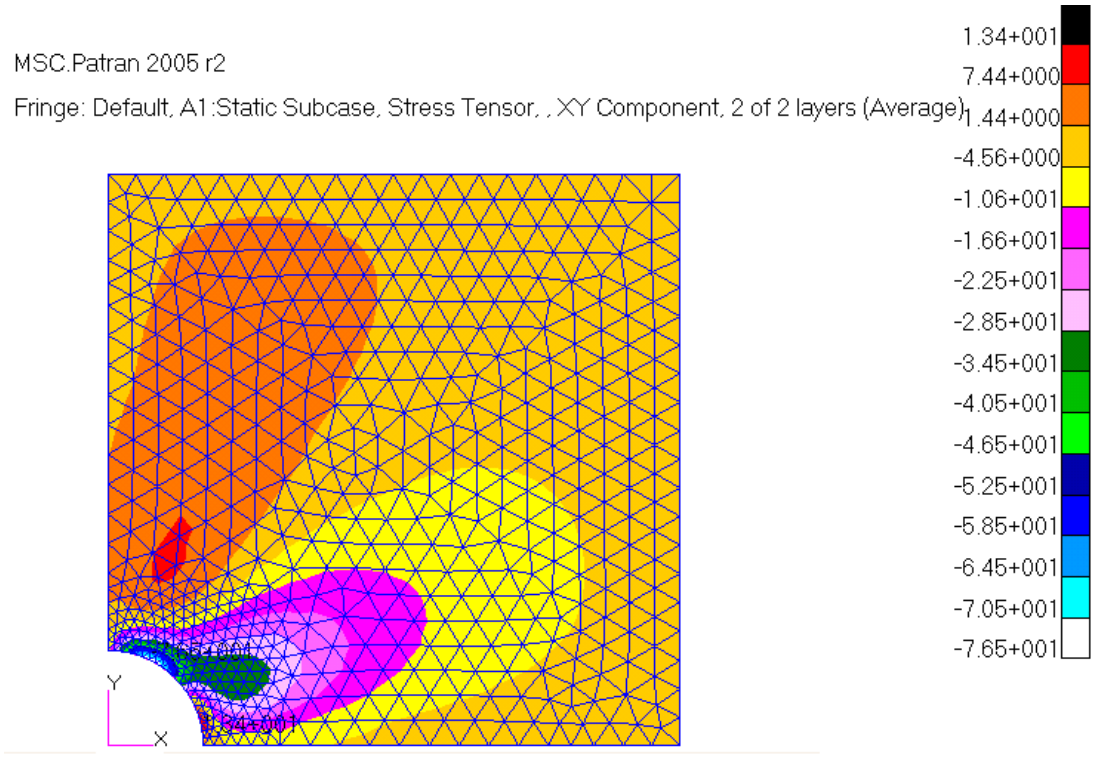

Figure 4.3.21 σ_{xy} distribution obtained by Patran/Nastran

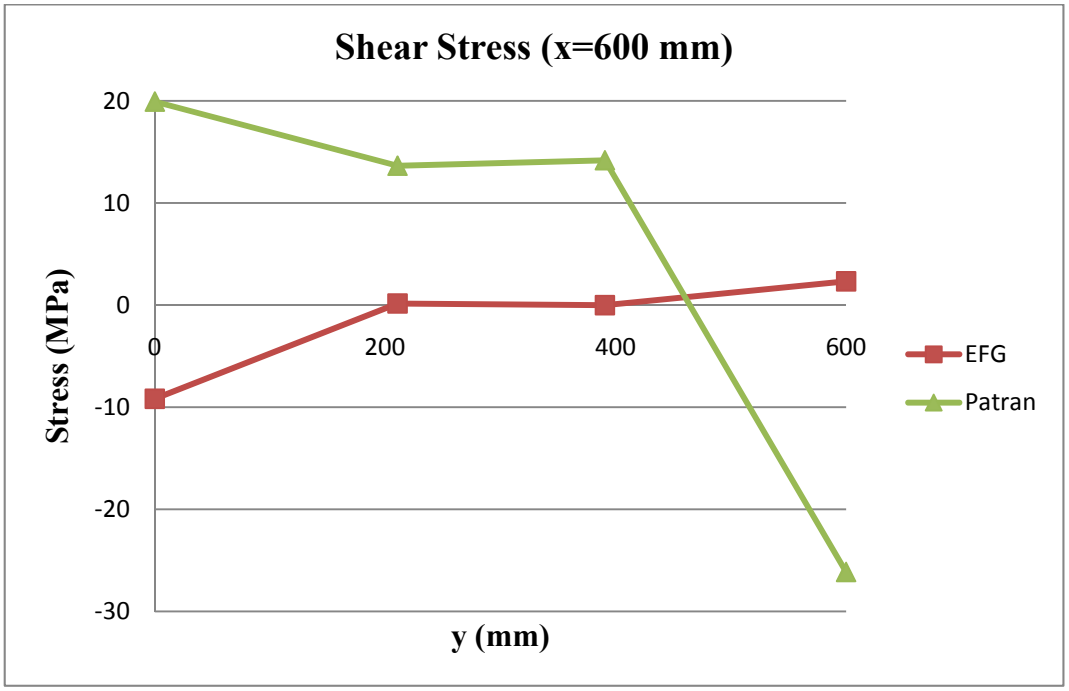

Figure 4.3.22 Graphical comparison of σ_{xy} results

For the third run, the same problem is solved by using the previous background mesh but increasing the number of integration points. There are 1154 elements in the background mesh. The nodes are defined at the center and vertices of each element and thirteen Gauss integration points are used for each element.

Table 4.3.11 and Figure 4.3.23 show the displacement results in x direction calculated by EFG program and finite element method;

Table 4.3.11 Comparison of the displacements in x direction

x	y	u EFG	u Patran	Error %
0	100	0.000	0.000	0.000
0	136	0.000	0.000	0.000
0	150	0.000	0.000	0.000
0	600	0.000	0.000	0.000
7	100	0.006	0.012	47.834
7	108	0.005	0.009	47.725
9	127	0.006	0.008	28.623
15	99	0.019	0.024	21.283
22	98	0.031	0.036	13.106
36	93	0.055	0.058	6.042
69	73	0.109	0.110	1.594
93	36	0.149	0.150	0.860
100	0	0.158	0.161	2.152
107	9	0.158	0.161	2.118
400	0	0.250	0.251	0.177
600	0	0.345	0.345	0.072
600	600	0.291	0.291	0.246

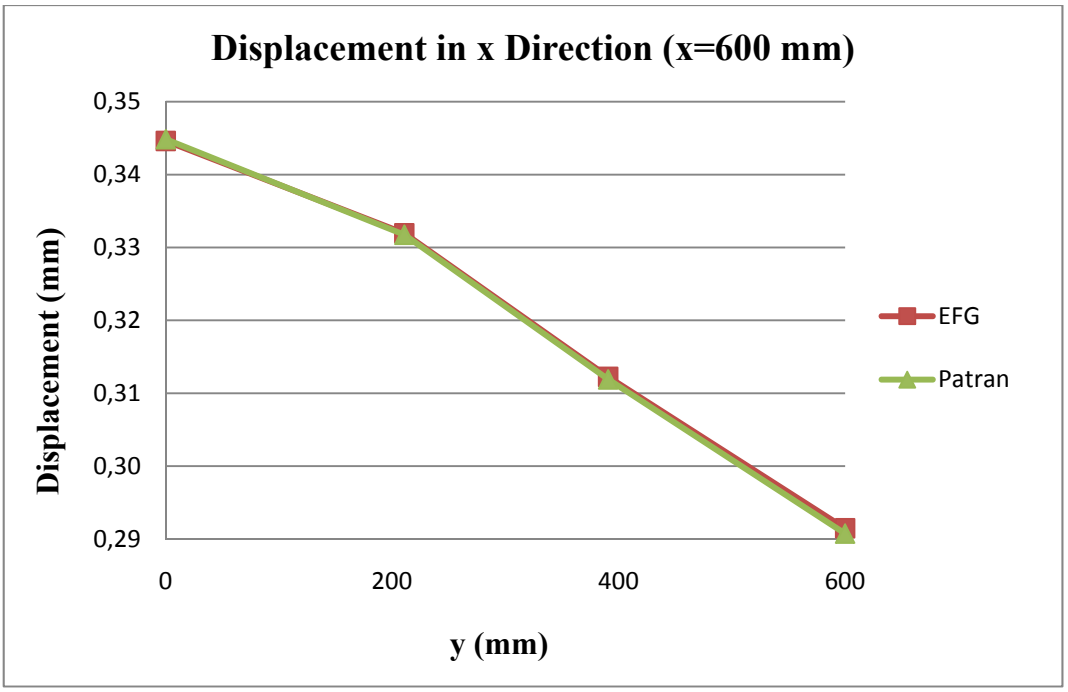

Figure 4.3.23 Graphical comparison of displacements in x direction

Table 4.3.12 and Figure 4.3.24 show the displacement results in y direction calculated by EFG program and finite element method;

Table 4.3.12 Comparison of the displacements in y direction

x	y	v EFG	v Patran	Error %
0	100	-0.059	-0.059	0.498
0	136	-0.063	-0.067	5.359
0	150	-0.064	-0.068	5.193
0	600	-0.118	-0.118	0.144
7	100	-0.058	-0.059	0.548
7	108	-0.061	-0.062	2.378
9	127	-0.063	-0.066	4.274
15	99	-0.057	-0.058	2.022
22	98	-0.056	-0.058	2.771
36	93	-0.054	-0.055	2.557
69	73	-0.041	-0.043	2.737
93	36	-0.018	-0.021	13.605
100	0	0.000	0.000	0.000
107	9	-0.001	-0.004	66.732
400	0	0.000	0.000	0.000
600	0	0.000	0.000	0.000
600	600	-0.071	-0.070	0.353

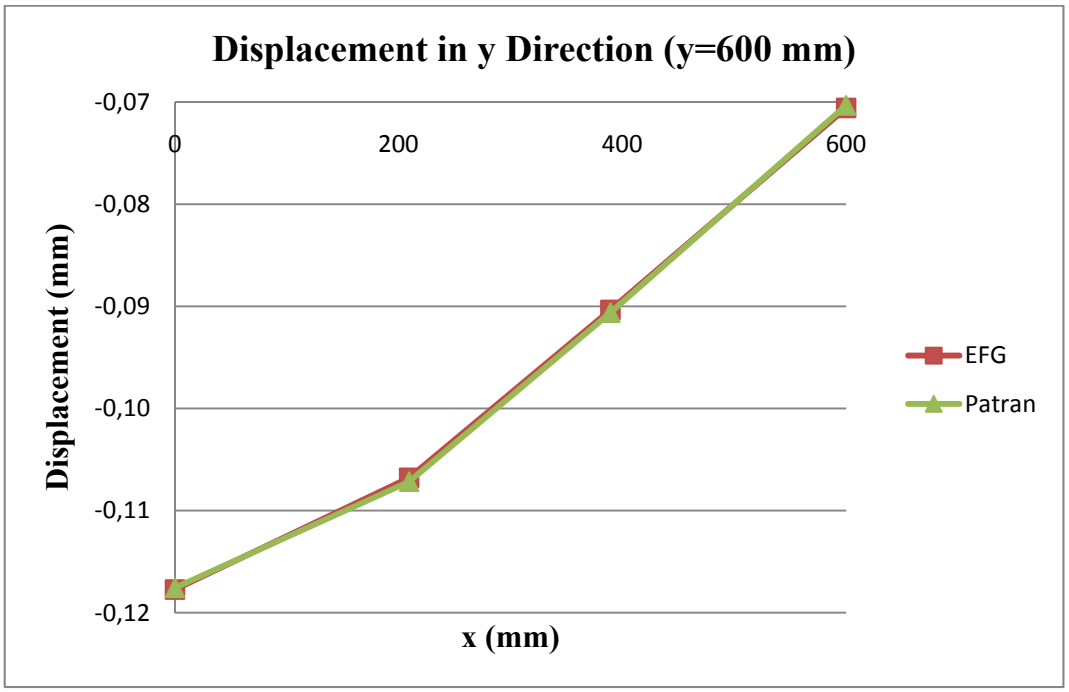

Figure 4.3.24 Graphical comparison of displacements in y direction

Table 4.3.13, Figure 4.3.25 and Figure 4.3.26 show the σ_x results calculated by EFG program and finite element method;

Table 4.3.13 Comparison of the σ_x results

x	y	σx EFG	σx Patran	Error %
0	100	292.026	296.044	1.357
0	136	164.563	184.966	11.031
0	150	145.837	163.198	10.638
0	600	91.651	90.801	0.927
7	100	250.061	303.290	17.551
7	108	215.236	270.965	20.567
9	127	138.747	198.814	30.213
15	99	333.990	292.198	12.513
22	98	279.785	274.073	2.041
36	93	241.354	226.493	6.157
69	73	65.153	76.158	14.450
93	36	-7.563	-0.888	88.262
100	0	0.847	-6.361	113.324
107	9	5.913	-3.278	155.430
400	0	90.817	91.537	0.787
600	0	106.590	99.833	6.339
600	600	106.921	99.993	6.480

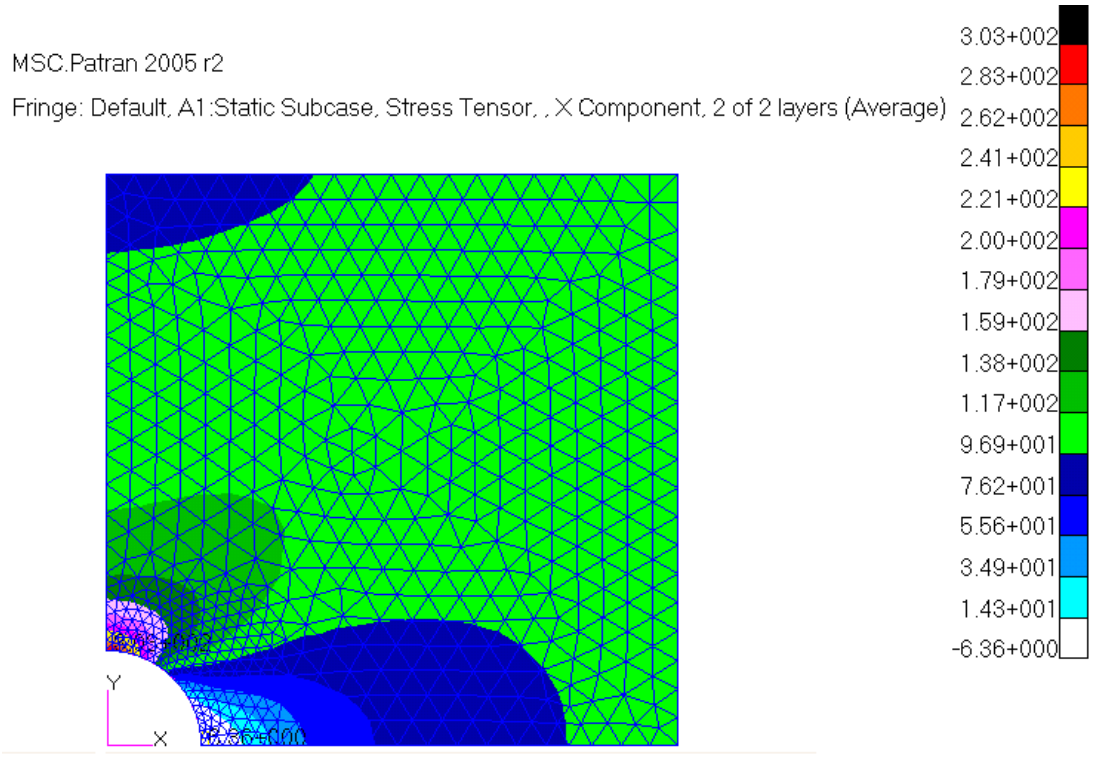

Figure 4.3.25 σ_x distribution obtained by Patran/Nastran

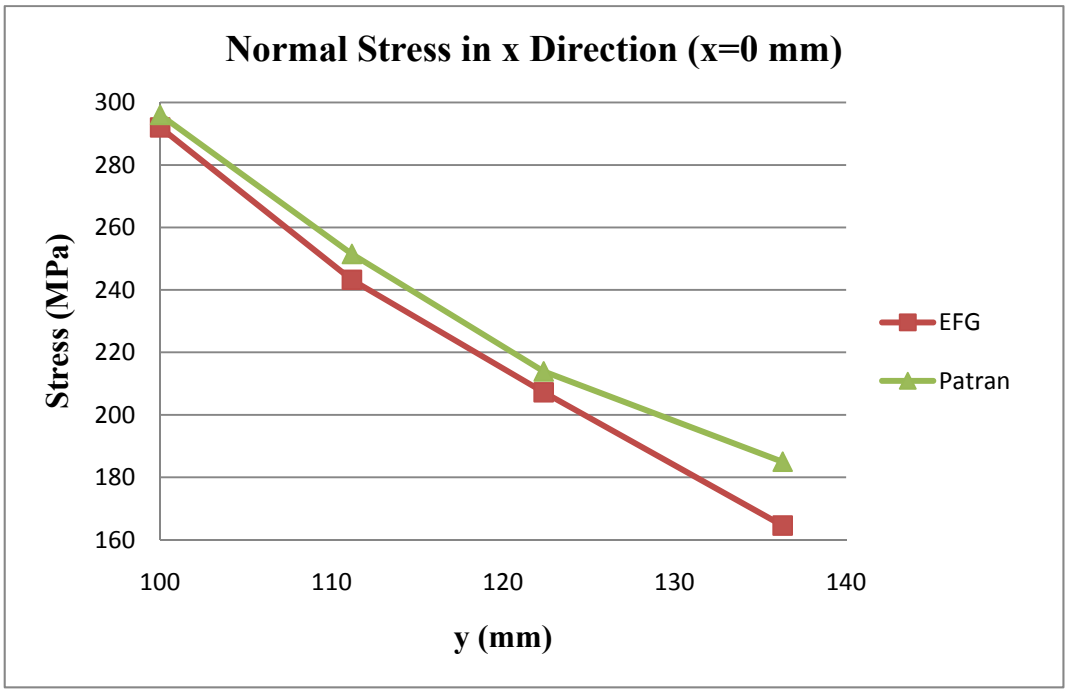

Figure 4.3.26 Graphical comparison of σ_x results

Table 4.3.14, Figure 4.3.27 and Figure 4.3.28 show the σ_y results calculated by EFG program and finite element method;

Table 4.3.14 Comparison of the σ_y results

x	y	σy EFG	σy Patran	Error %
0	100	3.178	17.157	81.476
0	136	35.903	37.929	5.342
0	150	36.794	37.648	2.268
0	600	0.025	0.121	78.932
7	100	5.948	14.645	59.385
7	108	10.329	20.073	48.545
9	127	29.146	36.190	19.465
15	99	0.408	17.706	97.695
22	98	9.434	23.480	59.822
36	93	33.434	36.343	8.005
69	73	54.358	38.058	29.987
93	36	-66.372	-52.861	20.356
100	0	-27.238	-98.600	72.376
107	9	-21.809	-82.446	73.548
400	0	6.278	4.948	21.182
600	0	15.403	17.617	12.567
600	600	-2.195	-0.006	99.740

Figure 4.3.27 σ_y distribution obtained by Patran/Nastran

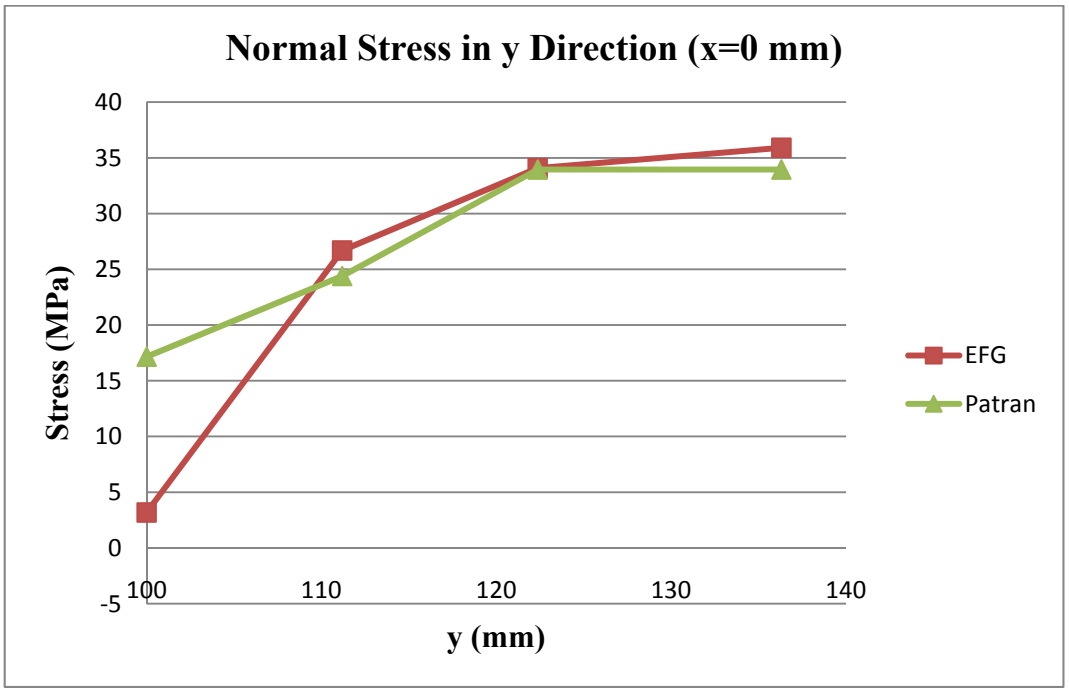

Figure 4.3.28 Graphical comparison of σ_y results

Table 4.3.15, Figure 4.3.29 and Figure 4.3.30 show the σ_{xy} results calculated by EFG program and finite element method;

Table 4.3.15 Comparison of the σ_{xy} results

x	y	σxy EFG	σxy Patran	Error %
0	100	3.115	-6.967	144.707
0	136	-2.071	0.151	107.311
0	150	0.087	1.484	94.122
0	600	0.177	0.180	2.004
7	100	-24.058	-21.144	12.113
7	108	-1.367	-11.451	88.067
9	127	-2.183	-3.306	33.972
15	99	-75.085	-38.630	48.551
22	98	-67.528	-52.888	21.680
36	93	-90.798	-72.432	20.228
69	73	-57.521	-51.039	11.270
93	36	25.953	9.223	64.463
100	0	0.121	1.264	90.393
107	9	-4.017	1.103	127.453
400	0	0.117	-1.144	110.191
600	0	-3.627	-0.238	93.450
600	600	3.439	0.023	99.327

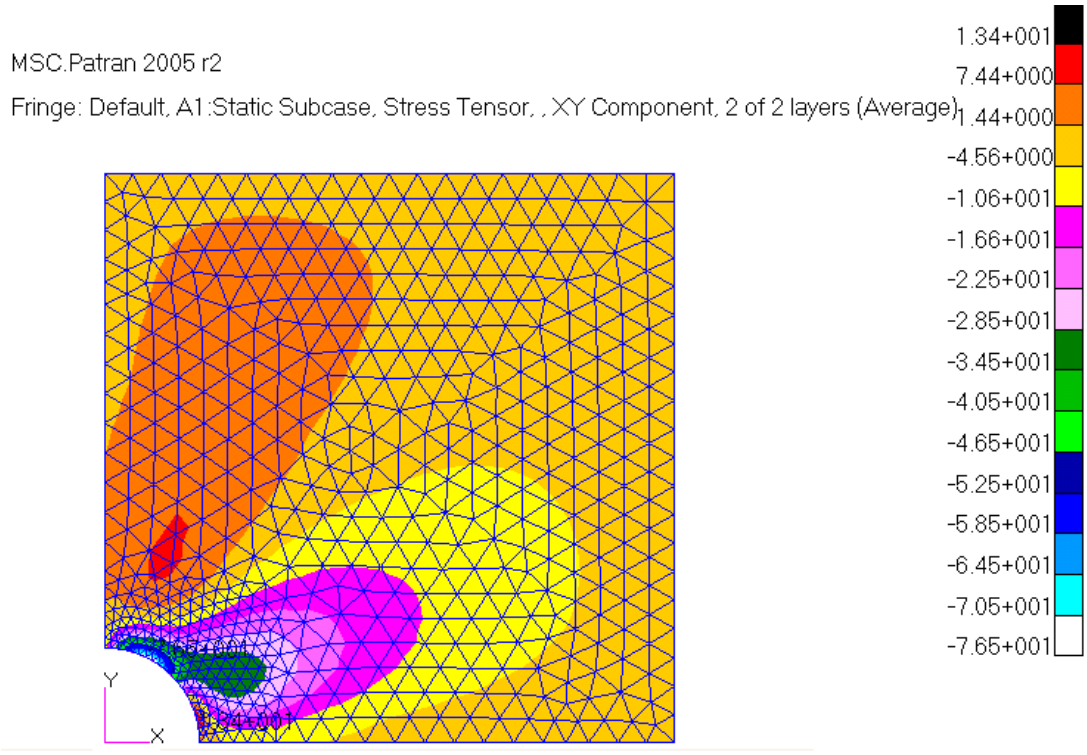

Figure 4.3.29 σ_{xy} distribution obtained by Patran/Nastran

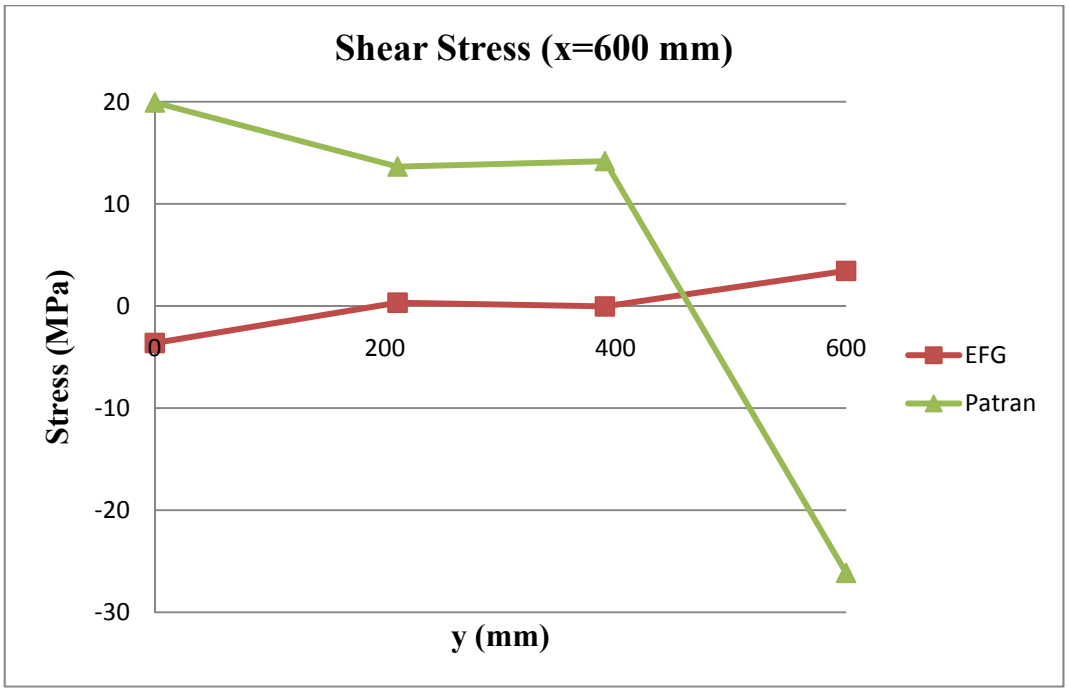

Figure 4.3.30 Graphical comparison of σ_{xy} results

The results obtained from the different EFG solutions are compared. Table 4.3.16 and Figure 4.3.31 show the displacement results in x direction calculated by finite element method and EFG program of runs 1, 2 and 3;

Table 4.3.16 Comparison of the displacements in x direction

x	y	u Patran	u EFG run 1	u EFG run 1	u EFG run 1
600	0	0.345	0.347	0.347	0.345
600	200	0.333	0.334	0.334	0.333
600	211	0.332	0.333	0.333	0.332
600	391	0.312	0.313	0.313	0.312
600	400	0.311	0.312	0.312	0.311
600	600	0.291	0.292	0.291	0.291

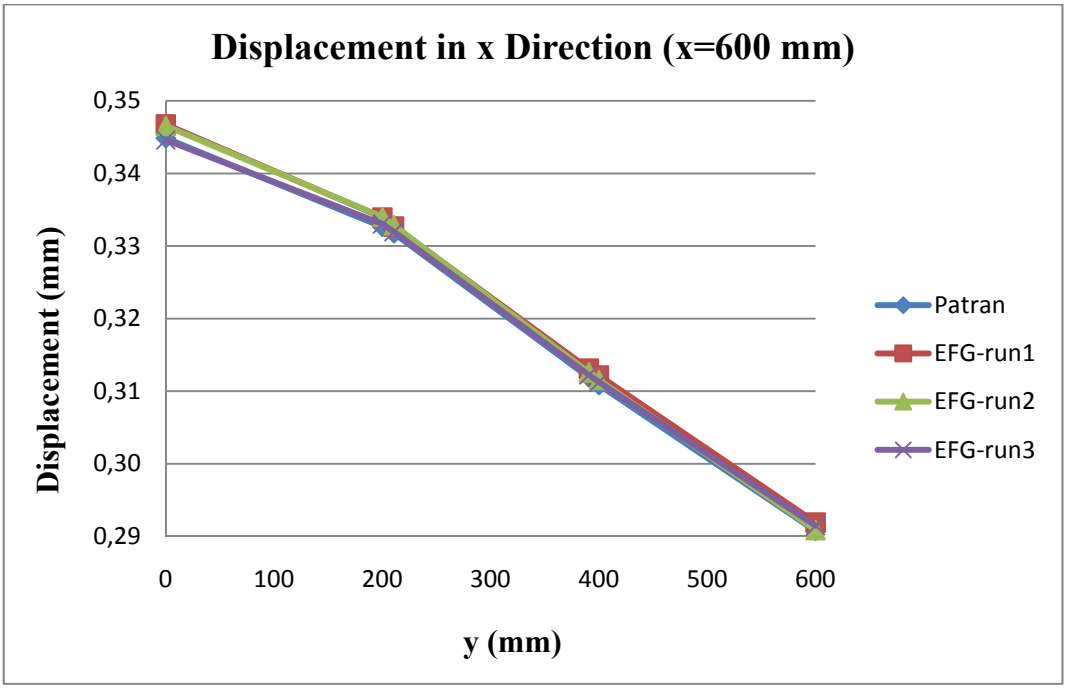

Figure 4.3.31 Graphical comparison of displacements in x direction

Table 4.3.17 and Figure 4.3.32 show the displacement results in y direction calculated by finite element method and EFG program of runs 1, 2 and 3;

Table 4.3.17 Comparison of the displacements in y direction

x	y	v Patran	v EFG run 1	v EFG run 1	v EFG run 1
0	600	-0.118	-0.117	-0.118	-0.118
200	600	-0.107	-0.108	-0.109	-0.108
209	600	-0.107	-0.107	-0.108	-0.107
389	600	-0.091	-0.091	-0.091	-0.090
400	600	-0.090	-0.090	-0.090	-0.089
600	600	-0.070	-0.071	-0.070	-0.071

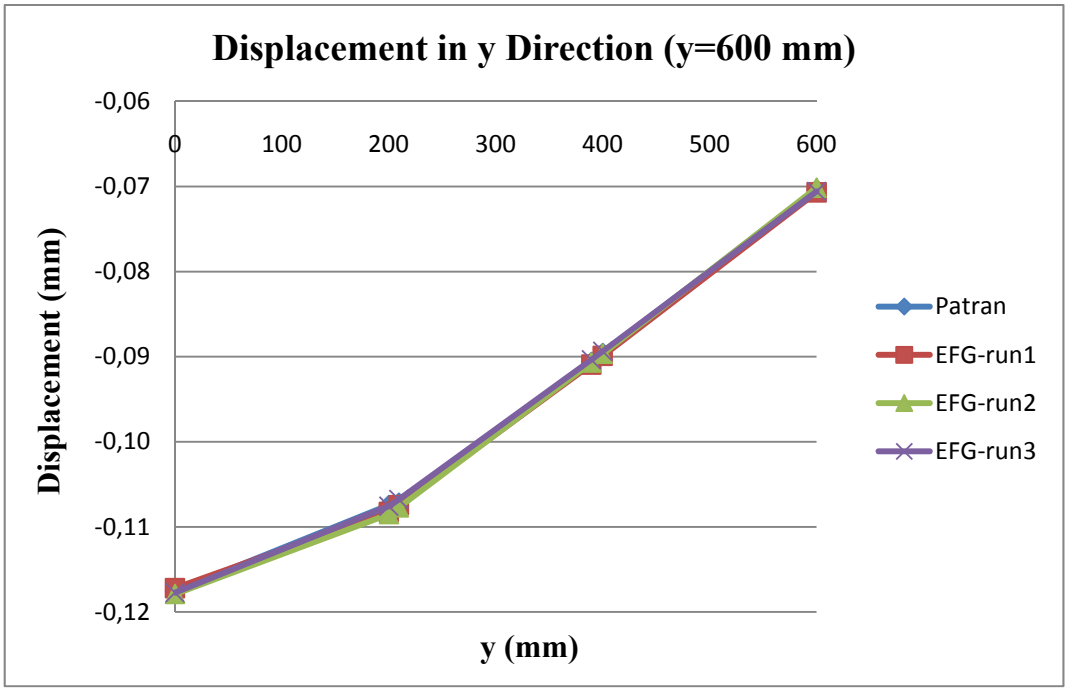

Figure 4.3.32 Graphical comparison of displacements in y direction

Table 4.3.18 and Figure 4.3.33 show the σ_x results calculated by finite element method and EFG program of runs 1, 2 and 3;

Table 4.3.18 Comparison of the σ_x results

x	y	σx Patran	σx EFG run1	σx EFG run2	σx EFG run3
0	100	296.044	308.088	288.623	292.026
0	111	251.485	264.772	247.449	243.231
0	136	184.966	200.194	170.358	207.219
0	150	163.198	164.942	149.669	164.563
0	217	122.100	122.857	130.055	136.795
0	300	110.265	108.702	114.596	125.624
0	452	100.690	102.129	102.047	107.844
0	600	90.674	107.937	87.434	91.651

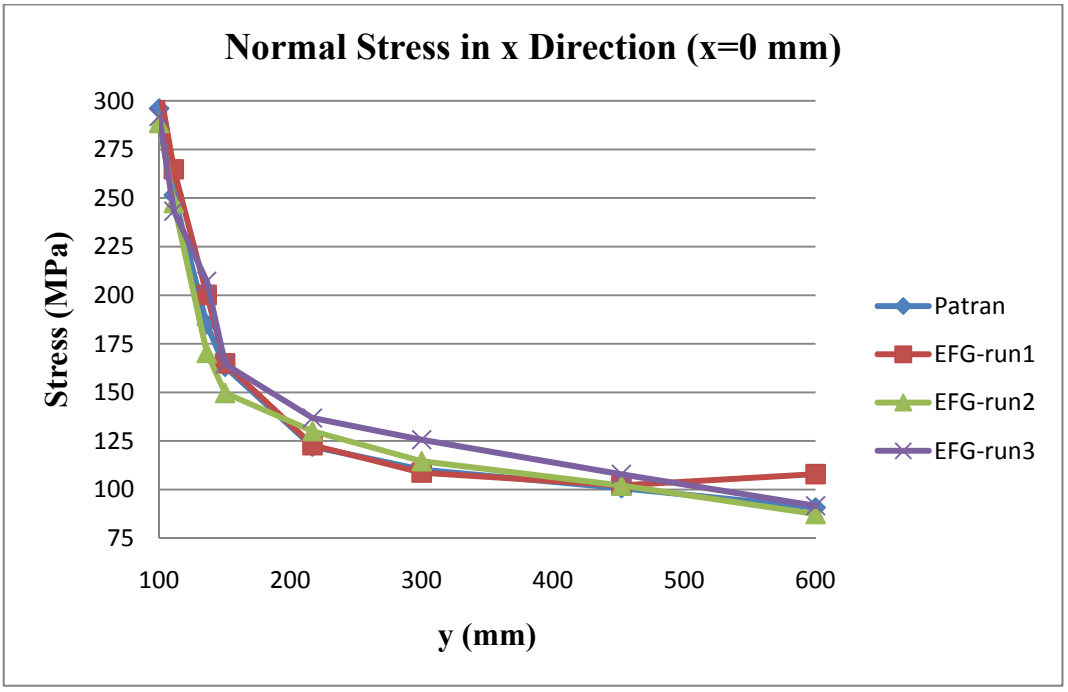

Figure 4.3.33 Graphical comparison of σ_x results

CHAPTER 5

CONCLUSION

The development of EFG method is a significant achievement in the improvement of mesh free methods. In this thesis, a FORTRAN program has been developed to analyze plane stress problems by EFG method. The results obtained are compared with analytical and FEM results.

In this study, three typical plane stress problems have been examined. First one is a cantilever beam subjected to parabolic end load, second is a cantilever beam subjected to uniform distributed transverse load and third one is a square plate having a hole at center and subjected to uniform distributed tension load.

In each sample analysis, the problem has been solved three times by changing the parameters. In the first run, the problem domain has been defined and a proper background mesh has been applied. A certain number of nodes and integration points have been selected. In the second run, the background mesh has been refined. This run serves to see the effect of mesh density. In the third run, the mesh density has been kept constant and the number of integration points has been changed.

It has been observed that the EFG method performed satisfactorily in each case and it compares favorably with the FEM results. The stress recovery is the best when four nodes per element and quintic Gauss integration are selected.

It has been observed that EFG gives more accurate results with respect to FEM at the same time computational cost.

The extension of EFG to bending problems such as beams and plates, different material models such as laminated composites, and nonlinear problems is straight forward by using the methodology presented in this thesis.

REFERENCES

[1] Wenjing Zhang, Maohui Xia and Lechun Liu, "Meshfree Radial Point Interpolation Method and Its Application for Two-Dimensional Elastic Problem", 3rd International Conference on Innovative Computing Information and Control, pp. 406, 2008.

[2] Liu, Gui-Rong, "Mesh Free Methods: Moving Beyond the Finite Element Method", CRC Press LLC, First Edition, pp. 3-4, 2003.

[3] Lucy, L. B., "A Numerical Approach to the Testing of the Fission Hypothesis", The Astronomical Journal, vol. 82, pp. 1013-1024, 1977.

[4] Monaghan, J. J., "Why Particle Methods Work", SIAM Journal of Scientific and Statistical Computing, vol. 3, pp. 423-433, 1982.

[5] Swengle, J. W., Hicks, D. L. and Attaway, S.W., "Smoothed Particle Hydrodynamics Stability Analysis", Journal of Computational Physics, vol. 116, pp. 123-134, 1995.

[6] Dyka, C. T., "Addressing Tension Instability in SPH Methods", Technical Report NRL/MR/6384, NRL, 1994.

[7] Liu. W. K., Jun, S. and Zhang, Y. F., "Reproducing Kernel Particle Methods", International Journal for Numerical Methods in Fluids, vol. 20, pp. 1081-1106, 1995.

[8] Johnson, G. R. and Beissel, S. R., "Normalized Smoothing Functions for SPH Impact Computations", International Journal for Numerical Methods in Engineering, vol. 39, pp. 2725-2741, 1996.

[9] Belytschko, T., Krongauz, Y., Fleming, M., Organ, D., and Liu, W. K., "Smoothing and Accelerated Computations in the EFG Method", Journal of Computational and Applied Mathematics, vol. 74, pp. 111-126.

[10] Bonet, J. and Kulasegaram, S., “Correction and Stabilization of Smooth Particle Hydrodynamics Methods with Applications in Metal Forming Simulations” International Journal for Numerical Methods in Engineering (IJNME), vol. 47, pp. 1189-1214, 2000.

[11] Nyroles, B., Touzot, G. and Villion, P. 1992, “Generalizing the Finite Element Method: Diffuse Approximation and Diffuse Elements”, Computational Mechanics, vol. 10, pp. 307-318.

[12] Belytschko, T., Lu, Y. Y., Gu, L., “Element-free Galerkin Methods”, International Journal for Numerical Methods in Engineering (IJNME), vol. 37, issue 2, pp. 229-256, 1994.

[13] Liu, G. R. and Gu, Y. T., “A Point Interpolation Method”, in Proc. 4th Asia-Pacific Conference on Computational Mechanics, Singapore, pp. 1009–1014, December, 1999.

[14] Duarte, C. A., Babuska, I. and Oden, J. T., "Generalized Finite Element Methods for Three Dimensional Structural Mechanics Problems", Computers and Structures, vol. 77, pp. 215-232, 2000.

[15] Duarte, C. A., and Oden, J. T., “H-p clouds and h-p Meshless Method”, Numerical Methods for Partial Differential Equations, vol. 12, pp.1-34, 1996.

[16] Vila, J. P., “On Particle Weighted Method and Smooth Particle Hydrodynamics”, Mathematical Models and Methods in Applied Sciences, vol. 9, pp. 161-209, 1999.

[17] Bouillard, P. and Suleau, S., “Element-free Galerkin Method for Helmholtz Problems: Formulation and Numerical Assessment of the Pollution Effect”, Computer Methods in Applied Mechanics and Engineering, vol. 162, pp. 317-335, 1998.

[18] Bonet, J. and Lok, T., “Variational and Momentum Preservation Aspects of Smooth Particle Hydrodynamics Formulations”, CEMAME vol. 180, pp. 97-115, 1999.

[19] Onate, E. and Idelsohn, S., “A mesh-free Finite Point Method for Advective-Diffusive Transport and Fluid Flow Problems”, Computational Mechanics, vol. 21, pp. 283-292, 2001.

[20] Atluri, S. N. and Zhu, T., “A New Meshless Local Petrov-Galerkin (MLPG) Approach in Computational Mechanics”, Computational Mechanics, vol. 22, pp. 117-127, 1998.

[21] Atluri, S. N., Cho, J. Y., and Kim, H. G., “Analysis of Thin Beams, using the Meshless Local-Petrov-Galerkin Method, with Generalized Moving Least Squares Interpolations”, Computational Mechanics, vol.24, pp.334-347, 1999.

[22] Atluri, S. N., Cho, J. Y., and Kim, H. G., “A Critical Assessment of the Truly Meshless Local Petrov-Galerkin (MLPG) and Local Boundary Integral Equation (LBIE) Methods”, Computational Mechanics, vol.24, pp.348-372, 1999.

[23] Lin, H., and Atluri, S. N., “The Meshless LocalPetrov-Galerkin (MLPG) Method for Solving Incompressive Navier-Stokers Equations”, Computational Modeling Engineering Science, vol. 2, pp. 117-142, 2001.

[24] Hennadiy Netuzhylov and Andreas Zilian, “Space-time Meshfree Collocation Method: Methodology and Application to Initial-Boundary Value Problems”. International Journal for Numerical Methods in Engineering (IJNME), vol. 80, pp. 350 - 380, 2009.

[25] Delaunay, B. “Sur la sphère vide, Izvestia Akademii Nauk SSSR”, Otdelenie Matematicheskikh i Estestvennykh Nauk, vol. 7, pp.793-800, 1934.

[26] Irons, B. M., "Numerical Integration Applied to Finite Element Methods", Conference on Use of Digital Computers in Structural Engineering, University of Newcastle, 1966.

[27] Irons, B. M. and Razzaque, A., "Experience with the Patch Test for Convergence of Finite Element Methods", Mathematical Foundations of the Finite Element Method, Academic Press, pp. 557-587, 1972.

[28] Zienkiewicz, O. C. and Taylor, R. L., “The Finite Element Method”, Butterworth-Heinemann, Fifth Edition, pp. 198-201, 2000.

[29] Timoshenko, S. and Goodier, J., “Theory of Elasticity”, Third Edition, McGraw-Hill, New York, 1987.

[30] Wikipedia Gaussian quadrature web site, http://en.wikipedia/wiki/ Gaussian quadrature, Last access date 13.January.2010.

[31] Abramowitz, M. and Stegun, I. A., "Integration", Handbook of Mathematical Functions (with Formulas, Graphs, and Mathematical Tables), Dover, pp. 885-887, 1972.

[32] CATIA, User's Manual for Version5 R17, "Creating Elements from an External File", Dassault Systèmes, 2007.

APPENDIX A

GAUSSIAN QUADRATURE

The definite integral of a function can be approximated by a quadrature rule in a numerical analysis. This rule is usually based on weights of specified points (IP, node etc.) in the integration domain.

Gaussian quadrature rule is introduced by Carl Friedrich Gauss and n-point Gaussian quadrature is constructed to yield an exact result for polynomials of degree 2n − 1 or less. The points and corresponding weights of them are represented by a suitable x_i and w_i (for i = 1... n) respectively.

The integration domain is usually taken as taken as [−1, 1], so the rule is stated as [30],

$$\int_{-1}^{1} f(x)\,dx \approx \sum_{i=1}^{n} w_i f(x_i) \qquad (A.1)$$

The i^{th} Gauss node, xi, is the i^{th} root of P_n (x) (Legendre polynomial having the n^{th} polynomial normalized to give P_n (1) = 1) and its weight is given by [31],

$$w_i = \frac{2}{(1-x_i^2)(P'_n(x_i))^2} \qquad (A.2)$$

Some low-order rules for solving the integration problem are listed in Table A.1 [30].

Table A.1 Abscissae and Weight Coefficients of the Gaussian Quadrature Formula

Abscissae and Weight Coefficients of the Gaussian Quadrature Formula used for Boundary Integration Points		
Number of points, n	**Gauss nodes, ± x_i**	**Weights, w_i**
1	0	2
2	$\pm\sqrt{1/3}$	1
3	0 $\pm\sqrt{3/5}$	8/9 5/9
4	$\pm\sqrt{(3-2\sqrt{6/5})/7}$ $\pm\sqrt{(3+2\sqrt{6/5})/7}$	$\frac{18+\sqrt{30}}{36}$ $\frac{18-\sqrt{30}}{36}$
5	0 $\pm\frac{1}{3}\sqrt{5-2\sqrt{10/7}}$ $\pm\frac{1}{3}\sqrt{5+2\sqrt{10/7}}$	128/225 $\frac{322+13\sqrt{70}}{900}$ $\frac{322-13\sqrt{70}}{900}$

For the boundary weights between the two nodes on the boundary line of the whole problem domain, the following Gaussian quadrature formula is used [28];

$$\int_{-1}^{1} f(x)\,dx \approx \sum_{i=1}^{n} w_i f(x_i) \qquad (4.1)$$

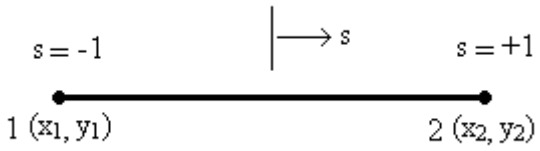

Figure A.1 Boundary line between two nodes

Table A.2 represents the gauss nodes and weight coefficients calculated for the 10 points;

Table A.2 Abscissae and Weight Coefficients of the Gaussian Quadrature Formula used for Boundary Integration Points [28]

Abscissae and Weight Coefficients of the Gaussian Quadrature Formula used for Boundary Integration Points		
Number of points, n	**Gauss nodes, ± x_i**	**Weights, w_i**
1	0	2.000000000000000
2	0.577350269189626	1.000000000000000
3	0.774596669241483	0.555555555555556
	0.000000000000000	0.888888888888889
4	0.861136311594053	0.347854845137454
	0.339981043584856	0.652145154862546
5	0.906179845938664	0.236926885056189
	0.538469310105683	0.478628670499366
	0.000000000000000	0.568888888888889
6	0.932469514203152	0.171324492379170
	0.661209386466265	0.360761573048139
	0.238619186083197	0.467913934572691
7	0.949107912342759	0.129484966168870
	0.741531185599394	0.279705391489277
	0.405845151377397	0.381830050505119
	0.000000000000000	0.417959183673469
8	0.960289856497536	0.101228536290376
	0.796666477413627	0.222381034453374
	0.525532409916329	0.313706645877887
	0.183434642495650	0.362683783378362
9	0.968160239507626	0.081274388361574
	0.836031107326636	0.180648160694857
	0.613371432700590	0.260610696402935
	0.324253423403809	0.312347077040003
	0.000000000000000	0.330239355001260
10	0.973906528517172	0.066671344308688
	0.865063366688985	0.149451349150581
	0.679409568299024	0.219086362515982
	0.433395394129247	0.369266719309996
	0.148874338981631	0.295524224714753

APPENDIX B

VISUALIZATION

B.1 Creating Elements from an External File

The results generated by the EFG method via solving the system equations are usually in the form of a vast volume of digital data. The results have to be visualized in such a way that they can be easily interpolated, analyzed, and presented. The visualization is performed by the postprocessor that comes with the software package. Most of these processors allow users to display 3D objects in many convenient and colorful ways on the screen. The object can be displayed in the form of wire frames, collections of elements and collections of nodes. The user can rotate, translate, and zoom in/out on the objects. Field variables can be plotted on the object in the form of contours, fringes, wire frames and deformations. There are usually tools available for users to produce iso-surfaces and vector fields of variables. Tools to enhance the visual effects are also available, such as shading, lighting, and shrinking. Animation and movies can also be produced to simulate dynamic aspects [32].

The EFG method gives the displacement of each node and integration points. Since the coordinates of the those points are already known before the application of the loading, the only need for visualization of the deformation is to calculate the final coordinates of the nodes and integration points by adding the displacement to initial coordinate of each point and then enter initial and final coordinates data to the program.

The visualization of the parts' deformations are performed by CATIA (Computer Aided Three-dimensional Interactive Application) which is a multi-platform CAD/CAM/CAE commercial software suite developed by the French company Dassault Systèmes and marketed worldwide by IBM. The Version5 R17 is suitable and this version is used in this thesis.

CATIA creates points, curves, and multi-sections surfaces from a Microsoft Excel spreadsheet which contains macros. In those macros, one can define:

- the points space coordinates
- the points through which the curves pass
- the curves used as profiles for the multi-sections surface

The following is the procedure for extracting the points from an external Excel file into CATIA [32];

1 One opens any .CATPart document containing a Geometrical Set or an Ordered Geometrical Set into CATIA.

2 Opens the ElementsFromExcel.xls file from any directory saved in into Excel, and enables the macros. The excel document looks like the Figure B.1.1:

	A	B	C
1	StartMulti-SectionsSurface		
2	StartCurve		
3	0	-90	10
4	0	-30	60
5	0	50	60
6	0	110	20
7	EndCurve		
8	StartCurve		
9	50	-60	0
10	50	-10	40
11	50	50	40
12	50	70	0
13	EndCurve		
14	StartCurve		
15	100	-100	-10
16	100	-40	35
17	100	0	50
18	100	75	40
19	100	140	0
20	EndCurve		
21	EndMulti-SectionsSurface		
22	End		

Figure B.1.1 Sample Input Excel Sheet for the Macro [32]

The Excel sheet contains:

- Instructions, such as “StartMulti-SectionsSurface” and “EndMulti-SectionsSurface”, “StartCurve” and “EndCurve” are given between other instructions or numerical data.
- Numerical data are the point space coordinates: X, Y, Z respectively from the left to the right
- A final End instruction

In the above example, a multi-sections surface can be created based on three curves. The first and second curve pass through four points, and the third curve passes through five points.

The elements will be created from top to bottom, i.e. the four points of the first curve will be created, then the curve itself, then the points making up the second curve and the latter itself, and so forth.

One can add rows to create more elements or delete rows to edit elements and then save the spreadsheet.

1 From Excel, select the Tools -> Macro -> Macros menu item. The Macro dialog box is displayed.

2 Select the Feuil1.Main macro.

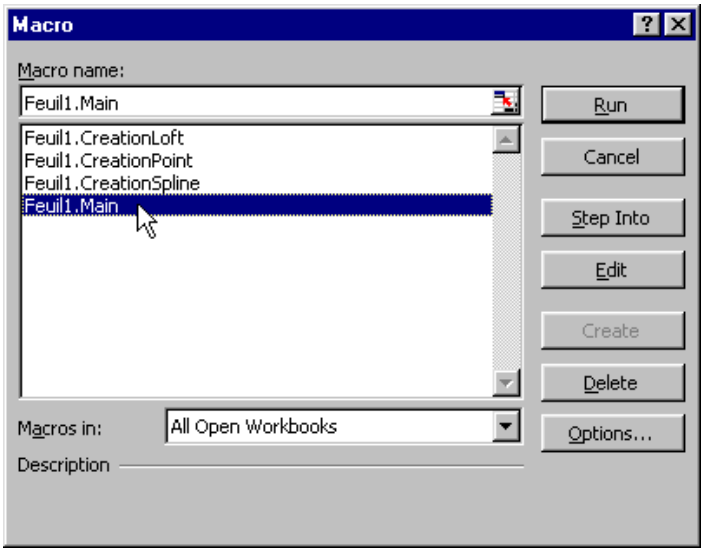

Figure B.1.2 Macro type list view

3 Click Run. The User Info dialog box is displayed.

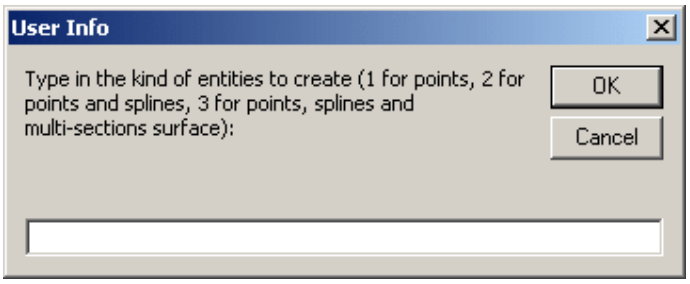

Figure B.1.3 Entity type selection view

4 Key in the type of element to be generated:

"1" for generation of only the point(s)
"2" for generation of the points and the curve(s)
"3" for generation of the points, curves and multi-sections surface(s)

5 Click OK. The elements (points, curves, and multi-sections surface) are created in the geometry. The specification tree is updated accordingly.

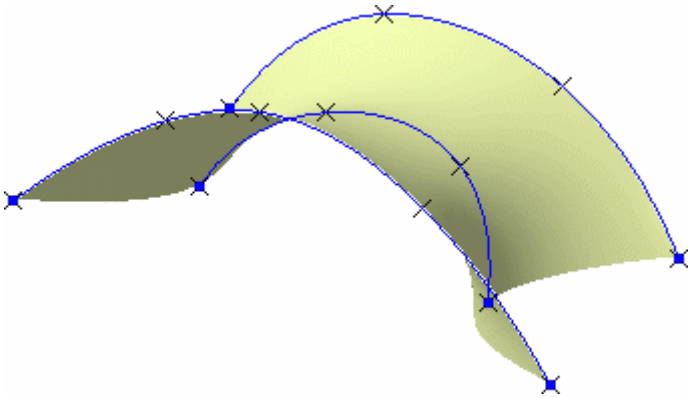

Figure B.1.4 A multi-sections surface created by extracting the points from an excel sheet [32]

The Generative Shape Design or Wireframe and Surface workbench needs not to be loaded, provided a CATIA session is running and a .CATPart document is loaded.

The curve definition is limited to 500 points, and the multi-sections surface definition to 50 splines.

However, the thesis problems have numerous numbers of points and they have to be arranged in the format of the excel macro. The macro performs lines according to the points entered between the commands of "StartCurve" and "EndCurve". In order to line up and prepare the excel sheet for the mesh free problems, other macros have been written and the following procedure should be applied:

B.2 Data Preparation Procedure for CATIA

1 Open the text file called "1_connectivity.txt" into TextPad version 5.0.3.0 (which is a text editor for the Microsoft Windows family of operating systems).

2 Run the macro written in TextPad called "connect_line" which lines the connected nodes one under the other.

3 Copy the output file of the TextPad (2 columns) into the excel file (called CATIAElementsFromExcel_line.xls) B and C columns.

4 Copy the "2_node coordinates.txt" file to the columns between H and K of the same excel sheet.

5 In the A column, write "*" sign to the cells starting from the 3rd row and increasing by 4 rows (e.g. 3rd, 7th, 11th … and so on).

6 Copy columns between A and D of the excel sheet into a new blank TextPad file.

7 Replace "*… N/A…" with "…EndCurve" and "… N/A…" with "…StartCurve".

8 Then copy back the changed file into the excel sheet columns between A and D.

9 Run the macro called "Feuil1.Main" of the excel sheet.

10 Click Run. "The User Info" dialog box is displayed.

11 Key in the type of element to be generated;
"1" for generation of only the point(s)
"2" for generation of the points and the curve(s)

Typing 3 does not work for the problems having more than 50 lines. The problems solved in this thesis has exceeding number of lines. However, at the same time the problems are plane stress problems which mean their three dimensions are reduced to two dimensions and one can create a surface using only the outer lines of the problem domain in CATIA Wireframe and Surface Design modules.

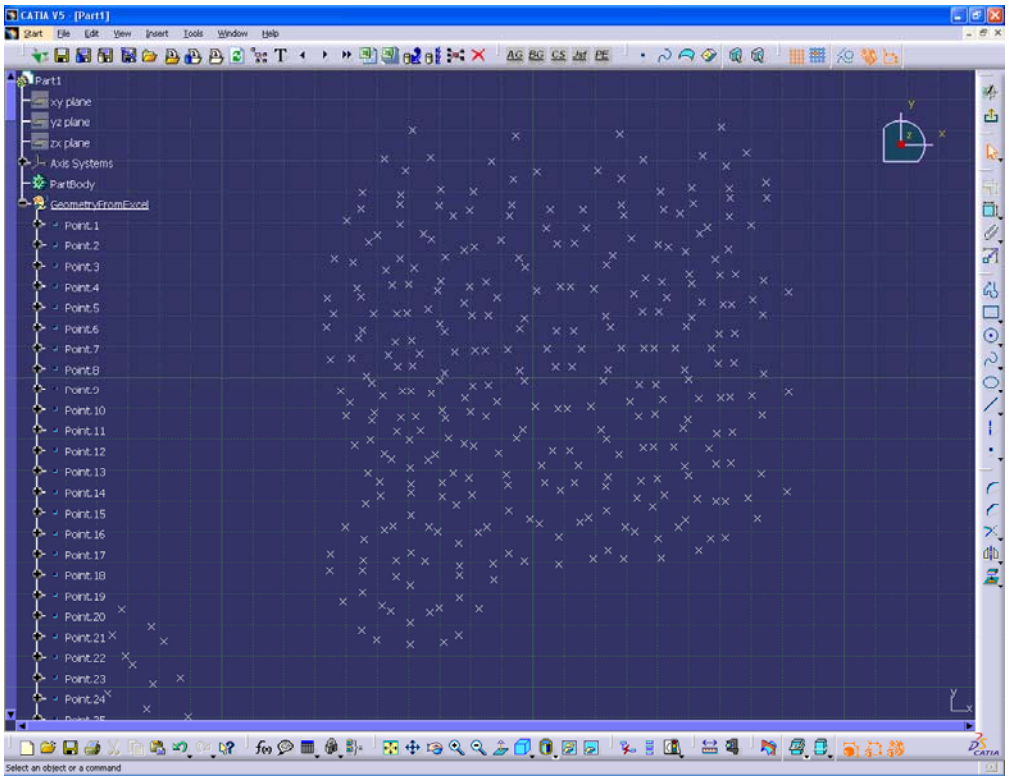

Figure B.2.1 Integration Points view in a CATPart

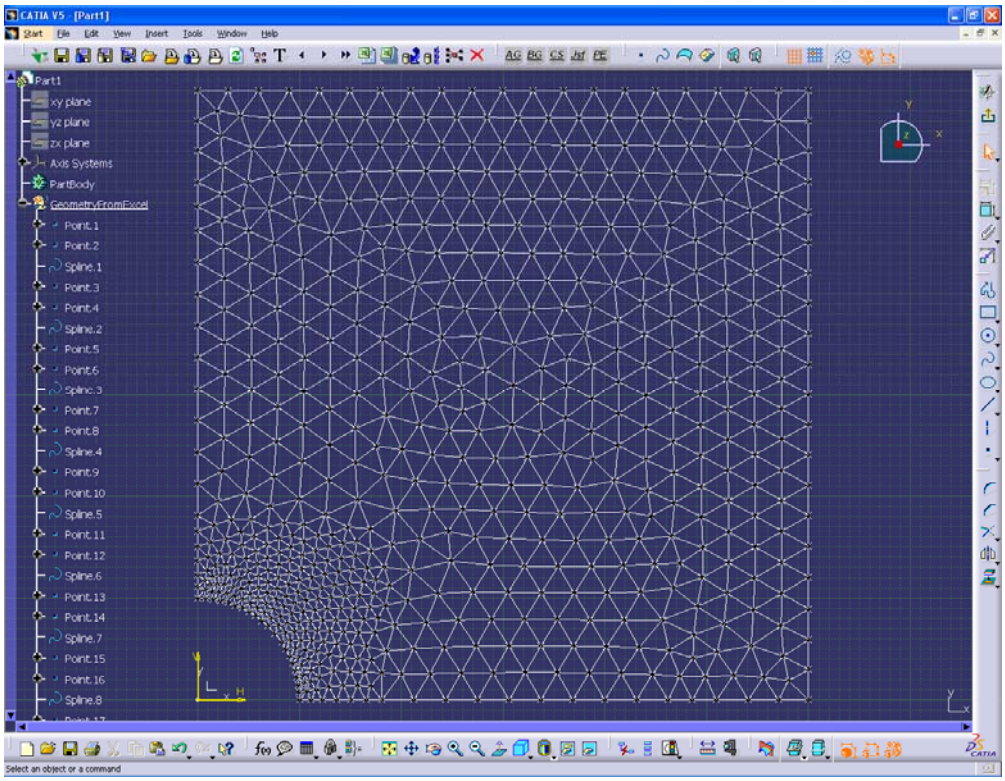

Figure B.2.2 Connected Lines (background meshes) view in a CATPart

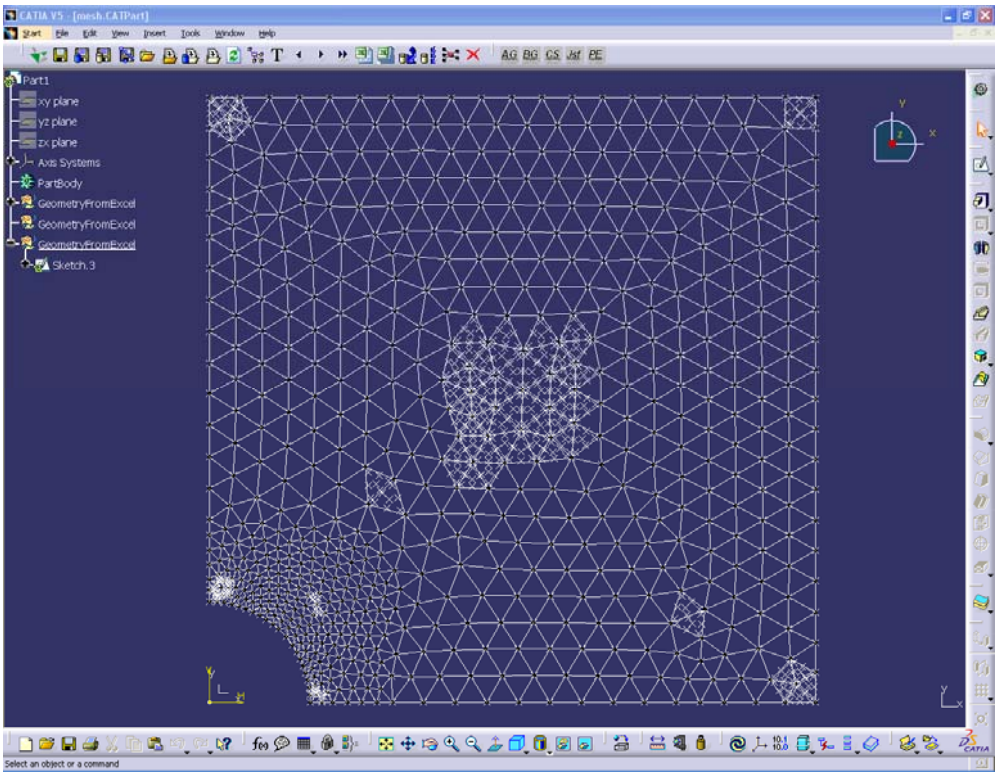

Figure B.2.3 Connected Lines and Integration Points together view in a CATPart

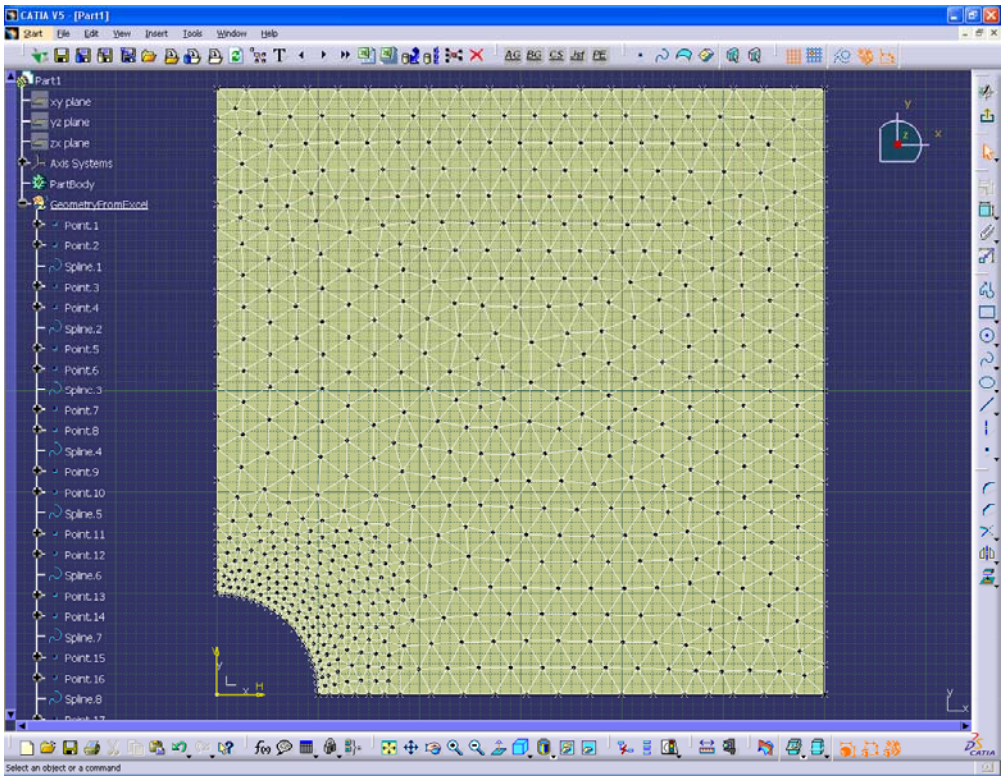

Figure B.2.4 Surface created by the connected lines view in a CATPart

APPENDIX C

CODE ALGORITHM